TRIUMF

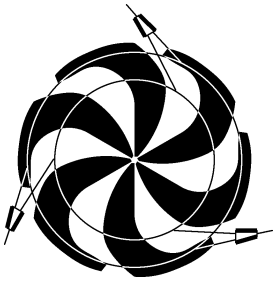

ANNUAL REPORT
SCIENTIFIC ACTIVITIES
2002

ISSN 1492-417X

CANADA'S NATIONAL LABORATORY
FOR PARTICLE AND NUCLEAR PHYSICS

OPERATED AS A JOINT VENTURE

MEMBERS:

THE UNIVERSITY OF ALBERTA
THE UNIVERSITY OF BRITISH COLUMBIA
CARLETON UNIVERSITY
SIMON FRASER UNIVERSITY
THE UNIVERSITY OF VICTORIA

ASSOCIATE MEMBERS:

THE UNIVERSITY OF MANITOBA
McMASTER UNIVERSITY
L'UNIVERSITÉ DE MONTRÉAL
QUEEN'S UNIVERSITY
THE UNIVERSITY OF REGINA
THE UNIVERSITY OF TORONTO

UNDER A CONTRIBUTION FROM THE
NATIONAL RESEARCH COUNCIL OF CANADA

DECEMBER 2003

The contributions on individual experiments in this report are outlines intended to demonstrate the extent of scientific activity at TRIUMF during the past year. The outlines are not publications and often contain preliminary results not intended, or not yet ready, for publication. Material from these reports should not be reproduced or quoted without permission from the authors.

Experiment 560
πp analyzing powers with the CHAOS spectrometer
(G.R. Smith, TRIUMF, G. Hofman, Colorado)

This experiment made use of the CHAOS spectrometer and a specially designed CHAOS polarized proton target (CPPT). The goal was to measure the analyzing powers (A_y) for $\pi^{\pm}p$ scattering to better than 0.05 between angles of 60° and 180° at several bombarding energies between 30 and 140 MeV. In 1995/1996 we made measurements at resonance energies only, due to persistent problems with the polarized target. In the fall of 1997, however, the target (and spectrometer) operated flawlessly, which permitted us to successfully explore the low energy region with incident π^- down to 51 MeV. Unfortunately, the beam time available to us in the fall of 1997 was insufficient to measure below 51 MeV, or to pursue the π^+ part of the low energy program.

Using the technique of partial wave analysis (PWA), the data obtained in this experiment are being used to improve the knowledge of the smaller scattering amplitudes. Analyzing power results in the forward angle (Coulomb nuclear interference) region for π^+p scattering, and in the $S-P$ interference region at backward angles near 50 MeV for π^- scattering are especially useful in this regard. With accurate πN partial waves, in particular at low energies, the physics goals of Expt. 560 are then to provide improved values for the πN coupling constant, to extrapolate to threshold where the πN scattering lengths can be obtained, and to extrapolate below threshold as well as to obtain a more accurate measure of the πN sigma term. The πN sigma term is an explicit measure of chiral symmetry breaking from which the strange sea quark content of the proton can be deduced. In addition there has been substantial interest in using πp observables to investigate isospin violations. These modern analyses use only data below about 100 MeV.

In 1997 the analysis of the resonance energy experiment was completed, and a Ph.D. thesis [Hofman, Physics, Univ. of British Columbia] was obtained based on those data. In 1998 the resonance energy results were published [Hofman *et al.*, Phys. Rev. **C58**, 3484 (1998)].

During the years 1998–2001 much effort was expended in designing and implementing an analysis procedure for the data which emphasized increased efficiency. The linear data streams were converted into a tree structure built around the CERN ROOT system. This led to an extremely fast, robust, and automated analysis that lets us adjust parameters such as kinematic cuts and angular binning, checking the new results in seconds rather than days.

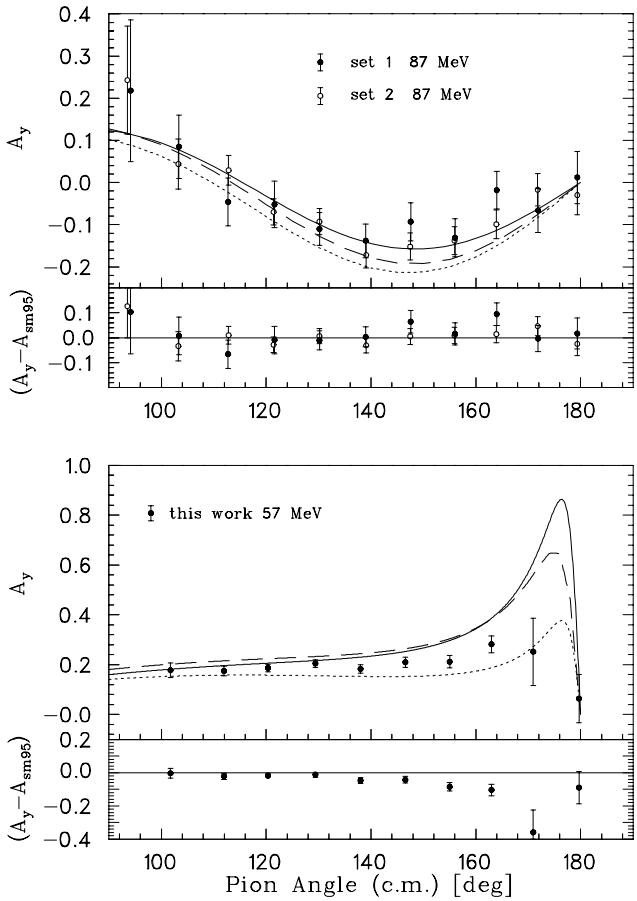

Fig. 30. The analyzing powers compared to phase shift solutions 87 and 57 MeV π^-. In each case the solid line is the SM95 phase-shift solution, the dotted line the SM02 solution and the dashed line the KH80 solution. The lower graphs show the new experimental analyzing powers subtracted from the SM95 solution.

The data analysis was performed by J. Patterson. Much effort went into reconstructing so called short tracks in CHAOS. Since the energy available to the recoil proton is very low, it does not penetrate all the detector planes. A special hardware trigger was developed to record events of this type and new off-line algorithms were required to reduce the large number of false tracks. Analysis was completed in late 2001 and a Ph.D. thesis (University of Colorado) submitted.

A typical result at the lowest energy of 57 MeV is shown in Fig. 30 and compared to 3 existing phase shift analyses. All the data have been submitted to the Virginia-GWU partial wave analysis group and were published [Patterson *et al.*, Phys. Rev. **C66**, 025207 (2002)].

Although the Expt. 560 program was (successfully) completed, the same spin polarized target was employed in Expt. 862 (see elsewhere in this Annual Report). As a by-product of that effort in summer, 2002, elastic πp analyzing power data were collected at 280 MeV. These have been analyzed and will be submitted for publication.

Experiment 704
Charge symmetry breaking in $np \rightarrow d\pi^0$ close to threshold
(A.K. Opper, Ohio; E. Korkmaz, UNBC)

Experiment 704 has final results from its precision measurement of charge symmetry breaking in the strong interaction. The observable of interest is the forward-backward asymmetry (A_{fb}) in $np \rightarrow d\pi^0$, which must be zero in the centre of mass if charge symmetry is conserved and has a predicted value that ranges between $(-35 \rightarrow +70) \times 10^{-4}$ [Niskanen, Few-Body Systems **26**, 241 (1999); van Kolck *et al.*, Phys. Lett. **B493**, 65 (2000)] depending on the strengths of the various contributions. The forward-backward asymmetry is defined as

$$A_{fb}(\theta) \equiv \frac{\sigma(\theta) - \sigma(\pi - \theta)}{\sigma(\theta) + \sigma(\pi - \theta)}$$

with the relevant contributions being the neutron-proton mass difference, exchange of an isospin mixed $\eta - \pi$ meson, and the effect of the d u quark mass difference on pion nucleon scattering.

The experiment was carried out with a 279.5 MeV neutron beam, a liquid hydrogen target, and the SASP spectrometer positioned at 0°. With these kinematics and the large acceptance of SASP the full deuteron distribution was detected in one setting of the spectrometer thereby eliminating many systematic uncertainties. Deuterons from this reaction form a kinematic locus in momentum vs. lab scattering angle, shown in Fig. 31.

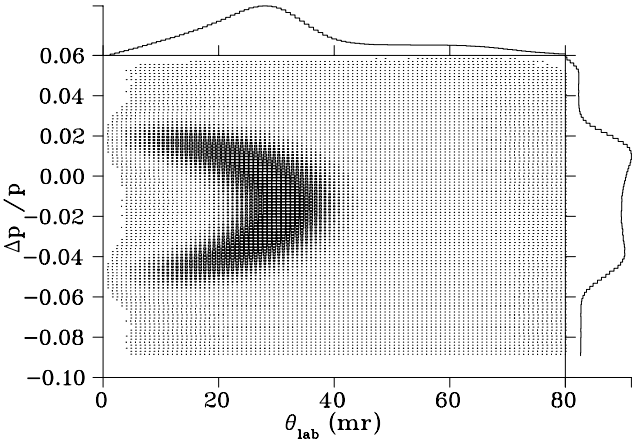

Fig. 31. Kinematic locus of all $np \rightarrow d\pi^0$ data.

Measurements of np elastic scattering with incident neutron beams that fill the same target space and produce protons that span the momentum distribution of the $np \rightarrow d\pi^0$ reaction provide a stringent test of the acceptance description of the spectrometer. With over seven million $np \rightarrow d\pi^0$ events and six million np elastic events the statistical uncertainty of this measurement is 8×10^{-4}. The systematic uncertainties add in quadrature to 5.5×10^{-4}.

Extraction of A_{fb}

The data have the accumulated effects of multiple scattering, energy loss, and other physical processes which make extracting A_{fb} directly from the locus impossible. As such, Monte Carlo techniques are used to extract the angle integrated A_{fb}. Close to threshold the $np \rightarrow d\pi^0$ cross section in the centre of mass frame is given by:

$$\frac{d\sigma}{d\Omega} = A_0 + A_1 P_1(\cos(\theta)) + A_2 P_2(\cos(\theta)) \,,$$

where P_i are Legendre polynomials, and θ is the centre of mass scattering angle [Hutcheon *et al.*, Nucl. Phys. **A535**, 618 (1991)]. The presence of charge symmetry breaking is reflected in the A_1 term as it is odd in terms of $\cos\theta$. The angle integrated form of A_{fb} is given by

$$A_{fb} = \frac{1}{2} A_1 / A_0 \,.$$

Due to the strong sensitivity of A_{fb} to the central momentum of the spectrometer (p_0), the LH_2 target thickness, and the average energy of the primary beam ($T_{\rm beam}$) the simulation spanned a four dimensional space defined by these three experimental parameters and A_1/A_0. This procedure required generating simulations at the nominal values, plus a canonical step, and minus a canonical step for each parameter. With a four dimensional parameter space needing to be covered, 81 (i.e. 3^4) independent simulations had to be generated. The comparison of data to these simulations produced a four dimensional χ^2 space and the values of the four parameters that gave a global minimum of that χ^2 space determined the value of A_1/A_0 and consequently A_{fb}.

Simulation

The simulation is based on GEANT and begins with a proton beam incident on a ^{7}Li target to reproduce the energy loss effects in that target. The model of the equipment is in agreement with the best known blueprints, "as-built" drawings, and recent measurements. The SASP dipole field used in the simulation is a map of that magnet at 875 A, scaled up to the running current of 905 A. Data were acquired in 19 different periods spanning two years and the simulation

"scheduled in" measured detector efficiencies, scintillator thresholds, and missing wires in a manner consistent with the actual running periods. Deuteron reaction losses, which account for 1–2% of all deuteron events, have a significant momentum dependence over the 8% momentum range of the experiment. These losses were parameterized from the world's data on deuteron elastic and reaction cross sections from hydrogen and carbon, and included in the simulation.

To reduce the possibility of psychological bias in matching simulation to data, a blind analysis technique was used which incorporated a "black box" subroutine into the simulation. This routine added a (hidden) offset to the A_1/A_0 asymmetry parameter used to set up the $np \to d\pi^0$ generator. After selecting the value for the offset, a member of the collaboration not involved in simulation development compiled the subroutine on all simulation computer clusters, mailed the source code to two people outside the collaboration, and deleted the source code.

Model of SASP acceptance

The acceptance of SASP is a complicated function of the position and angle at which the deuteron is produced and its momentum (X_i, θ_i, Y_i, ϕ_i, and δ). Describing this acceptance properly required an accurate model of the magnetic fields and interior surfaces of SASP because (1) deuterons can collide with interior surfaces of SASP and be lost from the locus and (2) the reconstructed momentum variable, which is a function of the focal plane variables X_f and θ_f, may be distorted in a momentum dependent way by an inaccurate model.

The np elastic scattering data provide the best means to determine the acceptance in that the incident beam of this reaction fills the target parameter space in a way that is similar to that of the $np \to d\pi^0$ reaction. The $np \to d\pi^0$ momentum space was spanned with np elastic scattering data taken with the SASP fields set to those used for the $np \to d\pi^0$ reaction and changing the energy of the primary proton beam so that the elastically scattered protons had momenta equal to -4, 0, and $+4$% of the central momentum of the deuterons of interest. To investigate momentum dependent effects, projections of θ_i and ϕ_i were made for slices in X_i and Y_i, respectively, and ratios of these distributions made for the –4% and +4% momentum sets. The basic features of these ratios are understood in terms of the focusing action of the SASP entrance quads, Q1 and Q2. These features appear in both data and GEANT but GEANT does not accurately represent the shoulder region where the acceptance in θ_i and ϕ_i begin to change. Consequently, we have determined cuts which exclude those portions of the acceptance that cannot be adequately modelled. These cuts are on target position and angle and define regions of uniform acceptance.

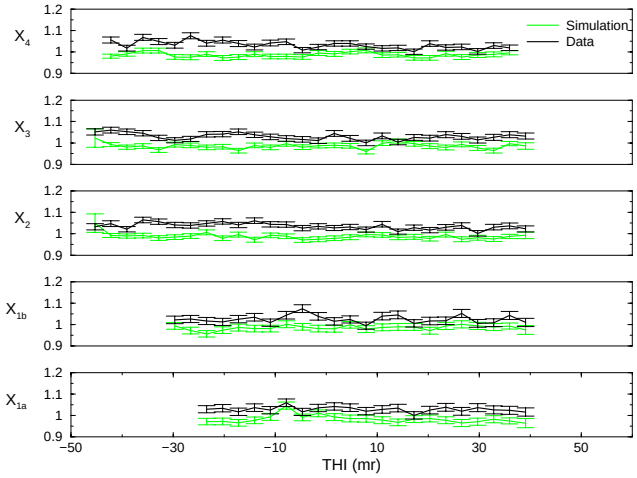

Fig. 32. Elastic np scattering ratio (–4%/+4%) vs. THI for five slices in X_i with final acceptance cuts applied.

Prior to August, position and angle acceptance cuts were only applied in the horizontal direction to avoid non-uniformities due to the dipole gap of SASP. Subsequent inspection of the (–4%/+4%) ratio in the vertical direction showed clear discontinuities and analogous cuts were determined for the vertical direction. Applying these acceptance cuts yields distributions of the (–4%/+4%) ratio that are essentially flat in θ_i and ϕ_i for all X_i and Y_i slices used; the magnitudes of the slopes of these distributions are all less than $5 \times (10)^{-4}$.

Verification of acceptance model

In a robust test of the uniformity of the acceptance, A_1/A_0 was extracted for various subsets of the target space and compared to the result for the full acceptance. Carrying out such a comparison for each data cycle was hampered by limited statistics so a group of cycles were analyzed together. Six of the ten data cycles have calibration data that allowed the relative target thickness for each cycle to be determined; these relative thicknesses were "scheduled" into the appropriate cycles of the simulation. This allowed the six "good LH_2 cycles" to be added together and treated as a single high statistics set in both data and simulation.

Figure 33 shows the value of [(A_1/A_0)+ black box offset] independently determined for the full acceptance and each of four acceptance subspaces for the six good LH_2 cycles. Note that while data in the bottom and top (left and right) subspaces are independent, they make up the data in the full acceptance. The values of [(A_1/A_0)+ black box offset] were determined both by analyzing the summed cycles (red squares) and by calculating the error weighted average of the individually analyzed cycles (black circles). These two methods give good agreement and the small differences

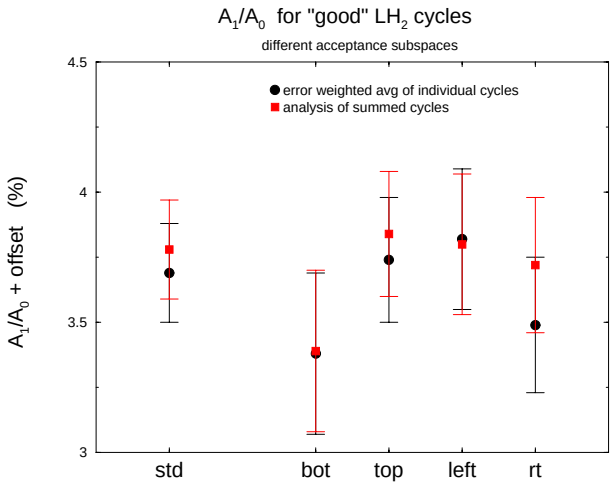

Fig. 33. A_1/A_0 for different acceptance subspaces.

in their results are thought to arise from effects that are not fully accounted for when data cycles are added together. The consistency of [(A_1/A_0)+ black box offset] for all acceptance subspaces suggested that the acceptance was well described in the simulation and the value of the black box offset was revealed.

Result and error budget

Simulation vs. simulation comparisons were carried out to determine how strongly experimental parameters are correlated with A_1/A_0. For each parameter this involved simulating kinematic locus scatter plots for a 3×3 grid of the experimental parameter vs. A_1/A_0, calculating the χ^2 of those 9 plots when compared to a plot simulated with nominal values, and fitting the χ^2 space. The correlation of A_1/A_0 with the experimental parameter was then obtained from the error matrix based on the curvature of the χ^2 space. Combining this correlation with the independently determined uncertainty of the parameter gives the systematic uncertainty of A_1/A_0 due to that experimental parameter.

Table I. Error budget.

	Uncertainty A_{fb} (10^{-4})
FEV threshold	2.5
FEC separation	2.5
Li target position	2.5
A_2/A_0	2
Deuteron losses	1.5
Efficiencies	1.5
$\sigma(T)$	1
Neutron angle	1
Background	1
FET threshold	0.5
Total systematics	5.5
Fit & statistics	8
Total uncertainty	10

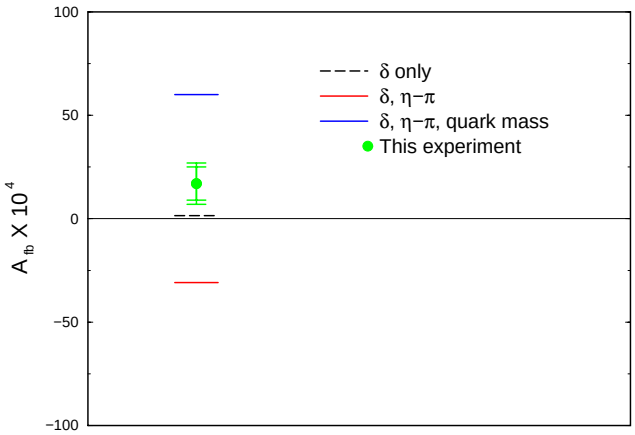

Fig. 34 A_{fb}, error weighted average of all ten cycles, standard acceptance. Incident $T_{\text{neutron}} = 279.5$ MeV.

The error weighted average of A_{fb} for all ten cycles with standard acceptance cuts applied is 17×10^{-4} and is shown in Fig. 34. This figure also shows the results of calculations done by van Kolck, Niskanen, and Miller which include contributions from the np mass difference effect on the OBEP (δ), the exchange of an isospin mixed $\eta - \pi$ meson, and the effect of the d u quark mass difference on π^0 nucleon scattering. A_{fb} can be expressed as

$$A_{fb} = -0.28\% \times \left[\frac{\langle \pi^0 | \mathcal{H} | \eta \rangle}{-0.0059 \text{GeV}^2} - \frac{0.87}{\text{MeV}} (\delta m_N - \frac{\bar{\delta} m_N}{2}) \right]$$

where the first term arises from the exchange of an isospin mixed $\eta - \pi$ meson and the second from π^0 scattering from the nucleon. The neutron proton mass difference can be expressed in terms of δm_N and $\bar{\delta} m_N$

$$m_n - m_p = \delta m_N + \bar{\delta} m_N = 1.3 \text{ MeV}$$

where δm_N is the ud quark mass difference and $\bar{\delta} m_N$ is the contribution due to electromagnetic effects.

Experiment 715
Weak interaction symmetries in β^+ decay of optically trapped ^{37,38m}K
(J.A. Behr, M. Pearson, TRIUMF; K.P. Jackson, TRIUMF/SFU)

TRIUMF neutral atom trap (TRINAT)

TRIUMF's neutral atom trap (TRINAT) captures radioactive atoms in a 1 mm-sized cloud using the pressure of laser light, with goals of precision standard model weak interaction tests in both the charged and neutral current sectors. To date, the trap techniques have shown great promise to provide greater precision in two broad types of experiments in nuclear β decay. The low-energy recoiling nuclei produced in the decays freely escape the trap, and by measuring their

momenta in coincidence with the β, the ν momentum can be deduced more directly than in previous experiments. In addition, the nuclei can be highly polarized by atomic techniques, and their polarization measured atomically independent of their decays. We have pioneered the β-recoil coincidence techniques at TRIUMF/ISAC, and are learning to polarize the nuclei to realize unique spin-correlation experiments.

Progess in ^{36}K trapping is updated in the Expt. 925 report.

Technical progress

Production

The $CaZrO_3$ production target has recently been replaced with a TiC target which can withstand 40 μA of 500 MeV proton beam, producing ^{37}K yields of 6×10^7/sec, a 6-fold increase.

Laser development

Laser development has been ongoing on two fronts within the TRINAT collaboration.

Firstly, in order to enhance the current trapping efficiencies, a second, basic titanium sapphire ring laser has been purchased. This ring is currently being pumped by an existing argon ion laser returned from long term loan to Expt. 497. Currently this new ring is capable of producing in excess of 2 W of single frequency, narrow linewidth laser power. Work is currently ongoing in order to frequency stabilize and control this laser. It will increase collection efficiency in the capture MOT by a factor of three.

With a view to producing a purely optical dipole force trap (see below), an existing standing wave titanium sapphire laser has been converted into a single mode ring laser. This has reduced its linewidth from a factory specification of 40 GHz to an unstabilised linewidth of less than 40 MHz. This transformation has ensured a narrow, low divergence, gaussian output that is required in order to produce a tight, diffraction limited focus to create the trap. In order to successfully load this trap using circularly polarized light (required for 100% polarization) the laser frequency has to be shifted by approximately 2 nm on a rapid ($\sim$1 μs) time-scale. A scheme for a reliable, controllable, method of operation has been devised using an electro-optic modulator to make controllable changes in the birefringence within the laser cavity. Arrangements have been made to borrow equipment for initial tests in order to ascertain the feasibility as well as the final design requirements.

Beta-neutrino correlations

The weak interaction is mediated by vector bosons with spin one. By measuring the β-ν angular distribution in the decay of ^{38m}K, which is one of the pure Fermi $I^\pi = 0^+ \rightarrow 0^+$ decays, we can test whether bosons with spin zero produce a scalar interaction contributing to β decay. The best present β-ν experiment is the Seattle/Notre Dame/ISOLDE collaboration's β-delayed proton decay of ^{32}Ar, with published result $a = 0.9989 \pm 0.0052 \pm 0.0039$.

We have taken data with statistical error in the β^+-ν correlation coefficient a of $\sigma_a \approx 0.33\%$. We are presently evaluating systematic errors, which will limit us to total σ_a between 0.5% and 0.7%. This accuracy will let us constrain the mass/coupling ratio of non-standard model spin-0 bosons as great as 4 times the mass of the spin-1 W boson. We analyze data taken in October, 2000 in two ways: 1) fitting the experimental time-of-flight spectra of the recoils as a function of β energy; 2) reconstructing the β-ν angle from the position and energy information in both detectors. With help from our new collaborator F. Glück, we have included radiative corrections in our full Monte Carlo simulations. These are dominated by the momentum perturbations caused by real bremsstrahlung photons. The perturbation of the recoil TOF spectra turns out to be small in our experiment, but the perturbation on the β^+ singles spectrum from which our energy calibration comes is larger and still being evaluated. We have published the main method in a conference proceedings [Gorelov *et al.*, Hyp. Int. **127**, 373 (2000)] and expect to publish a result soon.

By reconstructing the ν momentum, we have completed and published a missing mass search for heavy ν's with masses 0.7 to 3.7 MeV mixing with the electron ν, [Trinczek *et al.*, Phys. Rev. Lett., in press]. Although recent results exclude a sterile ν_x as an explanation for the atmospheric and solar neutrino anomalies, the small admixture limits for heavy masses explored by TRINAT are still allowed. The length of the ν pulse from SN1987A also allows ν_e to have relatively large admixtures with a ν_x with mass a few MeV, so experiment must constrain these.

Our kinematic coincidences reduce the 3-body kinematics to 2-body, allowing a search for peaks in a TOF spectrum instead of the more conventional search for kinks in continuous β spectra. Figure 35 shows the reconstructed zero-mass peak and a simulation of an admixture with a massive ν for a particular data cut, and the results. The admixture upper limits are as small as 4×10^{-3}, and are the most stringent for ν's (as opposed to $\bar{\nu}$'s) in this mass range, although there are stronger indirect limits from other experiments. This constitutes the first real physics measurement in β decay from neutral atom traps.

Polarized measurements

The weak exchange bosons also couple only to left-handed (negative helicity) ν's, and in that sense parity – mirror symmetry – is said to be fully violated.

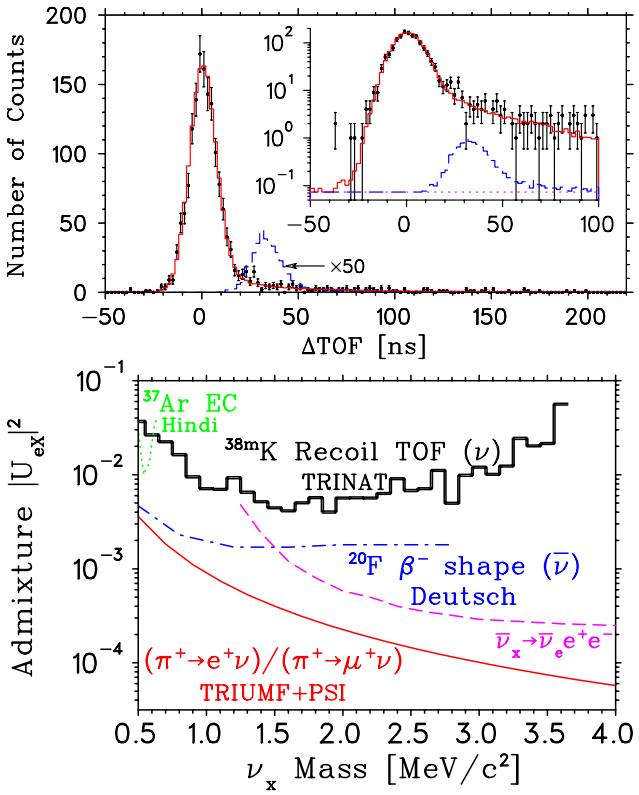

Fig. 35. Top: Kinematic reconstruction of events for $T_\beta = 1.7 - 1.9$ MeV bin, and simulation including a 1 MeV ν_x. Bottom: Present 90% CL upper limits, and those of other experiments.

By measuring β-ν angular distributions from the decay of polarized ^{37}K, we can search for production of right-handed ν's. Since β-decay is semileptonic, these experiments are complementary to the purely leptonic TWIST experiment. Measurements of the β asymmetry A_β and neutrino asymmetry B_ν in ^{37}K to accuracy 10^{-2} compete with the world average of neutron β decay, and experiments to $\leq 10^{-3}$ accuracy are necessary to be complementary to TWIST or collider searches for higher-mass extra W's. We also plan a search for non-standard model time-reversal violation in ^{37}K, flipping the nuclear spin to simulate the reversal of time in a correlation involving the nuclear spin and the β and ν momenta.

We have begun spin-correlation measurements in the mixed Fermi/Gamow-Teller decay of ^{37}K. We have achieved polarization precision 0.001 in trapped stable ^{41}K atoms, which has almost identical hyperfine splitting to ^{37}K. We are in the process of calibrating the absolute accuracy and applying the techniques to β-decaying ^{37}K.

We have implemented optical pumping in a geometry with back-to-back β^+ detectors along the optical pumping axis (Fig. 36). We use high-reflectivity dielectric mirrors on 0.1 mm thick fused silica substrates, to minimize energy loss and angle straggling. The circular polarization distortion from the 11° mirror is cancelled by a mirror with the same coating outside the vacuum rotated by the same angle in the other plane. The β^+ detectors are plastic/CaF_2(Eu) phoswiches designed to contain the 10 MeV β^+'s from ^{36}K. The electrostatic field electrodes are made from glassy carbon to minimize eddy currents when the trap B field is switched on and off.

Figure 36 also shows data from our recent ^{37}K run using this geometry. MCP position asymmetries are shown for the nuclear recoils in coincidence with β^+'s at 90° to the polarization axis (not shown in the figure). Assuming the standard model, the X asymmetry implies that $(107 \pm 5)\%$ nuclear vector polarization was achieved. The atomic probe also indicated over 95% polarization. When the polarization is known better, the ν asymmetry B_ν can be determined from this observable – the β^+ is detected at ≈90°, so that the recoil momentum is directly opposite the ν momentum. Preliminary results are in press in a refereed conference proceedings [Melconian *et al.*, EMIS14, Nucl. Instrum. Methods B, in press]. We have extracted polarization information from nuclear recoil singles in the past tests and will attempt to do this here as well. B_ν could be determined with $\sigma_{\rm stat} \approx 0.001$ in 1 month at demonstrated rates in this geometry.

We learned that β singles measurements in this geometry are difficult. See Expt. 925 report for details.

We will simultaneously search for time-reversal violation in the triple product of vectors involving the nuclear spin, the term D $\vec{J}_N \cdot (\vec{p}_\beta \times \vec{p}_\nu)$. We will look for distortions of the position spectrum along the axis perpendicular to the polarization when the spin is flipped, rather than looking at rate changes as in previous experiments. Unwanted polarization along this axis will be tested by recoil singles asymmetries. The location of the cloud is determined in 3D by photoionization using a small 355 nm frequency tripled diode-pumped Nd::YAG laser, and we have shown this method works for the radioactive ^{37}K (see below). Constraints on the β^+ detector position and orientation will come from measurements of the β^+ asymmetry in the silicon strip detector ΔE.

Polarization probe and calibration

Our most important recent advance is the demonstration that we can make measurements of the polarization of the same nuclei that are decaying by using atomic techniques *in situ* on ^{37}K. The atoms stop absorbing optical pumping light after they are fully polarized, and we monitor the vanishing atomic excitation with two-step photoionization. The knowledge of polarization is a limiting systematic in many experiments in this field, including those in neutron β-decay and μ decay.

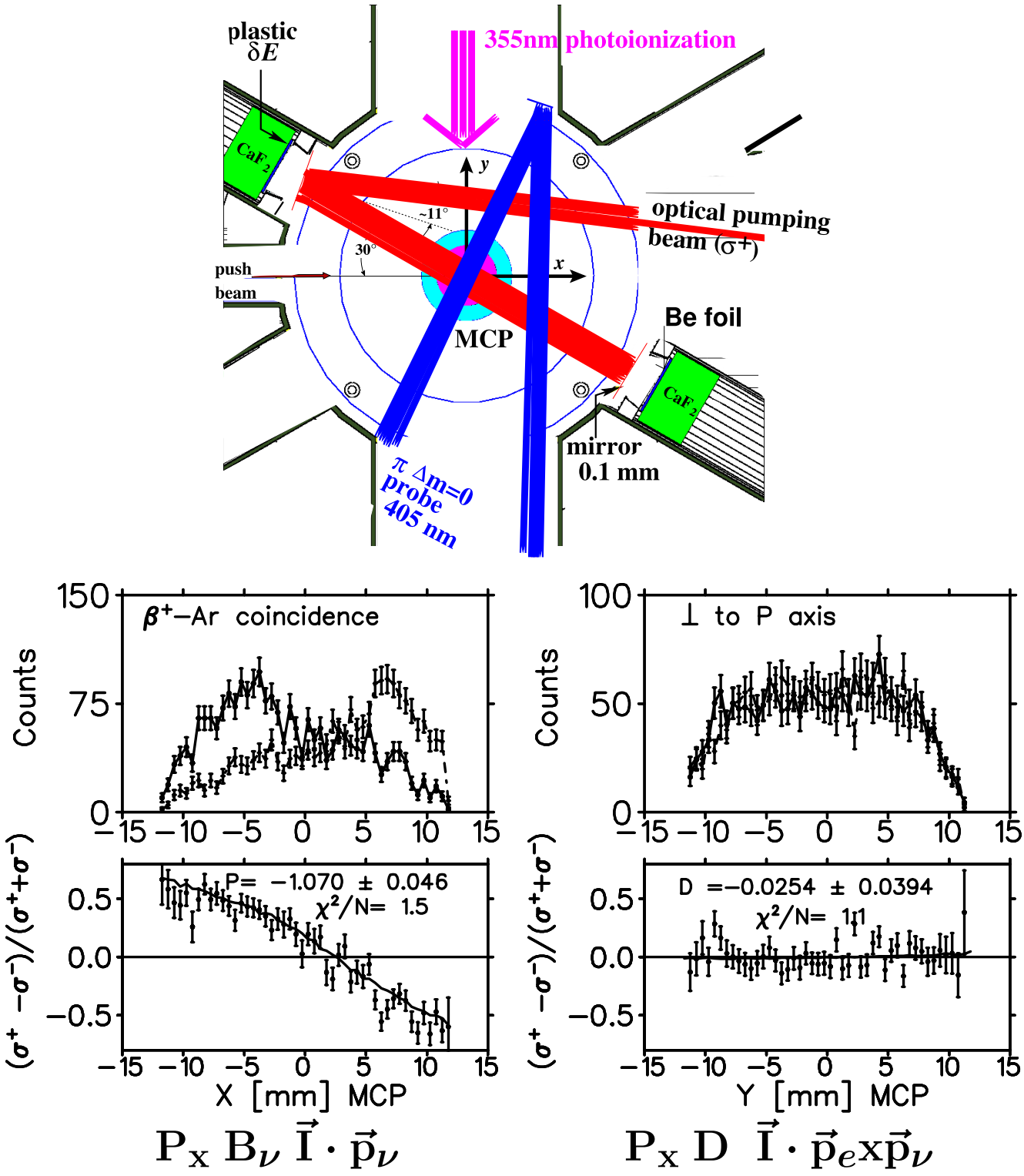

Fig. 36. Top: 2D side view of additional detectors and optical pumping light for polarized geometry, showing the 0.1 mm-thick mirrors, plastic/CaF_2(Eu) phoswiches, copper tungsten collimators, and 405 nm probe beam. Bottom: Asymmetry in MCP position for β^+-Ar coincidences for 1 day of data, with optical pumping polarization axis in X-direction. The X-asymmetry is dominated by B_ν; the standard model was assumed in this test to "measure" the polarization. The Y-asymmetry would be from a time-reversal violating D term (residual polarization will be tested by recoil singles asymmetries, not shown).

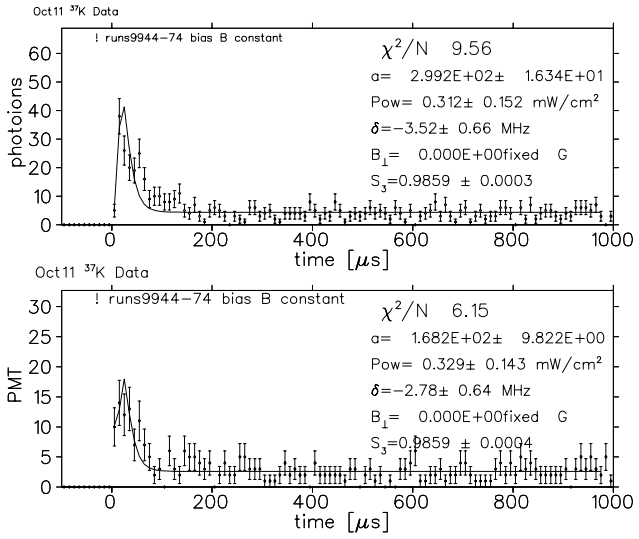

Fig. 37. Vanishing of fluorescence for ^{37}K atoms whose nuclear decays are shown in Fig. 36, showing P> 95%, for both signs of polarization.

We show in Fig. 37 the fluorescence spectrum determined by photoionization with the 355 nm laser for ^{37}K, showing the vector polarization P is greater than 95%. About half the size of the tail is from β^+ decay "backgrounds" that must still be subtracted.

The most direct way to probe the sub-level population is to Zeeman-split the sub-levels with a B field and use resonant fluorescence. Resolution is limited by the natural linewidth Γ of the excited states, which is 6 MHz for the $4P_{1/2,3/2}$ first excited states used for trapping and optical pumping. The $4P$ hyperfine splitting is very small in ^{41}K and ^{37}K, so B fields large enough to resolve the sub-levels will hurt the optical pumping process by decoupling the nuclear and atomic spin.

Instead, we use the second excited $5P_{1/2}$ state, where Γ=1.1 MHz. Diode lasers at 404 nm have recently become commercially available. We have not achieved routine operation, but a first scan over the ^{41}K Zeeman substructure measured polarization of 90%, in good agreement with the vanishing of fluorescence measured at the same time. When this method becomes more reliable, we will be able to absolutely calibrate the fluorescence vanishing in a model-independent way.

CFORT: A trap with perfect polarization

The future of these experiments lies in a remarkable dipole force trap using circularly polarized light developed at JILA. This will trap atoms in one magnetic substate only, with no known systematics to spoil the polarization; the resulting nuclear polarization should be better than 99.99%. 1 W of circularly polarized σ^+ light is focused to a diffraction-limited spot, with frequency between the D1 and D2 resonances. With light detuned just blue of the D1 resonance, repulsive dipole forces ("optical tweezers") expel all the spin sub-levels except M_F=F, whose coupling to the D1 vanishes for σ^+ light. The light is to the red of the D2 resonance, which produces a weaker attractive force that traps the M_F=F state only. This state (and this state only) is then trapped by the attractive force produced because the same light is red-detuned from the D2 resonance. This trap is unique to neutral atoms, and it would let us compete with the new generation of neutron β-decay experiments coming on line.

If the circular polarization of the light is imperfect, the trap becomes shallower but still only traps the one sub-level. The quantization axis will be determined by the laser light direction. (For gaussian beams the wavefronts are parallel at the focus, so even the small angle of the light focus does not spoil the polarization!) We have diverted 10 W of power from an existing Ar^+ laser to pump a ring laser constructed by us from a used standing-wave cavity. This trap will be the M.Sc. thesis for Erika Prime at UBC.

The potential of this technology is enormous, but this trap is extremely difficult to load. It took JILA approximately two years to load it for Rb atoms. Some of the atomic physics complications will be different for K atoms, and it is difficult to foresee when it will be ready. We will develop this in parallel with on-line experiments using the present optical pumping methods.

Expt. 956: search for tensor interactions in recoil nucleus singles in decay of polarized ^{80}Rb

The EEC has approved this experiment with medium priority. The recoiling nuclei in singles have spin asymmetry $A_{\rm recoil}$= A_β+B_ν, which vanishes for pure Gamow-Teller decays. Right-handed current effects also cancel. $A_{\rm recoil}$ is sensitive to fundamental tensor interactions, on which the best limits are from ^{6}He β-ν correlations. $A_{\rm recoil}$ measurements with error 1% accuracy would be competitive and, given the vanishing observable, it is foreseeable to do much better. We have made optical pumping tests in ^{80}Rb, and we can adapt methods developed in ^{37}K (for example using MCP pulse heights to distinguish ions from backgrounds) to ^{80}Rb. A heavy Gamow-Teller decay like ^{80}Rb will be ultimately limited by nuclear-structure dependent recoil order corrections. ^{8}Li is a case where nuclear structure-dependent corrections are better understood.

Fr atomic spectroscopy

Including Stony Brook collaborators, we (M. Pearson *et al.*) have submitted a LOI for hyperfine anomaly measurements in Fr isotopes. Comparison of precision hyperfine splitting measurements in $7S_{1/2}$ and $7P_{1/2}$ states is more sensitive to higher-order moments of the nuclear magnetism distribution than the magnetic

dipole. This is because the two atomic states have different overlap with the nucleus. The result is a probe of the spatial distribution of nuclear magnetism. Since the proton distribution is given by the charge radius to this order, it can be calculated, allowing the spatial distribution of the valence neutron to be deduced in odd-odd Fr isotopes. Among the physics interests are proton-rich isotopes with spin isomers, where differences in the spatial neutron distribution would come from higher-order interactions between the valence neutron and the core. The LOI was favourably received and it is hoped these measurements will begin when an actinide target is available.

Experiment 778
Pion proton cross sections in the Coulomb-nuclear interference region
(H. Denz, R. Meier, Tübingen)

Several quantities of fundamental importance to the strong interaction can be extracted from πp observables. Examples include the πNN coupling constant, the sigma-term of the proton and a measure of isospin breaking.

Presently, there is no agreement on the values of these quantities. For example, recent extractions of the pion nucleon sigma-term from elastic pion-proton scattering vary by up to a factor of 2, including results which imply a strangeness content of the nucleon of up to 25% in contrast with extractions of the sigma-term from baryon masses.

These discrepancies are at least partly due to the status of the πp data base, in particular at low energies. There are regions where information is still missing, and there are regions where the available experimental data are contradictory. New measurements of πp observables at low energies are aimed at providing additional information and resolving the discrepancies. The goal of Expt. 778 is to determine differential cross sections of pion proton elastic scattering at low energies, in particular at small scattering angles in the so-called Coulomb-nuclear interference (CNI) region.

This experiment received beam time in 1998, 1999, and 2000. The data were taken using the CHAOS detector. A planar liquid hydrogen target was used. For each event, the incoming particle and the outgoing reaction products were detected. At large scattering angles, both the elastically scattered pion as well as the backscattered proton were tracked. At forward scattering angles the protons had too low energy to leave the target, therefore only the outgoing pion track was seen. For normalization purposes, elastic scattering of muons was measured simultaneously using muons originating from a point close to the production target which could be separated from pions by the time of flight through the secondary beam line. A major difficulty for measurements in the Coulomb-nuclear interference region at low scattering angles was overwhelming muon background from pion decay close to the hydrogen target. These decay muons could only partly be separated from scattered pions by kinematical constraints. Therefore a muon-pion identification detector was built for this experiment and included in the CHAOS data acquisition.

Data were taken for $\pi^{\pm}p$ differential cross sections at 8 energies between 15 and 67 MeV, in an angular range from 8° to 180°.

The analysis efforts are ongoing. The raw data (4.7 TB) have been reduced by a factor of 10 by removing obvious decay events in a first analysis stage. Now enough disk space is available to keep all remaining information on disk and simultaneous analysis of the full data set at several energies is possible. This greatly facilitates the study of systematic effects. In the GEANT simulation for the experiment, further details have been incorporated, e.g. structural elements of the 4th wire chamber which are thick enough to affect pions at very low energies, thus modifying the acceptance of the detector.

In the forward angle region, the decay background poses a challenging problem. Most of it can be removed by applying the neural net for pion-muon identification, but the problem of background subtraction is not yet fully solved for a few angular bins. Preliminary results from the analysis of the larger angle data show good agreement of the shape of angular distributions with current phase shift analyses at the higher measured energies, but deviate at very backward angles and low energies. The currently applied absolute normalization, based on acceptances determined in Monte Carlo simulations, leads to reasonable agreement with phase shift analyses and previous experiments (where data exist), but the normalization uncertainty is still large. This uncertainty will be reduced by matching the angular distribution at larger angles with the forward angle data and the μp scattering which was measured simultaneously.

We expect to have final results for a subset of the data in 2003.

Experiment 781
Investigations of the $\pi\pi$ invariant mass distributions of nuclear $(\pi, \pi\pi)$ reactions with CHAOS
(N. Grion, INFN Trieste; M. Sevior Melbourne)

In earlier CHAOS experiments investigating nuclear pion induced pion production, data were collected at a single energy (280 MeV) for a variety of nuclei. Of particular interest we note that typical differential dis-

tributions such as the cross section as a function of the dipion invariant mass, $M^2_{\pi\pi}$, were reasonably well described by phase space for the isospin 2 reactions $(\pi^+,\pi^+\pi^+)$ on several nuclei. However, the same distribution for the isospin 0 reactions $(\pi^+,\pi^+\pi^-)$ on the same nuclei were not well described by phase space. In particular the process leads to strength in the low end of the $M^2_{\pi\pi}$ distribution for the reaction on nuclei relative to that on the nucleon. These results have generated considerable excitement because they are consistent with a modification of the $(\pi\pi)$ interaction due to nuclear matter when the interaction occurs in the $I = J = 0$-channel, which is conventionally called the σ-channel. This behaviour might be explained by the partial restoration of the chiral symmetry in nuclear matter, which was observed to occur at nuclear densities below the saturation density. Similar results were subsequently found in the crystal ball studies of the reaction $(\pi^-,\pi^0\pi^0)$ on several nuclei at the AGS [experiment: Starostin *et al.*, Phys. Rev. Lett. **85**, 5539 (2000); discussion: Camerini *et al.*, Phys. Rev. **C64**, 067601 (2001)], and in studies of photo pion production at MAMI by the TAPS collaboration [Metag *et al.*, nucl-ex/0205009 (2001)]. Although the coupling of the pions to particle hole and delta hole configurations may also play a role, its effect is much smaller.

In this experiment additional data were collected for the pion induced pion production reactions on ^{45}Sc at a variety of incident energies between 240 MeV and 320 MeV. Data were analyzed in Trieste using the same algorithm as in the earlier work.

The data were obtained in M11 using a solid slab of ^{45}Sc. Incident beam was detected with in-beam counters and observed in the two inner wire chambers. Particle identification is achieved with the CHAOS fast trigger array, which is composed of 20 segments, each with two layers of thin plastic scintillation counters (the second of which is segmented) and 3 lead glass Čerenkov detectors. CFT segments were removed for the incident and exit beam. Particle identification is generally achieved through the CFT detector pulse heights and the track momentum. Of particular importance is the separation of pions from electrons and positrons which is achieved to better than 95% per track using the lead glass Čerenkov detectors. The rate of misidentified electron-positron pairs is further reduced to about 0.1% by an opening angle cut at 3°.

Events of interest are binned in the angle and energy of both of the pions detected. All quantities, such as the $M^2_{\pi\pi}$ discussed above, the missing energy, and the opening angle between the pions, are then determined. The CHAOS geometry has a large acceptance near the horizontal plane, but no coverage beyond seven degrees out of the plane. In this work the in-plane acceptance has been determined with a Monte Carlo simulation, however, any out of plane correction necessarily has a model dependence. Fortunately, comparisons with theoretical predictions can be made within the CHAOS acceptance to avoid the impact of a model dependence. It is also possible to consider ratios of the various quantities between the reaction on nuclei and the reaction on ^{2}H, as a second approach to avoid the impact of any model dependence in forming the conclusions.

In order to determine a total cross section a correction reflecting the in-plane acceptance must, however, be applied. One choice would be to impose a phase space expectation as a model for out of plane extrapolation. In this work a different out of plane correction was determined. This correction factor is based simply on an interpolation between the dipion opening angles near 0° and near 180°. Clearly this choice preserves the shape of the in-plane distribution, which is dominated by the CHAOS acceptance.

As shown in Fig. 38, the shape and magnitude of the dipion invariant mass distributions for the pion production on ^{45}Sc in this work confirm earlier results on, for example, calcium [Bonutti *et al.*, Nucl. Phys. **A677**, 213 (2000)]. The phase space for the ^{45}Sc reactions is represented by the shaded regions in each part of the figure, and the curves are theoretical results of Vincente-Vacas *et al.* [Phys. Rev. **C60**, 064621 (1999)], determined within the CHAOS acceptance. One can readily see that the shape of the $M^2_{\pi\pi}$ near threshold for the reaction $(\pi^+,\pi^+\pi^+)$ on nuclei is essentially the same as that for the ^{2}H$(\pi^+,\pi^+\pi^+)$ reaction, whereas the shape changes dramatically for the reaction $(\pi^+,\pi^+\pi^-)$ on nuclei compared to that for the ^{2}H$(\pi^+,\pi^+\pi^-)$ reaction. This trend was reproduced throughout the energy range studied. An

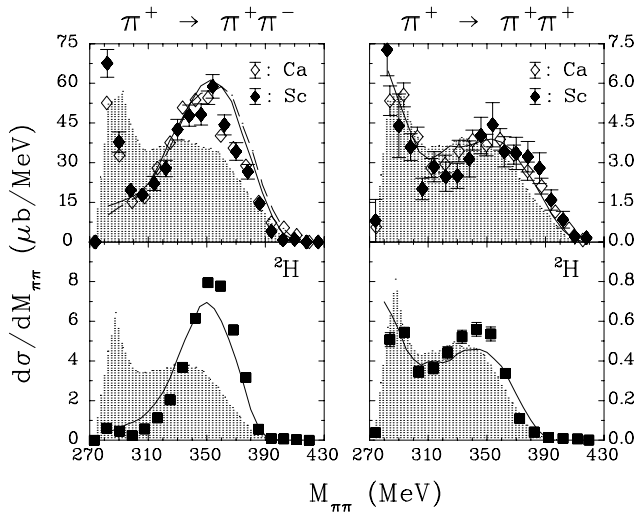

Fig. 38. Invariant mass distributions (see text for details).

interpretation of this trend is that the dynamical traits of the I=2, J=0 interaction are understood on nuclei as on the nucleon, whereas the I=0, J=0 interaction is specifically different in nuclei than on the nucleon.

Experiment 823
Pure Fermi decay in medium mass nuclei
(G.C. Ball, TRIUMF)

Precise measurements of the intensities for superallowed Fermi $0^+ \rightarrow 0^+$ β-decays have provided a demanding test of the CVC hypothesis at the level of 3 $\times$ 10^{-4} and also led to a result in disagreement with unitarity (at the 98% confidence level) for the CKM matrix. Since this would have profound implications for the minimal standard model, it is essential to address possible "trivial" explanations for this apparent non-unitarity, such as uncertainties in the theoretical isospin symmetry-breaking correction. Uncertainties in the calculated Coulomb corrections can be studied by extending the precision β-decay measurements to heavier ($A \geq 62$, $T_z = 0$) odd-odd nuclei where these corrections are predicted to be much larger [Towner and Hardy, Phys. Rev. **C66**, 035501 (2002)]. The primary goal of the Expt. 823 experimental program is to measure the half-lives and branching ratios for the superallowed β-decay of these radioactive nuclei produced at ISAC. The early measurements have focused on ^{74}Rb (see 1999–2001 Annual Reports).

High-precision β-decay branching-ratio measurements for ^{74}Rb

The goal of this experiment was to determine the branching ratio of the superallowed $0^+ \rightarrow 0^+$ transition from ^{74}Rb to the ground state of ^{74}Kr. However, the ground-state branch cannot be measured directly, but is determined by subtracting the (non-superallowed) feeding to excited levels from the total intensity of the decay. However, since the Q_{EC}-values are large ($\sim$10 MeV) for the heavier $T_Z = 0$ nuclei, there are a large number of excited 1^+ states in the daughter nucleus predicted to be populated through GT transitions [Hardy and Towner, Phys. Rev. Lett. **88**, 211801-1 (2002)]. These transitions, together with non-analogue Fermi (F) branches must be taken into account to determine the partial half-life of the superallowed transition. Yet their individual intensities are very small and many of them cannot be detected with high resolution gamma spectroscopy. In the present experiment we have shown that this problem can be overcome with the help of theory. It is not necessary to reconstruct the GT strength function of the ^{74}Rb decay, only the total amount of non-superallowed feeding must be determined. The low-lying levels in ^{74}Kr act as collector states for a large fraction of the non-superallowed feeding and by observing their de-excitation, the larger part of their feeding can be determined. The remaining component, which directly feeds the ^{74}Kr ground state can be estimated from shell-model calculations [Towner and Hardy, *op. cit.*] provided they reproduce well the relative feeding to excited levels in ^{74}Kr.

The experiment was carried out at ISAC in May, 2001. In this measurement the ^{74}Rb atoms were implanted into a $\frac{1}{2}$ in. wide conducting collector tape which was viewed by two LN-cooled Si(Li) diodes for the detection of conversion electrons, two large plastic scintillation counters (one thin ΔE and one thick E counter) to detect positrons and an ($\sim$80%) HPGe detector for γ-rays. A more complete description of the experiment together with preliminary results was reported previously in the TRIUMF 2001 Annual Report. Analysis of the data has now been completed. Table II summarizes the experimental feeding of the lowest six 0^+ and 2^+ levels in ^{74}Kr resulting either from the γ-decay of states above the third 2^+ level at 1742 keV (following GT or F decay) or from direct F decay to the lowest two excited 0^+ levels. The sum of the six feedings is equal to the sought branching ratio, namely the sum of all branches other than the superallowed branch in the β-decay of ^{74}Rb. This experimental sum shown at the bottom of the second column amounts to 0.336(20)%; however, this sum is incomplete since much of the γ-ray feeding of the ground state from states above 1742 keV likely remains unobserved in this experiment. Also shown in Table II are the predictions of recent shell model calculations [Towner and Hardy, *op. cit.*]. In these calculations, two quantities affect the total GT strength, namely the effective axial-vector coupling constant g_A and the excitation energies of the predicted 1^+ states in ^{74}Kr. In the published calculations g_A was set to 1.0 (a typical quenched value for shell model calculations in complete 0 hbar ω oscillator model spaces) and the lowest 1^+ state was at 3.2 MeV excitation energy. The results of this calculation appear in the fourth column of Table II, where it can be seen that they give relative feeding intensities in reasonable agreement with experiment but absolute values that are too large by a factor of two.

The purpose of the shell model calculations is to provide an estimate of the missing strength not seen in the experiment. To this end we have adjusted the calculation to reproduce the intensity of the strongest γ-ray transition seen, the $2_1{}^+ \rightarrow 0_1{}^+$ 456 keV transition. Since the model space is not that of a complete 0 hbar ω oscillator space, it is not clear what an appropriate quenched value of g_A should be: we now choose to use $g_A = 0.8$. Further, we raise the spectrum of 1^+ states relative to the 0^+ and 2^+ states such that the lowest 1^+ state occurs at 3.6 MeV. Again there is very little experimental data to guide us here. The

Table II. γ-ray and direct non-superallowed beta feeding to the 6 lowest states in ^{74}Kr, expressed per ^{74}Rb beta decay.

Level	Exp.	Theory			
	GT +F [$\times 10^5$]	GT[a] + F [$\times 10^5$]	GT[b] + F [$\times 10^5$]	GT[a] [%]	GT[b] [%]
gs, 0_1^+	12(2)	103	259	26.4	28.2
456, 2_1^+	142(18)	145	324	37.3	35.2
509, 0_2^+	39(11)	60+36	158+36	15.3	17.2
1204, 2_2^+	53(14)	41	87	10.6	9.4
1654, (0_3^+)	52(5)	20+23	46+23	5.0	5.0
1742, (2_3^+)	38(6)	21	46	5.4	5.0
Sum	336(20)	449	979	100	100

[a] lowest 1^+ level at 3.6 MeV, $g_A = 0.8$
[b] lowest 1^+ level at 3.2 MeV, $g_A = 1.0$

feeding intensities predicted by the adjusted shell model calculation, which are also shown in Table II, are in reasonable agreement with experiment. Notice that between the two calculations there is little difference in the relative feedings; the adjustments principally altered the absolute intensity. From the first row of Table II we estimate that the missing strength feeding the ground state is 0.10%. To place an error on this estimate we take the spread of the two calculations to give an upper error, while arguing that the missing strength is unlikely to be less than half our estimate to get the lower error. This results in a missing strength of 0.15(10)% with symmetrized errors. This missing strength is now added to the observed strength to get the summed branching ratio for all non-superallowed beta decays of 0.336(20) + 0.15(10) = 0.5(1) %.

The Q_{EC} value for the β-decay of ^{74}Rb can be predicted using the previously measured half-life [Ball *et al.*, Phys. Rev. Lett. **86**, 1454 (2001)], the present branching ratio, the average Ft value measured for the nine well-known superallowed emitters together with the theoretical corrections from Towner and Hardy [*op. cit.*]. The result, 10405(9) keV, is in agreement with the measured value of 10425(18) keV [Herfurth *et al.*, Eur. Phys. J. **A15**, 17 (2001)]. It is important to note that the error in the predicted Q_{EC} value is dominated by the theoretical uncertainty in the nuclear-structure dependent correction δ_C - δ_{NS} = 1.50(40)%.

The present experiment also provides a test for part of the analogue-symmetry breaking correction, δ_C, by observing limits on the strength of the Fermi transition to excited non-analogue 0^+ states (see below). For the ^{74}Rb decay, 80% of the non-analogue Fermi strength is predicted to be shared by the two lowest excited 0^+ levels. The predicted branches to the 0_2^+ and 0_3^+ levels are 36 $\times$ 10^{-5} and 23 $\times$ 10^{-5}, respectively, in agreement with the experimental upper limits of 50 $\times$ 10^{-5} and 57 $\times$ 10^{-5} (see Table II).

These results show that the precise determination of the superallowed branching ratio in the presence of non-negligible, strongly-fragmented GT branches is achievable and suggests improved results can be obtained by using refined experimental techniques. Such measurements using the reconfigured 8π spectrometer are planned [Svensson *et al.*, TRIUMF Expt. 909]. Finally, a paper describing these results has been submitted to Phys. Rev. C.

Measurement of the non-analogue $0^+ \rightarrow 0^+$ transition in ^{38m}K

The determination of the transition strengths for non-analogue $0^+ \rightarrow 0^+$ decays provides a critical test of the model predictions for superallowed β-decays. In particular, they provide a direct measurement of the isospin-mixing component of the Coulomb correction. Branching ratios for Fermi transitions to non-analogue states have been measured previously [Hagberg *et al.*, Phys. Rev. Lett. **73**, 396 (1994)] for ^{46}V and ^{54}Co. In this experiment it was only possible to set a limit for the non-analogue transition in ^{38m}K of <19 ppm corresponding to an isospin mixing correction of <0.28%. Recently, Towner and Hardy [*op. cit.*] have recalculated the nucleus-dependent corrections for the nine well-known superallowed β emitters for several shell model effective interactions. The values for ^{38m}K range from 0.062 to 0.186%.

An experiment designed to measure this weak decay branch was carried out in October. The measurement used the same basic method developed previously [Hagberg *et al.*, Nucl. Phys. **A571**, 555 (1994)] and modified as described in the 2000 Annual Report for the ^{74}Rb branching ratio measurements. The fast tape transport system was used to collect and move the ^{38m}K samples out of the vacuum chamber and position them between two thin plastic scintillator paddles each backed by a HPGe detector. However, the

large HPGe detectors used previously were replaced by two Compton suppressed (∼25%) HPGe detectors from the 8π spectrometer. As a result, the sensitivity for detecting the 1209 keV γ-ray following the β-decay of ^{38m}K($t_{1/2}$ = 0.925s) to the first excited $0_2{}^+$ state in ^{38}Ar at 3377 keV was greatly enhanced by the reduction in the background coming from the decay of the long-lived isobaric contaminant $^{38}K_{gs}$($t_{1/2}$ = 7.64 min) which emits a 2168 keV γ-ray with a branching ratio of 99.8%. The $^{38}K_{gs}$ contaminant was minimized by collecting the ^{38m}K samples for only 0.3 s. Unfortunately with the ISAC TiC target used to produce the ^{38m}K beam, the yield of the short-lived ^{38m}K isomer relative to the long-lived $^{38}K_{gs}$ was found to be substantially reduced (by a factor of ∼5) compared with that obtained using a $CaZrO_3$ target. As a consequence, the ratio of the $^{38m}K/^{38}K_{gs}$ initial activities was only ∼4:1. Under these conditions the background (during the initial 0.5 s counting period) coming from the decay of the long-lived $^{38}K_{gs}$ contaminant in the vicinity of 1209 keV is estimated to be approximately a factor of ten higher than the present upper limit for the non-analogue 0^+ decay branch for ^{38m}K. Approximately 2 × 10^{10} ^{38m}K β-decays were observed. Analysis of the data is in progress. These data should be sufficient to confirm the present upper limit of <19 ppm. However, we plan to repeat the measurement with a $CaZr0_3$ production target and the full 8π spectrometer.

Experiment 824
Measurement of the astrophysical rate of the ^{21}Na$(p,\gamma)^{22}$Mg reaction
(J.M. D'Auria, SFU)

Experiment 824 has essentially completed the data-taking phase using the new DRAGON facility in 2002 and several papers have been submitted for publication on the facility and some results of the experiment. The objective of this experiment is to measure for the first time the rate of the ^{21}Na$(p,\gamma)^{22}$Mg reaction at explosive stellar temperatures. This reaction is thought to play a key role in the production and destruction of the long-lived isotope, ^{22}Na, during nova and X-ray bursts. Unsuccessful searches in the universe for the observation of its unique (1274 keV) decay γ-ray in such cataclysmic events using γ-ray observatories, e.g. COMPTEL, have indicated that present models on the mechanism of such events require improvement [Iyudin *et al.*, Astron. & Astrophys. **300**, 422 (1995); Starrfield *et al.*, MNRAS **296**, 502 (1998); José and Hernanz, Astrophys. J. **494**, 680 (1998)]. In the energy region of interest, such radiative proton capture reactions are governed primarily by narrow resonances, requiring direct and indirect studies to elucidate. In order to perform this study directly, we require an intense beam of the radioactive isotope, ^{21}Na, a gaseous helium target and a detection system able to separate the relatively rare reaction products from the much more intense beam particles (∼1 in 10^{12}).

The DRAGON (Detector of Recoils And Gammas Of Nuclear reactions) facility consists of a windowless, recirculating gas target (with a cold cleaning trap), surrounded by a BGO gamma array (30 units) to detect the prompt reaction gamma, followed by a multi-component recoil mass separator (RMS) system to separate the recoiling reaction products. For Expt. 824 a DSSSD (double sided silicon strip detector) was used at a position just past the focal plane of the RMS to detect separated reaction recoiling ions. A more complete description can be found elsewhere [Hutcheon *et al.*, Nucl. Instrum. Methods A (in press); Liu *et al.*, *ibid.*].

Within the past 12 months considerable time was devoted to studying the performance of the DRAGON, particularly measuring the incident beam energy using the first magnetic dipole of DRAGON, studying the optics of the system, measuring the efficiency of the gamma array, and measuring the omega gamma of well-known resonances in order to "calibrate" DRAGON. These studies were performed using stable heavy ion beams, and a description of some of these studies can be found elsewhere in this Annual Report.

The stellar reaction rate, $N_A\langle\sigma v\rangle$, for a narrow resonance, expected for nova conditions, is directly proportional to the resonance strength, $\omega\gamma$, and depends exponentially on the resonance energy, E_R. In units of cm^3 s^{-1} mol^{-1}, it is given by [Fowler *et al.*, Ann. Rev. Astron. Astrophys. **5**, 525 (1967)]:

$$N_A\langle\sigma v\rangle = 1.54\times10^{11}(\mu T_9)^{-3/2}\omega\gamma\,\exp\left[-11.605\frac{E_R}{T_9}\right], \quad (1)$$

with N_A Avogadro's number, μ the reduced mass in amu, T_9 the temperature in units of GK, $\langle\sigma v\rangle$ the thermally averaged nuclear cross section and $\omega\gamma$ and E_R in MeV. The narrow resonance thick target yield, Y, at maximum is,

$$Y = \frac{\lambda^2}{2}\frac{M+m}{m}\omega\gamma\left(\frac{dE}{dx}\right)^{-1}, \quad (2)$$

with λ the centre-of-mass de Broglie wave length, M the (heavy) projectile nucleus mass, m the (light) target nucleus mass, and $\frac{dE}{dx}$ the energy loss per atom/cm^2(lab). Thus, measurement of the maximum thick target yield can determine the resonance strength, $\omega\gamma$.

Figure 39 shows the ^{22}Mg level scheme. Calculations of the Gamow window for the ^{21}Na$(p,\gamma)^{22}$Mg reaction at estimated ONe nova temperatures from

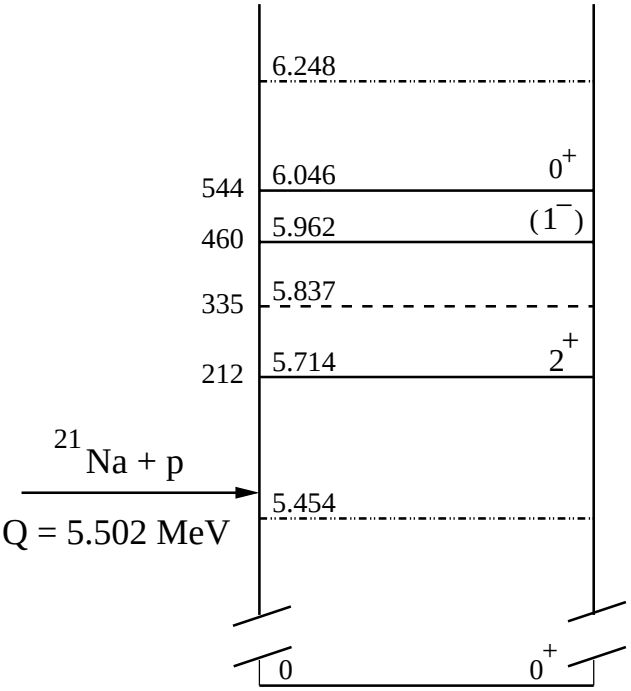

Fig. 39. The ^{22}Mg level scheme of those states of astrophysical interest for ONe nova, shown with solid lines. The numbers on the far left denote centre-of-mass energies ($E_x - Q$), in units of keV. The state at 5.837 MeV was observed once and not confirmed in other studies [Bateman *et al., op. cit.*; Michimasa *et al.*, Eur. Phys. J. **A14**, 275 (2002); Chen *et al.*, Phys. Rev. **C63**, 065807 (2001)].

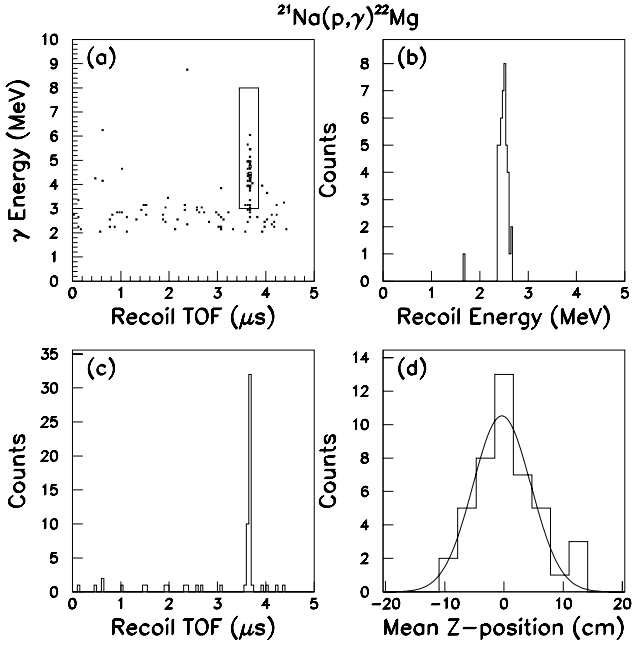

Fig. 40. Resonant-capture spectra for a ^{21}Na beam energy of 220 keV/u. (a) Valid events enclosed by a two-dimensional-cut box above a background of random-coincidence events, (b) the recoil-energy distribution of the events in the DSSSD, selected by the box in (a), (c) the recoil TOF distribution for events above the γ-ray threshold energy, (d) distribution of box-selected γ-ray events observed in the BGO array along the target length, with a Gaussian fit.

0.2 to 0.35 GK at peak temperature suggest that throughout the duration of the outburst the 212 keV, $l = 0$ resonance will be dominant in the nucleosynthesis of ^{22}Na.

The experiment was carried out at the TRIUMF-ISAC radioactive beam facility. A radioactive beam of pure ^{21}Na ($q = 5^+$) at typical intensities up to 5×10^8 s^{-1} was delivered to the DRAGON hydrogen gas target (4.6 torr). The gas target received a total of $\sim 10^{14}$ ^{21}Na atoms for this study. Data-taking was done in both singles and coincidence modes; the coincidence mode required a "start" timing signal from the γ-array in coincidence with a "stop" timing signal from the DSSSD. Figure 40 shows resonant-capture spectra for a beam energy of 220 keV/u. Counts within the box in Fig. 40a were considered to be valid capture events. Their recoil energy distribution is presented in Fig. 40b. Figure 40c is the recoil time-of-flight spectrum for events satisfying the cut on γ-ray energy. The distribution of the hit BGO detector position along the beam axis (Fig. 40d) shows that the resonance was near the centre of the gas target at beam energy 220 keV/u ($E_{\rm cm}$= 211 keV).

The beam energies were measured by adjusting the field of the first magnetic dipole in the separator so as to position the beam on the ion-optical axis at an energy-dispersed focus. Using the design bending radius of the dipole (1 m), it was possible to calculate beam energy in terms of the dipole field. The expected relationship was confirmed by measuring a number of known resonances with stable beams. The lower panel of Fig. 41 shows the yield curve for one of these studies, the ^{24}Mg$(p,\gamma)^{25}$Al reaction, demonstrating our agreement (inflection point of 214.4 ± 0.5 keV) with the literature resonance energy of 214.0 ± 0.1 keV [Uhrmacher *et al.*, Nucl. Instrum. Methods **B9**, 234 (1985)]. As shown in the upper panel, we find the energy (inflection point) for the ^{21}Na(p,γ)^{22}Mg resonance to be 205.7 ± 0.5, and not 212 keV (see Fig. 39), the difference between the Q value and the level excitation energy, 5713.9 ± 1.2 keV [Endt, Nucl. Phys. **A521**, 1 (1990)]. Given that the latter value is based upon a direct gamma de-excitation measurement of the 5713.9 keV level, this disagreement could be explained by a modified mass excess for ^{22}Mg; our data imply a value of –403.2 ± 1.3 keV rather than –396.8 keV.

Figure 41 (upper panel) shows the thick target yield curve corrected/scaled for various factors listed in Table III. The efficiency of the BGO array as a function of γ-ray energy and resonance position in the target was calculated using the GEANT program. The variation of resonance position with beam energy resulted in the

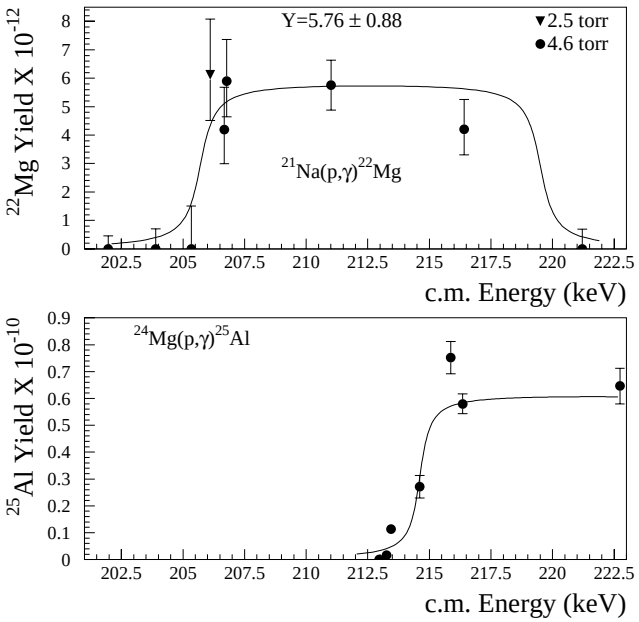

Fig. 41. The upper panel displays the thick target yield data for the ^{21}Na$(p,\gamma)^{22}$Mg reaction, with the solid line showing the nominal target thickness for 4.6 torr. Yield of the ^{24}Mg$(p,\gamma)^{25}$Al reaction for the resonance at $E_{\rm cm} = 214$ keV, used for beam energy calibration, is displayed in the lower panel. Statistical errors only are displayed in both.

Table III. Summary of systematic errors.

Factors	Value	Syst. error
BGO array efficiency (211 keV)	0.48	12%
Separator transmission	0.98	2%
DSSSD efficiency	0.99	1%
Charge state fraction	0.44	3%
Integrated beam (211 keV)	3.62×10^{13}	4%
dE/dx (eV/(atom/cm^2))$_{\rm lab}$	8.18×10^{-14}	5%

following calculated efficiencies: 45% for 202 keV $\leq$ E $\leq$ 207 keV, 48% at 211 keV, and 46% above 216 keV. The systematic error was deduced from values of the array efficiency measured with stable beam reactions. The separator transmission (98%) and DSSSD detection efficiency (99%) were determined separately, and the fraction of the charge state selected (44%) was measured with a ^{24}Mg beam of 220 keV/u. At 4.6 torr, charge state equilibrium in H_2 gas was measured to be attained within 4.4 mm [Liu *et al., op. cit.*]. The energy loss in the target (4.6 torr) was measured to be 14.4 keV/u (lab) or 8.18×10^{-14}eV/(atom/cm^2), in agreement with SRIM [Biersack and Haggmark, Nucl. Instrum. Methods **174**, 257 (1980)].

The data of Fig. 41 (upper panel) were obtained by maximum likelihood combination of several runs at each energy. The error bars on the zero counts seen at off-resonance energies are 68% confidence limits. Table III presents a summary of systematic

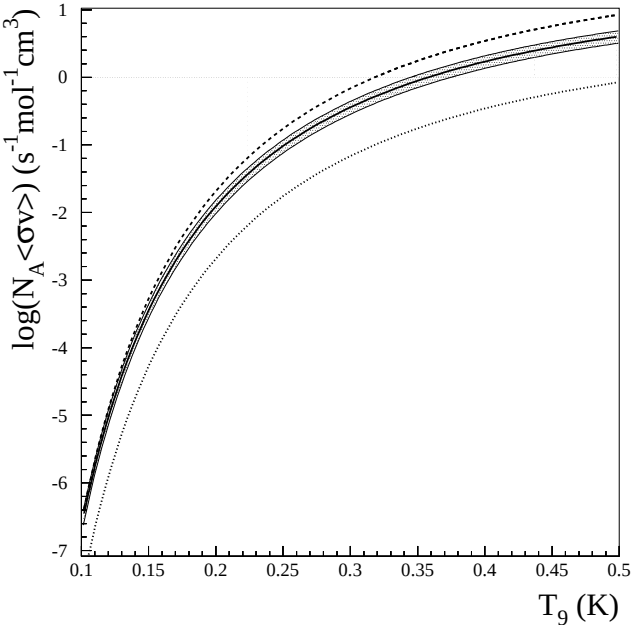

Fig. 42. ^{21}Na$(p,\gamma)^{22}$Mg reaction using Eq. 2 with typical novae temperatures and our measured values for $\omega\gamma$ and $E_{\rm R} = 0.206$ MeV (solid line with hatched area reflecting errors), in comparison with other works; upper curve [Bateman *et al., op. cit.*] and lower curve [José *et al., op. cit.*].

errors. Using Eq. 2 and only the mid-target data point (211 keV), a yield of $(5.76 \pm 0.88) \times 10^{-12}$ per incident ^{21}Na results in a resonance strength of $\omega\gamma = 1.03 \pm 0.16_{\rm stat} \pm 0.14_{\rm syst}$ meV.

The effect of these results on the calculated stellar reaction rate is shown in Fig. 42. The rate is reduced over that determined by shell model calculations of $\omega\gamma$ as reported in Bateman *et al.* [Phys. Rev. **C63**, 035803 (2001)], and enhanced over that found in José *et al.* [Astrophys. J. **520**, 347 (1999)]. An analysis of the impact of the new measurements on the synthesis of ^{22}Na in novae was performed. A new model of a nova outburst, using an ONe white dwarf of 1.25 solar mass, has been computed from the onset of accretion up to the explosion and ejection stages, by means of a spherically symmetric, implicit, hydrodynamic code, in Lagrangian formulation (see José and Hernanz [*op. cit.*] for details). Results have been compared with a model evolved with the previous prescription of the ^{21}Na$(p,\gamma)^{22}$Mg rate [José *et al., op. cit.*]. As a result of the higher contribution of the 5.714 MeV level (Fig. 42), a slightly lower amount of ^{22}Na (a mean mass fraction of 2.8×10^{-4}, compared with the previous estimate of 3.5×10^{-4}) is found. The small decrease in the ^{22}Na yield results from the fact that increasing the proton capture rate on ^{21}Na favours the synthesis path through ^{21}Na$(p,\gamma)^{22}$Mg$(\beta^+)^{22}$Na, hence reducing the role of the alternative ^{21}Na$(\beta^+)^{21}$Ne$(p,\gamma)^{22}$Na path. In these newly derived conditions of increased proton

capture on ^{21}Na, ^{22}Na production takes place earlier in the outburst, at a time when the envelope has not yet significantly expanded and cooled down (contrary to the case when a lower ^{21}Na(p,γ) rate is adopted), and hence the temperature in the envelope is still high enough to allow proton captures on ^{22}Na, that reduce its final content in the ejecta.

Up to now, γ-ray flux determinations were limited by a large uncertainty in the ^{21}Na(p,γ) and ^{22}Na(p,γ) rates, which translated into an overall uncertainty in the ^{22}Na yields of a factor of $\sim$3. The maximum detectability distance was, accordingly, uncertain by a factor of $\sim$2. Such uncertainty, mainly due to the previously unknown reaction rate, has been largely reduced with the present experimental determination of $\omega\gamma = 1.03 \pm 0.16_{\rm stat} \pm 0.14_{\rm syst}$ meV. These results provide a firmer basis for predictions of the expected γ-ray signature at 1.275 MeV associated with ^{22}Na decay in ONe novae, and confirm the previous determination of 1 kiloparsec for a typical ONe nova [Gómez-Gomar *et al.*, MNRAS **296**, 913 (1998); Hernanz *et al.*, Proc. 4$^{\rm th}$ Integral Workshop Exploring the Gamma-Ray Universe (ESA SP-459, ESA Publ. Div.:ESTEC, Noordwijk, 2001) p.65] observed with ESA's (European Space Agency) INTEGRAL spectrometer, SPI. Furthermore, the smaller uncertainty in the rate also indicates that the predicted ^{22}Na yields are not in conflict with the upper limits derived from several observational searches.

Additional details of this study can be found elsewhere [Bishop *et al.*, Phys. Rev. Lett. (in press); Bishop, "The ^{21}Na$(p,\gamma)^{22}$Mg reaction and O-Ne Novae" (Ph.D. thesis, SFU, in preparation)].

Experiment 862
Analyzing powers in the $\vec{p}(\pi,\pi\pi)$ reactions with CHAOS

(E.L. Mathie, Regina)

In this experiment, the Canadian High Acceptance Orbit Spectrometer, CHAOS, was used to observe at least two charged reaction products from 280 MeV negative pion interactions with polarized protons in the CHAOS polarized proton target. Of particular interest are reactions with two pions in the final state, which have proven to be excellent tests of the predictions of chiral perturbation theory (ChPT). Tests of ChPT at energies near threshold constitute some of the rare tests of QCD possible at low energies. Comparisons of the theory with experiment afford the opportunity to determine low energy constants (LEC) of the theory. Previously only total and differential cross sections could be used for this purpose. Experiment 862 is the first attempt to measure a polarization observable. The pion energy was chosen as a compromise between $\vec{p}(\pi,\pi\pi)$ cross sections, which rise steeply above threshold, and the near threshold kinematic regime, where the theory is best understood.

The polarization observable is sensitive to the spin orientation of the target proton and is defined in terms of the differential cross sections σ^+ (σ^-) for positive (negative) target polarization according to

$$A = \frac{1}{P_{\rm tgt}} \frac{\sigma^+ - \sigma^-}{\sigma^+ + \sigma^-}$$

where $P_{\rm tgt}$ refers to the magnitude of target polarization and σ refers to any one of several differential cross sections which may be determined. In earlier CHAOS experiments, such as Expt. 624, it has been demonstrated that the differential distributions for $(\pi,\pi\pi)$ reactions can be expressed in terms of: the square of the dipion invariant mass, $M^2_{\pi\pi}$; the square of the momentum transfer to the nucleon, t; and the angle between the two final state pions in the dipion system. The essentially full horizontal angle coverage of CHAOS permits the determination of two distributions for any one differential cross section, where for example the dipion system is moving to the left of the beam and to the right.

The polarized target was first developed for CHAOS experiment Expt. 560. The control system was extensively changed to operate in a more modern control environment. The orientation of the proton spins is accomplished in an external, high homogeneity magnetic solenoid. The target material is first cooled to low temperatures using a helium 3-4 dilution refrigerator. Bombardment with suitably tuned microwaves induces polarization of the electron system, which is subsequently transfered to the proton system. Upon completion of this dynamic phase, the microwaves are turned off, leading to a rapid drop in temperature and the proton spin relaxation time to increase suddenly, effectively freezing the proton spin polarization. Once frozen, the target was physically moved from the polarizing solenoid above CHAOS into the spectrometer, where the normal magnetic field serves to preserve the polarization for days. During the actual movement of the target, a third small superconducting magnet, local to the target cryostat, was used to preserve the polarization.

The target polarization may be determined either by calibration of the NMR with the signal due to the small natural polarization arising from thermal equilibrium, or through measurement of a nuclear reaction with a known analyzing power. Numerous target studies including optimizing the NMR system, thermal equilibrium calibrations, and thermal equilibrium buildup studies at different temperatures were completed.

In previous pion production experiments, limitations to the maximum data acquisition rate meant the trigger had to discriminate against the prolific pion proton elastic scattering reaction. Recent improvements in data acquisition meant that this was no longer required, and new data for pion proton elastic scattering were simultaneously obtained. These new pion proton elastic scattering data may be used to improve the current appreciation of the analyzing power or alternatively, knowledge of the analyzing power can be used to provide an independent determination of the target polarization.

Experiment 862 received beam in the summer of 2002. However, from early in the running period it became clear that the septum magnet at the entrance to the channel had an ever worsening coolant leak. The magnet is located in a very difficult location, immediately downstream of the meson production target with vacuum connections to beam line 1A as well as the meson channel, M11. A valiant effort was made to repair the magnet remotely, however, the leak grew worse steadily until its operation was untenable and it became impossible to run M11. During this time data were collected for three cycles of the target polarization (both spin orientations form a cycle) and for one series of measurements with the background target configuration.

In principle the improved trigger arrangement allowed the simultaneous collection of data for $\vec{p}(\pi^-, \pi^-\pi^0)p$, however, the reaction rate is low and, due to the meson channel failure, the amount of data even for the reaction $\vec{p}(\pi^-, \pi^-\pi^+)n$ is minimal. Furthermore, the truncated run limits the scope of systematic checks which are normally a strong point in polarization experiments.

Analysis effort since the end of the run has primarily been focused upon the thousands of NMR spectra and temperature calibrations to determine the target polarization for all runs. Analysis of these data continues in 2003.

Experiment 863
Ground state magnetic moments of ^{75,77,79}Ga (LTNO)

(P. Mantica, Michigan State)

The focus of Expt. 863 is to study the evolution of the single-particle structure of medium-mass nuclides above $_{28}$Ni toward the $N = 50$ shell closure. A well-known shape transition from spherical to moderate deformation ($\beta_2 \approx 0.2$) occurs in the neutron-rich $_{31}$Ga and $_{32}$Ge isotopes between $N = 40 - 42$. Since the ground state magnetic dipole moment can serve as a sensitive probe of the nuclear ground state wavefunction, the experimental determination of the magnetic moments of heavy, odd-A Ga isotopes can address the extent to which quadrupole deformation persists toward $N = 50$.

A low energy beam of ^{75}Ga was produced at the TRIUMF-ISAC facility using a surface ion source equipped with a Ta production target. The ^{75}Ga nuclei were implanted into an iron foil mounted on the cold finger inside the ^{3}He/^{4}He dilution refrigerator of the LTNO. The nuclear orientation of ^{75}Ga was monitored by measuring the angular distribution of β particles emitted from the radioactive parent ($T_{1/2}(^{75}\text{Ga}) = 126$ s). Two plastic scintillator ΔE-E telescopes were placed at 0° and 180° relative to the external magnetic field provided by a superconducting split-coil magnet surrounding the ^{75}Ga implantation position. Three Ge detectors were also placed around the sample position at 0°, 90°, and 180° relative to the external magnetic field. These detectors were used to monitor the γ-rays emitted from the ^{60}Co<u>Fe</u> thermometer as well as the ^{75}Ga γ-ray activity.

The angular distribution of β particles can be written in the form $W_\beta(\theta) = 1 + AP\cos(\theta)$, where P is the fractional polarization of the sample and A is the β-decay asymmetry parameter which depends on the spins and parities of all populated levels in the daughter nucleus, as well as their absolute branching ratios. Since only relative intensities were known for β-delayed γ-rays from ^{75}Ga, absolute γ-ray intensities were first measured in order to determine A, and hence the fractional polarization P from the measured angular distribution of β particles from ^{75}Ga.

In order to extract absolute branching ratios, care was taken to evaluate spectra from runs where the ^{75}Ge daughter activity was saturated, thus ensuring that the activities of the parent and daughter were in

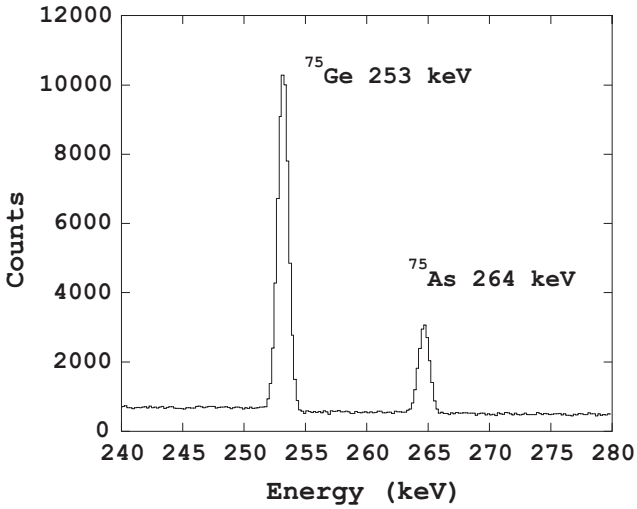

Fig. 43. Summed γ-ray spectrum in the range 240–280 keV taken with the 0° Ge detector during runs with an equilibrium of ^{75}Ga and ^{75}Ge activity.

equilibrium. Absolute γ-ray intensities in the stable ^{75}As granddaughter populated by the decay of ^{75}Ge ($T_{1/2}$ = 82.78 m) are known, hence all that is required for determining absolute branching ratios from parent ^{75}Ga is knowledge of relative intensities of daughter ^{75}Ge γ-rays combined with the total activity of the sample. Since the most intense γ-ray transitions in the ^{75}Ge daughter and ^{75}As granddaughter are close in energy (253 keV and 264 keV, respectively, see Fig. 43), the peak efficiency for each γ-ray can be assumed to be identical. Thus the ratio of counts at 253 keV to 264 keV can be used to determine absolute branching ratios from the parent ^{75}Ga.

Taking into account the deduced branching ratios and assuming the β-decay in this neutron-rich system to be pure Gamow-Teller, $A = -0.40(3)$ was obtained. This value permits the determination of the polarization of ^{75}Ga.

Experiment 870
The ^{17}O$(p,\alpha)^{14}$N reaction – a probe of the O isotope ratios in giant stars
(D. Groombridge, York)

Phase I of the He gas target tests was carried out in May/June. This preliminary test was unsuccessful due to a fault with the initial design of the gas target that caused unacceptable rates of scattered beam into our detection system. Following a small modification to the initial design of the gas target, the TUDA collaboration is pleased to announce that phase II of the tests, carried out in December, were successful.

The aims of these tests were (a) to commission the new gas target using a stable beam, in preparation for use with a ^{18}Ne beam (Expt. 870) and (b) to demonstrate the success of the experimental set-up in reconstructing the trajectories of the reaction protons and in the identification of the elastic proton background originating from the window at the entrance of the gas target.

Past experience of (α, p) measurements have shown that it is crucial to have a more complete understanding of the proton background. With this in mind, a ^{20}Ne beam was requested at a similar energy to that which will be used in the future ^{18}Ne measurement. In the attempt to fulfil the second aim, it was our intention to use a stable beam that also had the potential of yielding some astrophysically interesting physics. The ^{17}O$(p,\alpha)^{14}$N reaction affects the ^{16}O/^{17}O isotope ratio in intermediate mass stars undergoing hot bottom burning on the asymptotic giant branch. A measurement of the ^{14}N$(\alpha,p)^{17}$O reaction at high energies was performed. The (p,α) rate can be inferred using the principle of detailed balance and the resulting rate extrapolated down to stellar energies.

The gas target consists of a cylindrical chamber, 226 cm^3 in volume with a 0.75 μm Ni entrance window (8 mm dia.) and a 6 μm Ni segmented exit window. A thick Ta foil centered on the exit window served to stop the beam in the target. These windows were designed to hold He gas at a pressure of 250 mbar.

The beams were generated by ISAC using the offline ion source (OLIS). Typical beam currents on target were 180 pA, and during the experiment a ^{14}N beam at 1.45 MeV/u and a ^{20}Ne beam at 1.0 MeV/u were requested.

Detection of the elastic and reaction protons was acheived using 4 MSL type QQQ (single sided) 45 μm strip detectors in the "CD" configuration and 8 MSL type YY1 strip detectors in the "LEDA" configuration. These were placed at distances of 11 cm and 35 cm downstream of the entrance window, respectively. One feature of this set-up is that protons can be tracked to a position of origin within the gas target. This information, used together with energy loss information, has the advantage of reducing any ambiguity in the assignment of the final state.

Data were obtained with both ^{14}N and ^{20}Ne beams which indeed looked promising on-line, and detailed analysis of these data is currently being undertaken.

Experiment 871
Meson and quark effects in nuclear β-decay of ^{20}Na
(K. Minamisono, JSPS Postdoctoral Fellowship/TRIUMF; K. Matsuta, T. Minamisono, Osaka)

In preparation for the measurement of the alignment correlation terms in the β-ray angular distribution of ^{20}Na, several test experiments using Na isotopes (on the mass A = 20, 21, 26, and 28) have been performed. These were to demonstrate both nuclear polarization by optical pumping of neutral Na atoms in the ISAC polarized beam line and the preservation of that polarization following implantation of the activity in a lattice of single crystals. In addition, hyperfine studies were needed to find a suitable crystal in which spin manipulation could be used to convert the laser-induced nuclear polarization into nuclear alignment. As a result, a large nuclear polarization of $\sim$50% was produced by the laser-pumping method for four Na isotopes and successfully maintained in the crystal lattice (NaF and TiO_2 single crystals). The electric quadrupole coupling constant eqQ/h of ^{20,21}Na in TiO_2 and the asymmetry parameter η of the field gradient in the crystal were also determined for the first time.

Introduction

Alignment correlation term

The β-ray angular distribution from oriented nuclei is given by $W(E,\theta) \sim 1 + APp/E(1+\alpha E) + \hat{A}\alpha E$, where A is the asymmetry parameter, P the polarization, p and E the momentum and energy of the electron, respectively, $\hat{A}$ the alignment, and α the alignment correlation coefficient given by [Holstein, Rev. Mod. Phys. **46**, 789 (1972)]

$$\alpha_{\mp} \sim \frac{1}{3M}\left(\mp\frac{b}{c} + \frac{d_{\rm I}}{c} \pm \frac{d_{\rm II}}{c} - 1\right).$$

Here $\mp$ is for the electron and positron decays, respectively, M the nucleon mass, b the weak magnetism, c the Gamow-Teller matrix element, $d_{\rm II}$ the G-parity irregular induced tensor term, and $d_{\rm I}$ the nuclear structure dependent time component in the main axial vector current, which is known to have a huge enhancement relative to a value calculated by impulse approximation because of the meson exchange effect inside the nucleus. Taking advantage of the symmetry between the mirror pair, ^{20}Na and ^{20}F in the mass $A = 20$ system, we can extract the induced tensor term from the difference of the alignment correlation coefficients if the weak magnetism is known.

$$\alpha_- - \alpha_+ = -\frac{2}{3M}\left(\frac{b}{c} - \frac{d_{\rm II}}{c}\right).$$

On the other hand, the time component can be purely obtained from the sum as $\alpha_- + \alpha_+ = 2\left(d_{\rm I}/c - 1\right)/3M$. Here, the higher order matrices are neglected for simplicity. The polarization term also has α but since the parity violating large term 1 prevents us from extracting very small α ($\sim$0.01), the alignment term is the best observable to extract $d_{\rm II}$ and $d_{\rm I}$.

Hyperfine interaction

One important key for measurement of the alignment terms is to create a purely nuclear spin aligned Na nucleus. For this purpose, the spin manipulation technique is used, which is an artificial interchange and/or equalization of the population of the magnetic sublevels. For the spin manipulation, the Na atoms are implanted into the single crystal, which has a proper electric field gradient q, under a strong magnetic field H_0. The quadrupole interaction between q inside the crystal and the quadrupole moment Q of the nucleus, superposed on the magnetic interaction between the magnetic moment μ of the nucleus and H_0, changes the energy between each magnetic sublevel so that the single nuclear magnetic resonance (NMR) frequency splits into $2I+1$ lines depending on the nuclear spin I. Thus, a transition between specific two magnetic substates can be induced applying an rf field and it becomes possible to convert a polarization into an alignment. Accurate knowledge of the quadrupole interaction is required for a reliable spin manipulation and artificial creation of alignment.

Experiment

Production of Na atoms and laser-pumping method

The experiment was performed at the radioactive beam facility ISAC. The 500 MeV proton beam from the TRIUMF cyclotron was used to bombard a thick production target, which is coupled to the ionization source. For the production of ^{20}Na, a SiC target and a surface ionization source were used. ^{20}Na ions were extracted at an energy of 40.8 keV, mass separated, and transferred to the polarized beam line at the ISAC experimental hall, where Na atoms were polarized by the laser-pumping method. The atomic polarization was created by pumping Na atoms on the D_1 transition with circularly polarized light. Both ground state hyperfine levels were pumped to achieve high polarization. Essentially the same technique was used as the previous work [Levy *et al.*, Proc. 9$^{\rm th}$ Int. Workshop on Polarized Sources and Targets (World Scientific, 2002) p.334] but the optical pump laser was a coherent 899-21 frequency stabilized dye ring laser pumped by a 7 W argon-ion laser. The NMR vacuum chamber was placed 40 cm downstream of the polarimeter and a NMR magnet made of permanent magnet (5250 Oe at the centre) was used.

β NMR

The polarized Na ions were stopped on the surface of the crystal (catcher) placed at the centre of the NMR magnet and the β-rays from the stopped Na were counted by a set of plastic-scintillation counter telescopes placed above and below the catcher relative to the polarization axis. The solid angle was 2.6% in total. Each telescope consisted of three thin plastic-scintillation counters and a veto counter to reject the scattered β-rays from the NMR magnet. The amount of polarization was deduced from the asymmetry measured by the β-ray counting ratio between up and down counters. The NMR signals were measured as a function of applied rf frequencies.

Results

Measured asymmetry and polarization

First of all, Na ions were implanted into a NaF single crystal, which is known to keep 100% of Na polarization created by the laser-pumping method. The ground state properties of the Na isotopes measured in the experiment and the results are summarized in Table IV. The measured asymmetry AP depends on the asymmetry parameter A, the spin-lattice relaxation time T_1, the timing program used to measure AP, and other corrections. In Table IV, a typical value of

Table IV. Measured Na isotopes. Here A is the asymmetry parameter, which is the integrated value of all measured decay branch, AP the measured asymmetry, T_1 the spin lattice relaxation time, P_0 the initial polarization created by laser-pumping method (corrected value for A and T_1), eqQ/h the electric quadrupole coupling constant, and η the asymmetry parameter of the electric field gradient.

Catcher	Structure		^{20}Na	^{21}Na	^{26}Na	^{28}Na
		$T_{1/2}$	447.9 (ms)	22.49 (s)	1.072 (s)	30.5 (ms)
		I^π	2^+	$3/2^+$	3^+	1^+
		A	0.33	0.81	–0.94	–0.76
NaF	cubic	AP (%)	16.0 ± 0.4	21.8 ± 0.5	–46.6 ± 1.1	–35.9 ± 2.5
		T_1 (s)	9.9 ± 3.1	9.0 ± 0.2	24.6 ± 4.2	–
		P_0 or P (%)	51.0 ± 1.3	61.9 ± 1.4	52.8 ± 1.3	47.3 ± 3.3
TiO_2	rutile	AP (%)	5.3 ± 0.3	13.7 ± 0.3	–44.8 ± 0.5	–34.1 ± 2.5
		T_1 (s)	3.4 ± 1.3	13.0 ± 0.5	32 ± 11	–
		P_0 or P (%)	18.3 ± 1.5	24.0 ± 0.5	46.8 ± 0.9	44.9 ± 3.3
		eqQ/h (MHz)	2.2 ± 0.2	5.20 ± 0.03	–	–
		η	0.33 ± 0.03		–	–
$LiNbO_3$	ilmenite	AP (%)	4.3 ± 0.3	5.3 ± 1.6	–40.4 ± 0.6	–26.3 ± 3.0
		T_1 (s)	1.8 ± 0.5	1.3 ± 0.3	5.3 ± 0.5	–
		P_0 or P (%)	17.0 ± 1.7	56 ± 28	51.8 ± 1.5	34.7 ± 4
MgF_2	rutile	AP (%)	–	–	–18.6 ± 0.6	–
		T_1 (s)	–	–	7.4 ± 2.0	–
		P_0 or P (%)	–	–	22.3 ± 1.3	–
Pt	ccp	AP (%)	–	–	–14.5 ± 0.4	–
		T_1 (s)	–	–	0.78 ± 0.08	–
		P_0 or P (%)	–	–	55.0 ± 5.9	–

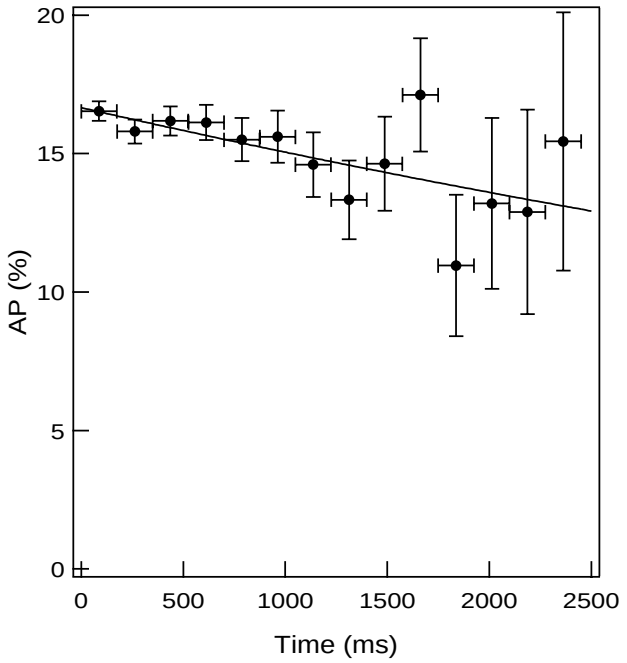

Fig. 44. A typical result of spectrum of spin–lattice relaxation time of ^{20}Na in NaF. Solid line is best fit.

measured AP during the run and the corrected value P_0 for T_1 and A are listed. For the run, in which T_1 was not measured, a value P corrected for A is presented. The typical result of T_1 measurement of ^{20}Na in NaF is shown in Fig. 44, where a pulsed-beam method was employed and the beam was chopped at time 0. Because of the limited beam time, the electro-optic modulators (EOMs) for the laser pumping were not fully optimized to cover the line width of the hyperfine splitting of the ground state in D_1 transition. Thus a higher asymmetry can be expected for the future run.

Quadrupole interaction of ^{20,21}Na in TiO_2: preliminary results

For the spin manipulation to create an alignment, TiO_2 single crystal will be used as a catcher. For this purpose, the quadrupole coupling constant eqQ/h and the asymmetry parameter η of the field gradient of ^{20,21}Na in TiO_2 were determined for the first time. η is defined as $\eta = (V_{XX} - V_{YY})/V_{ZZ}$, where the electric field gradient is defined by the principal components of $V_{ii} = d^2V/dX_i dX_i$ as $|V_{XX}| \leq |V_{YY}| \leq |V_{ZZ}|$ and $V_{ZZ} = q$. NMR spectra of ^{21}Na in TiO_2 were measured with crystal orientations c // H_0 and $c \perp H_0$ and eqQ/h and η were extracted as listed in Table IV. Then, using the obtained information, we measured the NMR spectrum of ^{20}Na in TiO_2, c // H_0, which is shown in Fig. 45, where the solid circles were the data measured with rf modulation of ± 150 kHz and open circles with FM = ± 50 kHz. From the measured coupling constant listed in Table IV, we have

$$\frac{Q(^{20}\mathrm{Na})}{Q(^{21}\mathrm{Na})} = 0.43 \pm 0.03 \ : \ \textit{preliminary.}$$

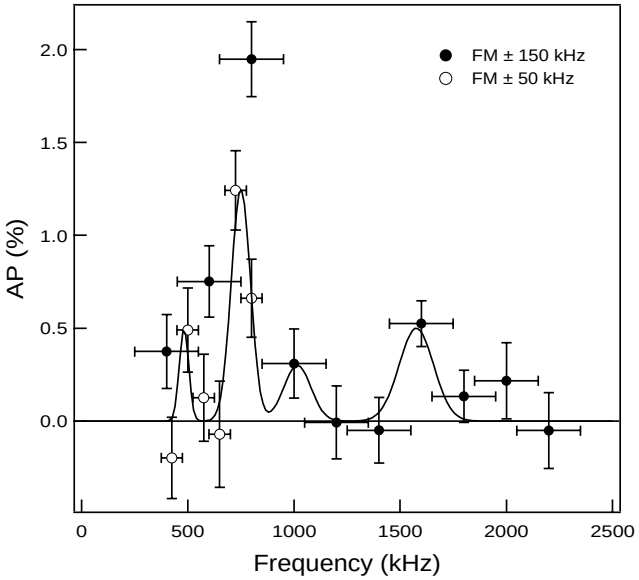

Fig. 45. NMR spectrum of ^{20}Na in TiO_2, c // H_0. The solid circles are the data measured with FM = ± 150 kHz and open circles with FM = ± 50 kHz. Solid line is best fit.

The Q moment of ^{21}Na has been measured as $Q(^{21}\mathrm{Na}) = 50 \pm 37$ (mb) [Touchard *et al.*, Phys. Rev. **C25**, 2756 (1982)] and thus the Q moment of ^{20}Na can be extracted as $Q(^{20}\mathrm{Na}) = 22 \pm 16$ (mb). To have a more precise value, we have to measure eqQ/h of a Na isotope in TiO_2 whose Q moment has been precisely measured.

In the next run, we will confirm the spectrum of ^{20}Na in TiO_2 and measure the alignment correlation term. The precise measurement of the Q moment of ^{20,21}Na is also planned.

Experiment 875
MuScat: muon scattering in low *Z* materials for muon cooling studies
(R. Edgecock, RAL)

As explained in the Annual Reports for 2000 and 2001, MuScat is making a precise measurement of the multiple scattering of muons in the momentum range 150–200 MeV/c as input to cooling studies for both a neutrino factory and a muon collider [MUCOOL Collab., Fermilab Proposal P904 (1998)]. Due to the complexity of the cooling process and the fact that ionization cooling has never been demonstrated to work, MuScat is one of three cooling projects. The second of these, MuCool, is studying the components of a cooling channel, while the third, the international Muon Ionisation Cooling Experiment (MICE), will show that a cooling channel can be built and will work.

The layout of MuScat during the first run in 2000 is shown in Fig. 46 and its performance was described in the 2000 Annual Report. As a result of this, it was

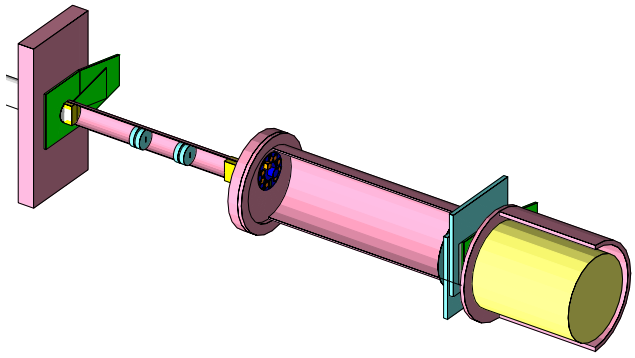

Fig. 46. The layout of the MuScat experiment in 2000, shown from below.

decided to make a number of modifications to the experiment for a second run. These are described in the 2001 Annual Report, and summarized in the following.

New tracking detectors

Three new chambers, using scintillating fibres, have been built. These consist of two offset planes of 1 mm thick fibres in each dimension, to give a uniform efficiency and two dimensional readout. There is a total of 1024 fibres per chamber. The light from the scintillating fibres is transmitted to photomultipliers using clear fibres. The PMTs used are Hamamatsu R5900 L16s (see http://cat1.hpk.co.jp/Eng/catalog/ETC/R5900U-L16_TPMH1146E06.pdf) and contain 16 anodes, each 16 mm long and 0.8 mm wide. Bundles of 16 by 16 clear fibres are formed to match these anodes, thus giving a 16-fold multiplexing. To ensure that signals can be de-convoluted, the scintillating fibres are read out at both ends and the PMTs at each end are rotated by 90° with respect to each other. One of the chambers, with the bundles of clear fibres clearly visible, is shown in Fig. 47. The PMTs sit outside the vacuum vessel and the fibre arrays form the vacuum seal. Tests show that the leak rate from these is sufficiently small to allow a vacuum of less than 10^{-6} torr.

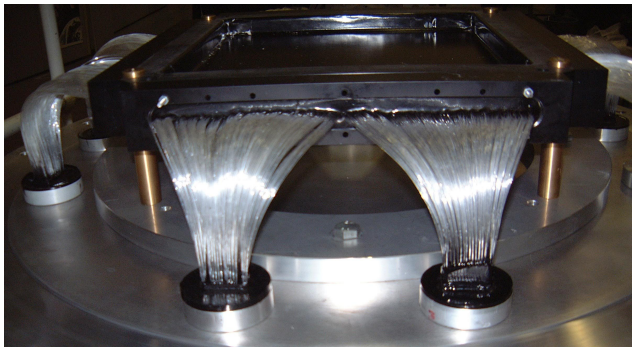

Fig. 47. One of new scintillating fibre detectors.

Collimation system

The performance of the collimation system has been improved by making a number of changes. In particular, the existing collimator disks in the collimator tube have been moved to the ends, two to each, to increase the thickness of the 40 mm and 160 mm thick end collimators. The disks have been replaced by another four, each 10 mm thick, but with 2 cm radius holes through the centre. As well as reducing the penetration through the collimators, this dramatically reduces large angle scatters off the internal faces of all the collimators. The large angle scatters will be further reduced as the collimator tube has been wrapped with 6 mm thick lead sheet and the thickness of the front flange of the main vacuum vessel doubled. Finally, an active collimator has been added to the front face of the 160 mm collimator block. This was done by placing small blocks of scintillator above and below the slit of the collimator. This will eliminate particles that just clip this edge of the collimator. These improvements are demonstrated in Fig. 48.

Targets

In the 2000 run, nine different solid targets were used, mounted on the ten hole target wheel. The tenth hole was used for measuring the intrinsic distribution of the beam. For the run in 2003, a twelve hole wheel has been created. This will allow nine targets of the same type as in 2000 to be used, but thicker to allow for the use of a higher beam energy than originally expected. In addition, one target from 2000 will be reused, to have a comparison with the previous data. Finally, it is hoped to use a lithium hydride target, if a solid piece of the required size can be obtained. However, the main change compared to 2000 will be two liquid hydrogen targets, one 100 mm thick and the other 150 mm. These have been built by the Cryogenics Group at TRIUMF. Two thicknesses are to be measured to make it easier to de-convolute the effects of the target windows.

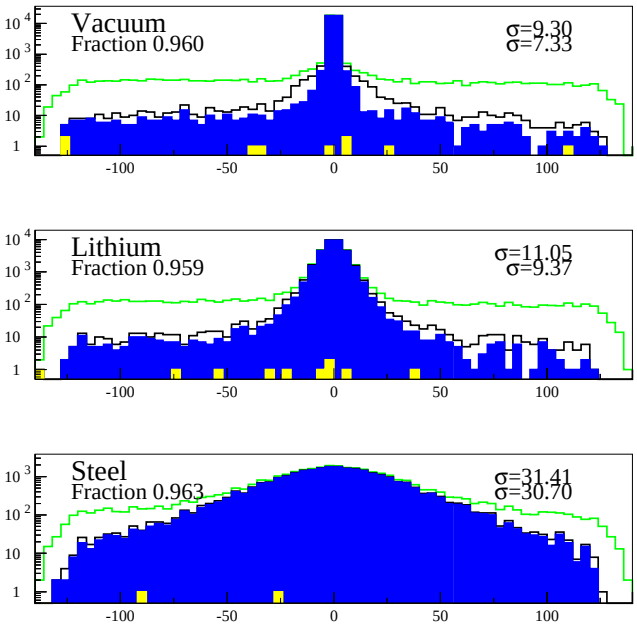

Fig. 48. A comparison of simulated scattering distributions with no target, 10 mm of lithium and 2 mm of iron using the old and new collimation systems. In each case, the upper line is the old collimation system, with no software cuts, the middle line is the new system and the dark shaded area is the new system using the active collimator. The light shaded blocks are from decays in flight.

Vacuum vessel

Due to the new scintillating fibre detectors and the liquid hydrogen targets, a new main vacuum vessel has been built.

The construction of the new version of the experiment was completed in the middle of 2002 and the rest of year was used to test it, especially the new tracking detectors, in a proton beam from the ISIS accelerator at RAL. The first results of these tests are described in the next section.

Beam tests

The new tracking chambers were tested with beams of protons and muons at a variety of energies. The entire experiment is shown in the HEP test beam line at RAL in Fig. 49. When the collimation system was used, a reasonable trigger rate could only be achieved using protons at 700 MeV/c. The bulk of these data were taken just before Christmas and are still being analyzed. Nevertheless, two plots are shown in Figs. 50 and 51. The first shows the number of photo-electrons measured on individual fibres from a proton hit. From these individual fibre hits, clusters are formed in each projection and then combined into a space point in the

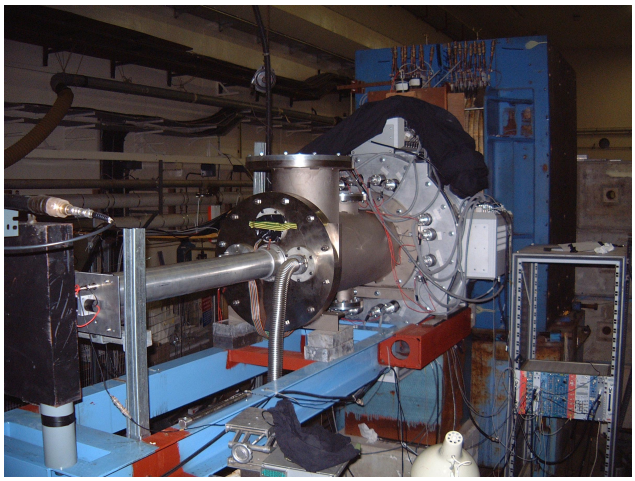

Fig. 49. The MuScat experiment in the test beam line at RAL.

chamber. Figure 51 shows the total number of photo-electrons in these space points.

Although the analysis of the data taken is not yet complete, it is sufficiently well advanced for us to be confident that the new detectors will work as required during our run in TRIUMF in 2003.

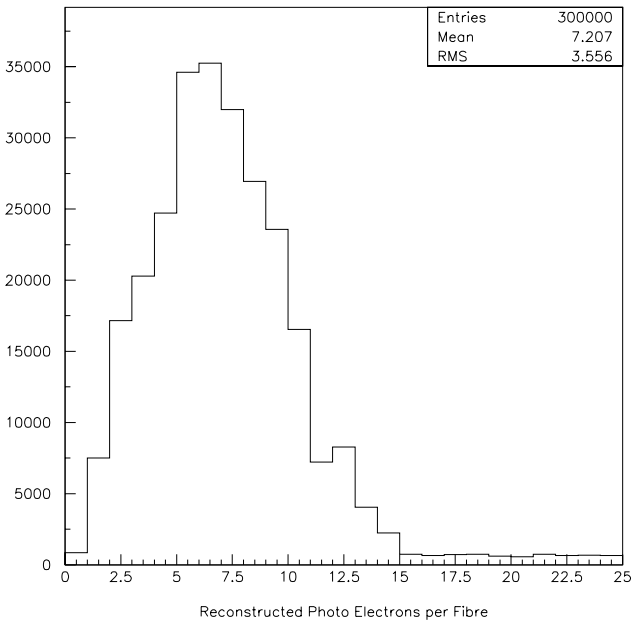

Fig. 50. The number of photo-electrons seen on individual fibres from 700 MeV/c protons.

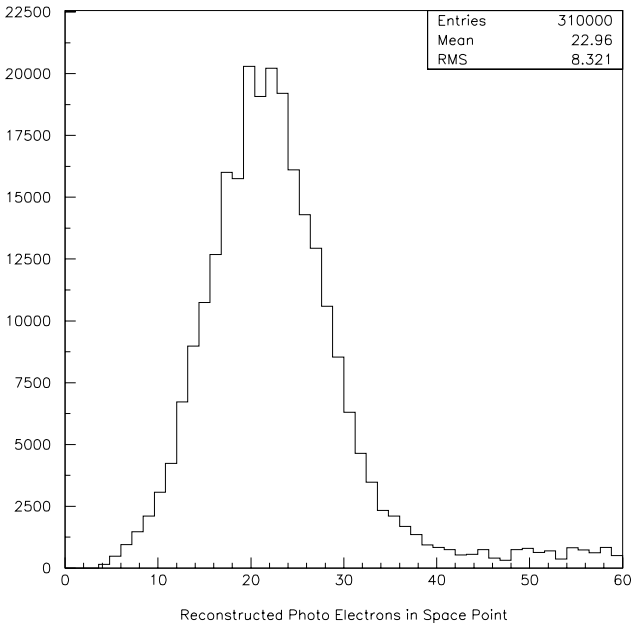

Fig. 51. The number of photo-electrons in a reconstructed space point in a single chamber.

Experiment 893
The hyperfine field of Rb in Fe, Ni and Co (LTNO at ISAC)
(P. Delheij, TRIUMF)

Principle

In the low temperature nuclear orientation set-up, a polarized nuclear ensemble is created by implanting the radioactive beam from the ISAC facility into a ferromagnetic target foil which is kept at a temperature near 10 mK. For these systems the polarization is determined by the factor μH/kT through the Maxwell Boltzmann distribution. Here, μ is the magnetic moment, H the hyperfine field, T the temperature and k the Boltzmann constant. This polarization produces an anisotropy in the emission of the decay products which depends on nuclear structure properties like spins, multipole mixing and parity mixing. By raising the temperature, the normalization (isotropic distribution) is measured. The normalized anisotropies determine the parameter values.

If two of the three parameters in μH/kT are known for the parent ground state, the third one can be determined. In this way (because μ and H are known) the temperature is determined by attaching a long lived source like ^{60}CoFe (for which μ and H are known) to the cold finger that cools the target foil.

The product μH can be determined directly with rf irradiation (NMRON technique). As the frequency of the rf field is stepped, the anisotropy of any subsequent transition is measured to detect the change of this anisotropy when the Larmor frequency is passed. This technique avoids the complication of the temperature determination. Then the accuracy is typically improved by an order of magnitude. Either the magnetic moment or the hyperfine field can be determined if the other quantity is known.

Development

A major disassembly included removing the refrigerator from the set-up to replace the O-rings on the actuator shafts for the baffles and the needle valves of the supply line to the 1 K pot. Also, a vacuum leak had developed in the cold beam line. This occasion was used to redesign the bellows section of the cold beam line which contains the iris to introduce more mechanical flexibility at that point.

To improve the diagnostics for the beam tuning, several changes were implemented. Microswitches were mounted on the 4 K shield below the target to verify the position of the movable Faraday cup. Furthermore, a Faraday cup was built that can be inserted to replace the cold finger with the target. In this way 90–100% transmission was obtained during tuning with stable

beam from the on-line source. These modifications performed very well.

On-line measurements

At ISAC the on-line ion source that was available was of the surface ionization type which is particularly suitable to produce alkali beams like Rb. The calculated and experimental values of the hyperfine field for Rb implanted in Fe differ by a factor 5. The best isotope to solve this problem is ^{79}Rb. The hyperfine field for alkalis is typically rather small compared to, e.g., noble gases or halogens. This feature of the experimental data is counter to what one would expect intuitively. Nevertheless, we observed sizable polarization for implanted ^{79}Rb. It has a number of other favourable properties. The decay scheme provides several internal consistency checks. Furthermore, the lifetime of 22 min is long enough to close off the beam after a few minutes of implantation. This provides a fixed source and allows the target to cool a few mK.

From several production targets enough ^{79}Rb intensity (20 pA) can be produced to take wirescans and measure the beam position every few hours. However, due to problems with the production target in the past year this goal could not be met. The intensity was also too low for NMRON measurements. An integral measurement at a temperature of 16 mK showed an anisotropy from which a preliminary lower limit of 14.5 ± 1.5 T is determined for the hyperfine field. It is assumed for this result that all the implanted ions experience the full hyperfine field. An NMRON measurement will verify this condition.

Off-line measurements

After the on-line measurements it was decided to verify quantitatively with a long lived source the status of the set-up. ^{60}Co was diffused into a thick Fe foil (0.25 mm thick). In Figs. 52 and 53 the intensity of the ^{60}Co γ-rays is shown as a function of the rf frequency for the detectors that were mounted parallel to the polarization direction. A magnetic field of 0.2 and 0.5 T respectively was applied to the sample. For this geometry an anisotropy in the gamma emission produces a reduction in the intensity. At the Larmor frequency the gamma anisotropy is reduced by the rf irradiation and therefore the measured intensity increases towards the normalization value wcts. From a gaussian fit to the data it follows that the destroyed fraction of the anisotropy exceeds 30%. The resonance frequency ν_2 of 165.1 MHz and the width W of 1.07 MHz agree very well with previous observations. In each graph an error bar is plotted for the measurements with the highest and lowest value.

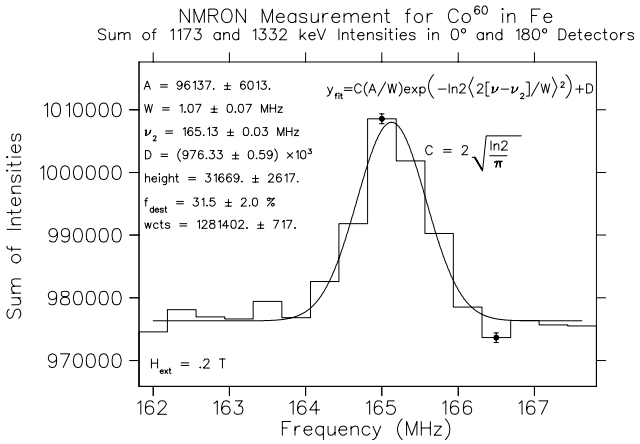

Fig. 52. NMRON resonance for ^{60}CoFe at 0.2 T.

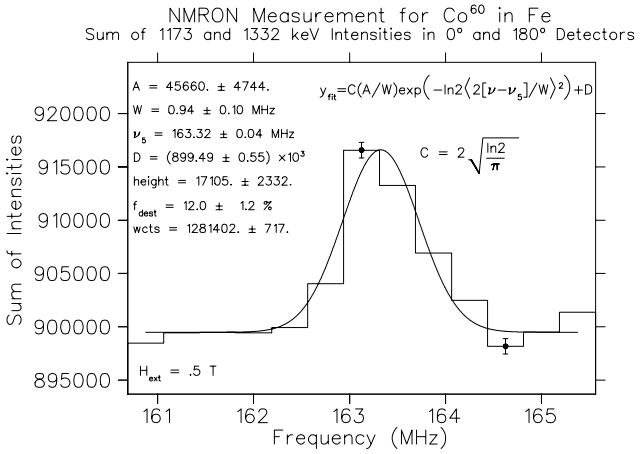

Fig. 53. NMRON resonance for ^{60}CoFe at 0.5 T.

The shift of 1.8 MHz in the resonance frequency reflects exactly the magnetic field shift of 0.3 T (Fig. 53). The reduction of the destroyed anisotropy fraction follows the decrease of the tipping angle at higher external magnetic field.

The isolated spin assumption is verified by measuring the intensities with the frequency modulation on (N_{on}) and off (N_{off}) for equal time intervals at each rf frequency (Fig. 54). Their difference is the destroyed anisotropy which is normalized with the undisturbed anisotropy(N_{warm} – N_{off}). These time intervals were split in four equal parts of 150 s each.

From the dropoff in intensity, when the modulation is turned off (Fig. 55), a longitudinal relaxation time of approximately 50 s is determined, as expected.

Through these off-line measurements it has been demonstrated quantitatively that the sample fabrication and the cryogenic set-up for NMRON measurements as well as the sample fabrication are operating very well.

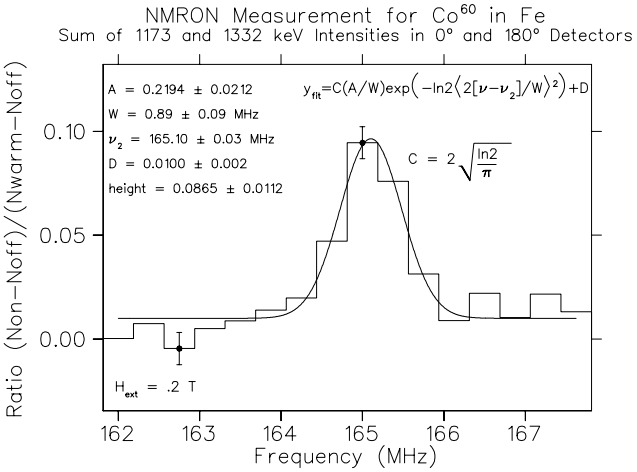

Fig. 54. NMRON resonance as determined by toggling the frequency modulation on and off at each frequency.

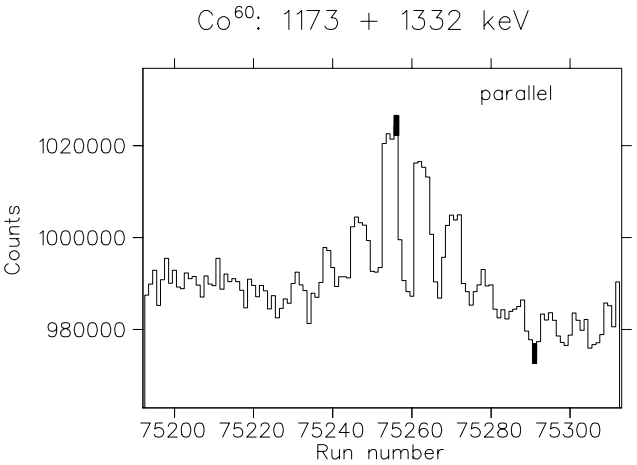

Fig. 55. Raw data with frequency modulation that is toggled every fourth run.

Experiment 903
Spectroscopic study of ^{11}Be with polarized ^{11}Li beam

(T. Shimoda, Osaka)

Although the establishment of a level scheme is of primary importance to understanding the nuclear structure, essentially no "firm" spin-parity assignments have been made for a neutron-rich nucleus ^{11}Be, except for the famous abnormal parity ground state ($1/2^+$) and the first excited state (0.320 MeV, $1/2^-$). This experiment aims at establishing firm spin-parity assignments and level scheme of ^{11}Be by observing β-delayed neutrons and γ-rays from a spin-polarized $^{11}\mathrm{Li}_{\mathrm{g.s.}}$. The present method takes advantage of the fact that the allowed β-decay from a polarized nucleus shows significantly different asymmetry depending on the spin values of both the initial and final states. The difference comes from the asymmetry parameter A as shown in the following expression of the β-ray angular distribution $W(\theta)$ as a function of the emission angle θ with respect to the polarization axis,

$$W(\theta) \propto 1 + AP\cos\theta,$$

where P is the polarization of the parent nucleus. In the allowed transition from $^{11}\mathrm{Li}_{\mathrm{g.s.}}$ ($I^\pi = 3/2^-$, $T_{1/2}$ = 8.5 ms, $Q_\beta = 20.61$ MeV) the asymmetry parameter A is restricted to very discrete values of -1.0 or -0.4 or $+0.6$, corresponding to the final state spin-parity of $1/2^-$ or $3/2^-$ or $5/2^-$, respectively, of ^{11}Be. The spin polarization P can be evaluated from the β-ray asymmetry coincident with the γ-ray from the first excited state at 0.32 MeV ($1/2^-$) to the ground state in ^{11}Be. Thus, from the β-ray asymmetry measurements of β-n and β-n-γ coincidence for other states in ^{11}Be, the associated A's can be determined, and consequently their spin-parities can be assigned, in addition to the level scheme of ^{11}Be and the decay schemes of $^{11}\mathrm{Li}_{\mathrm{g.s.}}$ and $^{11}\mathrm{Be}^*$. Highly polarized radioactive nuclear beams at ISAC are best suited for this kind of experiment.

Since the proposal of Expt. 903 has been approved in the beginning of 2001, preparation for the experiment has been made extensively in the following three major parts: (i) development of spin-polarized ^{11}Li beam, (ii) construction of the Osaka beam line which delivers the polarized ^{11}Li beam to the area where the present experiment is performed, (iii) development of the detector system for the β-n and β-n-γ coincidence measurements.

Polarized ^{11}Li beam

Polarization of ^{8}Li beam as high as $\sim$70% has been achieved in August, 2001 after introducing a set of EOMs into the pumping laser system so as to match the laser line width to the broadened absorption line of the neutral ^{8}Li beam [Levy *et al.*, PST2001 (World Scientific, 2002) p.334; Hatakeyama *et al., ibid.* p.339]. The same scheme is applicable for ^{11}Li beam. After installing a ring dye laser system, $\sim$50% polarization of ^{11}Li was achieved in July, 2002.

Detector system

A schematic of the detector set-up is shown in Fig. 56. The spin-polarized ^{11}Li beam is stopped in a thin Pt stopper foil in vacuum. The polarization is preserved with the help of a static magnetic field applied by a pair of permanent magnets. The β-ray asymmetry is measured with two sets of plastic scintillator telescopes placed along the polarization direction, free from spurious asymmetry due to the detector geometry or efficiency by inverting spin orientation. The inversion is achieved by flipping the laser helicity for optical pumping. High energy β-delayed neutrons (E_{n} = 0.5–9 MeV) are detected with six TOF plastic scintillators

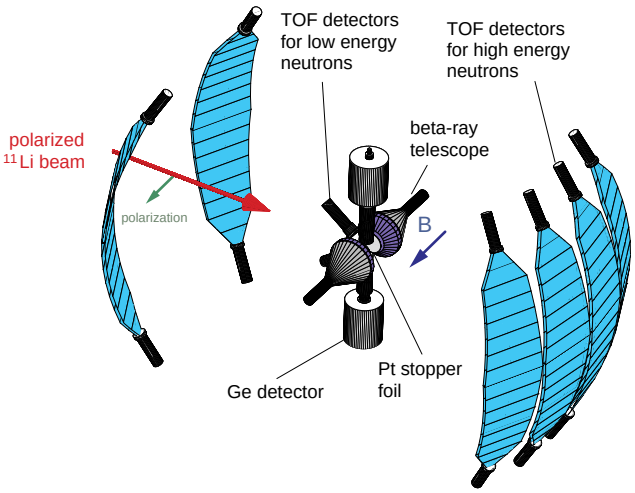

Fig. 56. Detector system for β-n and β-n-γ coincidence measurements from spin-polarized ^{11}Li.

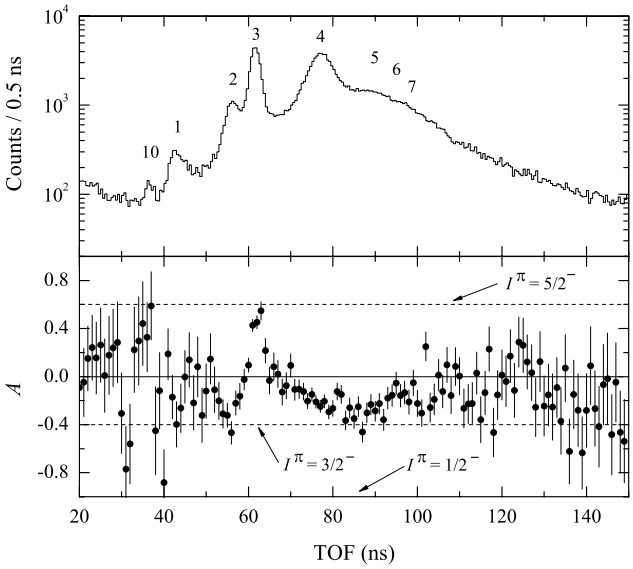

Fig. 57. Neutron TOF spectrum and associated β-ray asymmetry.

with an arc shape. Low energy β-delayed neutrons (E_n = 10–500 keV) are detected with two TOF Li-glass scintillators. γ-rays from ^{11}Li and ^{11}Be are detected with two HPGe detectors placed above and below the Pt stopper.

Results of July, 2002 run

Following the first test experiment in December, 2001 to examine the performance of the low energy neutron detectors, the second test experiment with polarized ^{11}Li beam and full detector set-up was performed in July, 2002. Even with many troubles such as the limited beam intensity to ∼200 pps (10 times less than expected) and not optimum laser conditions, significantly high polarization brought fruitful results as follows.

In the upper and lower panels of Fig. 57, the neutron TOF spectrum with the high energy neutron detectors and the observed asymmetry parameters A for β-rays coincident with the neutrons are shown, respectively, as a function of the flight time. The expected A values for β-decay to a specific spin state in ^{11}Be* are shown by horizontal lines in the lower panel. Better time resolution and less background than the previous works at fragment separator facilities [Aoi *et al.*, Nucl. Phys. **A616**, 181c (1997); Morrissey *et al.*, Nucl. Phys. **A627**, 222 (1997)] enabled observation of a new peak 10 which corresponds to the neutron decay from a state at E_x = 10.6 MeV in ^{11}Be to the ground state of ^{10}Be. For the peak 1 Aoi *et al.* proposed a neutron decay from a "new state" at E_x = 8.03 MeV, but Morrissey *et al.* assigned the peak 1 as due to the neutron decay from the known 10.6 MeV state to the first excited state in ^{10}Be(3.368 MeV, 2^+). Our observation of the peak 10 shows that these are decays from the 10.6 MeV state, and our β-n-γ coincidence measurements also indicate decay from the 8.03 MeV state. Table V lists the observed neutron energy, the states in ^{11}Be from which the neutrons are emitted, the measured asymmetry parameter A, and the spin-parity assignments, for the prominent neutron peaks.

The spin-parities of the state decaying to the ground state of ^{10}Be are decisively assigned. Namely, the states at E_x = 2.69, 8.03, and 10.6 MeV are assigned to be of $3/2^-$, $3/2^-$, and $5/2^-$, respectively. The

Table V. Results of β-n coincidence measurements for prominent neutron peaks observed with the high energy neutron detectors.

Peak number	TOF (ns)	E_n (MeV)	E_x in ^{11}Be (MeV) [Ajzenberg-Selov]	A (measured)	I^π (assigned)
10	36.2 ± 0.5	8.86 ± 0.25	10.6	$+0.89 \pm 0.52$	$5/2^-$
1	41.9 ± 0.5	6.61 ± 0.15	8.03, 10.6	-0.33 ± 0.14	$3/2^-$
2	55.7 ± 0.5	3.74 ± 0.07	8.03, 10.6	-0.42 ± 0.09	$3/2^-$
3	60.8 ± 0.5	3.14 ± 0.05	3.89, 3.96	$+0.44 \pm 0.05$	$5/2^-$
4	76.8 ± 0.5	1.97 ± 0.03	2.69	-0.36 ± 0.02	$3/2^-$

observed asymmetry of +0.44 for the peak 3, which is due to neutron decays from both the states at E_x = 3.89 MeV and 3.96 MeV to the ground state of ^{10}Be, indicates that one of these states, of which neutron yield dominates the other one, is of $5/2^-$ and the other state is of either $1/2^-$ or $3/2^-$.

Figure 58 shows the TOF spectrum with the low energy neutron detectors. A large peak at ∼20 ns is due to efficiency enhancement by the resonance of n + ^{6}Li ($E_x(^7\mathrm{Li})$ = 7.460 MeV, $5/2^-$, E_n = 0.245 MeV). Peaks 8 and 9 are most possibly due to decays from the 3.89 MeV and 3.96 MeV states, respectively, to ^{10}Be(3.368 MeV, 2^+). After correcting for detection efficiency, the neutron energy and the branching ratio (the ratio normalized to a parent nucleus $^{11}\mathrm{Li}_{g.s.}$) were determined as listed in Table VI.

Aoi *et al.* observed 80 keV neutrons with plastic scintillators, but their detectors were not sensitive to the 17 keV neutrons. They ignored such neutron decay in their decay scheme, according to Liu *et al.*'s assignment for the 3.89 MeV state to be $3/2^+$ from DWBA analyses of the ^{9}Be(t,p)^{11}Be reaction [Liu and Fortune, Phys. Rev. **C42**, 167 (1992)]. On the other hand, Morrissey *et al.* included the β-decay to the 3.89 MeV state and the successive 17 keV neutron decay, although they did not observe low energy neutrons. Their decay scheme was presumably claimed after Azuma *et al.* [Phys. Rev. Lett. **43**, 1652 (1979)] who have

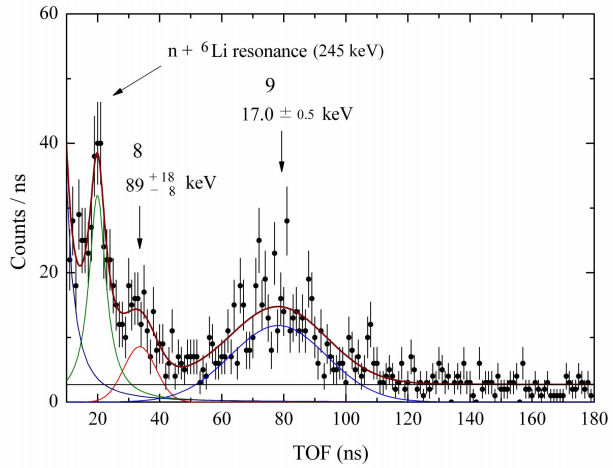

Fig. 58. Neutron TOF spectrum with low energy neutron detectors.

observed 18 keV neutrons as well as the 80 keV neutrons with ^{3}He proportional detectors. Our results apparently support the work by Azuma *et al.* Therefore, the 3.89 MeV state must be of minus parity.

Although the small statistics of the low energy neutron spectrum make it impossible for us either to deduce β-ray asymmetries for the neutron peaks 8 and 9 or to examine the β-n-γ coincidence, we could assign the spin values of the 3.89 and 3.96 MeV states. The key quantities are the branching ratios and asymmetries concerning the first excited state of ^{10}Be (E_x = 3.368 MeV, 2^+): We determined (i) the branching ratios of the neutron decays from the 3.96 MeV and 3.89 MeV states to the 2^+ state of ^{10}Be as 5.3% and 14.0%, respectively, (ii) the branching ratio and asymmetry of the γ-decay from the 2^+ state of ^{10}Be to the ground state as 37.0% and +0.16, respectively, (iii) the branching ratio and asymmetry of the γ-decays leading to the ^{10}Be(2^+) state as 12.7% and $A = -0.27$, respectively. Therefore the following relation must be fulfilled,

$$A_{3.96} \times \frac{0.053}{0.370} + A_{3.89} \times \frac{0.14}{0.370} + (-0.27) \times \frac{0.127}{0.370} + \overline{A} \times \frac{0.060}{0.370} = +0.160,$$

where A_i is the asymmetry parameter of the labelled state and $\overline{A}$ is the average asymmetry for all states which decay to the 2^+ state of ^{10}Be by emitting neutrons. For all possible combinations of A_i, $\overline{A}$'s were evaluated. From the condition that $-1.0 \leq \overline{A} \leq 0.6$, there are three possible cases where the spin-parity of the 3.89 MeV state is always $5/2^-$. Thus, the spin-parity of the 3.89 MeV must be $5/2^-$. As for the 3.96 MeV state, any of three possible spin values can not be excluded because of large errors in $A_{3.96}$. For this state two groups have proposed $3/2^-$ assignment from the DWBA analyses of the ^{9}Be(t,p)^{11}Be reaction at E_t = 23 MeV [Ajzenberg *et al.*, Phys. Rev. **C17**, 1283 (1978)] and at 15 MeV [Liu and Fortune, *op. cit.*], and the energy-level compilation [Ajzenberg-Selov, Nucl. Phys. **A506**, 1 (1990)] has adopted this assignment. In the next beam time with higher beam intensity and higher polarization, the spin-parity assignments of the 3.89 and 3.96 MeV states will be confirmed.

Table VI. Low energy neutron peaks detected with the low energy neutron detectors.

TOF (ns)	E_n (keV)	FWHM (keV)	Branching ratio (%)	E_x in ^{11}Be (MeV) [Ajzenberg-Selov]
$75^{+1.1}_{-2.1}$	17.0 ± 0.5	16.4	$14.0 \pm 2.4(\mathrm{stat})^{+2.1}_{-4.0}(\mathrm{syst})$	3.89
$32.7^{+1.5}_{-2.9}$	89^{+18}_{-8}	65.8	$5.3 \pm 1.9(\mathrm{stat})^{+4.0}_{-0.8}(\mathrm{syst})$	3.96

Many neutron decays leading to the excited states of ^{10}Be exhibit neutron peaks overlapping with each other as typically shown in the energy region below that of peak 4 in Fig. 57. The neutron peaks were decomposed by the β-n-γ coincidence analyses with the help of β-ray asymmetry, and the neutron decay paths were determined. In the case that the small statistics prevented such analyses, the following γ-ray shape analyses were very successful: Some of the γ-rays from ^{10}Be* showed significantly broader line shapes than the detector resolution. This is due to the neutron recoil effect. The line shapes were analyzed by assuming the neutron decay paths and by taking into account the stopping process of ^{10}Be* in the Pt stopper foil and the lifetimes of the γ-ray emitting states of ^{10}Be*, similarly to the Doppler shift attenuation method. It was found, for the first time, that the 8.82 MeV state in ^{11}Be decays to the 6.263 MeV state of ^{10}Be(2^-). In addition, the β-ray asymmetry coincident with the subsequent γ-decay in ^{10}Be (6.263 MeV state (2^-) $\rightarrow$ 3.368 MeV state (2^+)) was measured to be $-0.44(33)$. The neutron decay intensity from the 8.82 MeV state exhausted the γ-decay intensity. Therefore, it is strongly suggested that the 8.82 MeV state is of $3/2^-$. Other neutron decay paths determined from the γ-ray line shape analyses were very consistent with those determined by the β-n-γ coincidence analyses.

Neutrons with $\sim$96 ns flight time in Fig. 57 ("6") are due to the decay from the 5.24 MeV state in ^{11}Be to the 2^+ state of ^{10}Be [Aoi *et al., op. cit.*; Morrissey *et al., op. cit.*]. This was also confirmed by the β-n-γ coincidence measurement in the present work. The β-ray asymmetry in this region in Fig. 57 tends to increase toward positive value. This strongly suggests $5/2^-$ assignment, because the $5/2^-$ state uniquely gives positive asymmetry. Somewhat smaller asymmetry than the expected value of +0.6 is due to the many overlapping peaks in this region and the asymmetry cancellation occurs to a large extent. We therefore assign the 5.24 MeV state to be of $5/2^-$ with high probability.

From the β-n-γ coincidence we could determine the widths of the neutron peaks 5 and 7 which are due to the decay from the 8.03 MeV state. The widths were much smaller than assumed by Aoi *et al.* The widths for other states are known from the ^{9}Be(t,p)^{11}Be reaction [Liu and Fortune, *op. cit.*]. By assuming all the assigned states and decay paths, we reproduced the TOF spectrum and asymmetry as shown in Fig. 59a, but we failed to reproduce the experimental results to a large extent. Therefore, we assumed, in addition, three unknown states in ^{11}Be at 5.61 MeV ($1/2^-$ or $3/2^-$), 9.1 MeV ($3/2^-$), and 10.0 MeV ($5/2^-$) so as to better reproduce both the TOF spectrum and asymmetry. The experimental data are reproduced rather well, as

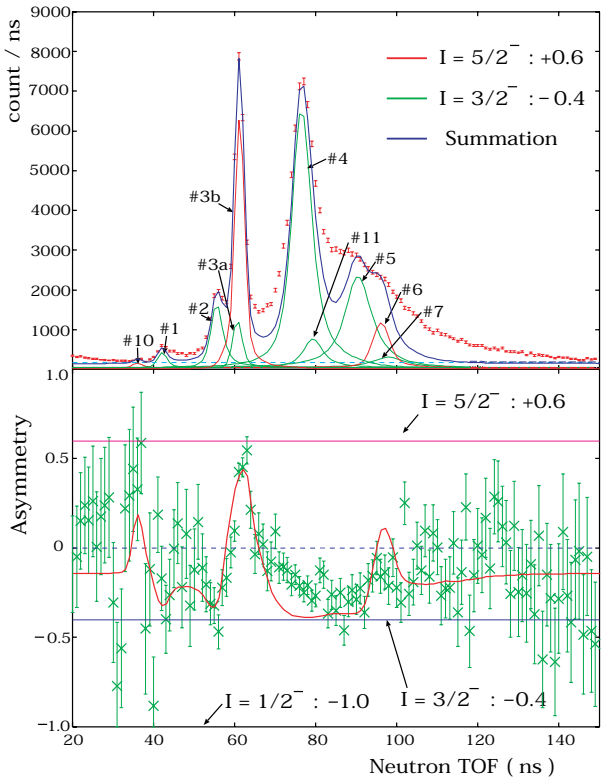

Fig. 59a. Reproduction of TOF spectrum and asymmetry with known states and presently assigned I^π and branching ratio.

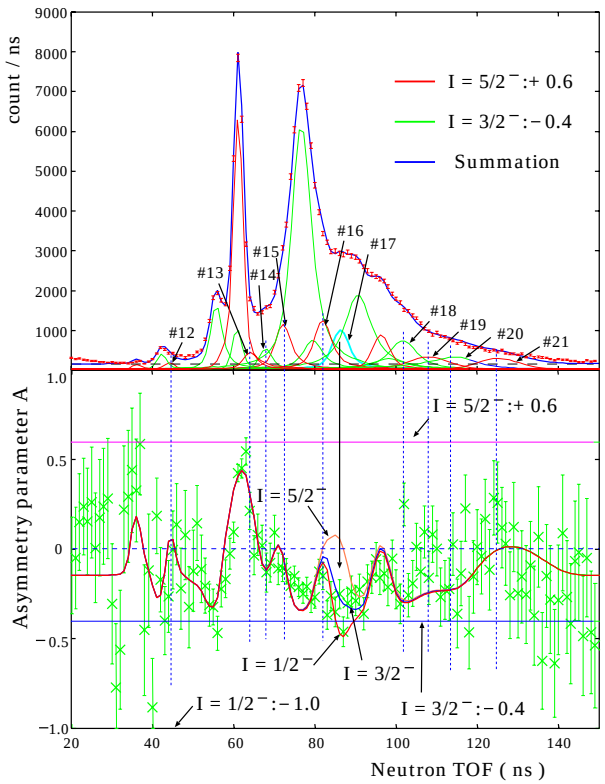

Fig. 59b. Reproduction of TOF spectrum and asymmetry with three more assumed states at 5.61 MeV ($1/2^-$ or $3/2^-$), 9.1 MeV ($3/2^-$), and 10.0 MeV ($5/2^-$).

Table VII. Assigned energy levels in ^{11}Be and logft values of the β-decay of ^{11}Li$_{\rm g.s.}$ to these states. The AMD calculations were made for two cases with different spin-orbit interactions. Very strong interaction of $u_{\ell s} = 3700$ MeV was used so as to reproduce the level inversion of the ground state $1/2^+$ and the first excited state $1/2^-$, but Kanada-En'yo *et al.* recommend $u_{\ell s} = 2500$ MeV to describe the excited states of ^{11}Be.

I^π	$E_{\rm x}$	logft			
		Present work	AMD by Kanada-En'yo *et al.*		
	(MeV)		$u_{\ell s} = 3700$ MeV	$u_{\ell s} = 2500$ MeV	K^π
$1/2^-$	0.32	5.67(8)	5.0	5.5	$1/2^-$
$3/2^-$	2.69	5.0(1)	4.4	5.0	$1/2^-$
$5/2^-$	3.89	4.80(7)	4.5	5.0	$1/2^-$
$3/2^-$	3.96	5.3(1)	4.9	6.2	$3/2^-$
$5/2^-$	5.24	5.55(8)			$3/2^-$
$3/2^-$	8.03	4.30(8)	3.9	4.3	
$3/2^-$	8.82	4.46(7)			
$5/2^-$	10.6	4.13(12)			

shown in Fig. 59b. We therefore claim these three new states in ^{11}Be. These speculations will be confirmed by the asymmetry associated with the β-n-γ coincidence measurements with much higher statistics in the next beam time.

Comparison with theoretical prediction

So far we have assigned spin-parities of some of the levels in ^{11}Be and decay schemes of ^{11}Li and ^{11}Be. The results were compared with theoretical predictions level by level. A recent shell model calculation by Millener [Nucl. Phys. **A693**, 394 (2001)] predicted an excited state with $I^\pi = 3/2^+$ located at 3.89 MeV with the 1-$\hbar\omega$ configuration and another state of $5/2^-$ at 3.96 MeV with the 0-$\hbar\omega$ configuration. Both predictions do not agree with the present assignments. On the other hand, the level sequence and the logft-values are in good agreement with predictions by a fully microscopic calculation of anti-symmetrized molecular dynamics (AMD) [Kanada-En'yo *et al.*, Nucl. Phys. **A687**, 146c (2001); Phys. Rev. **C66**, 024305 (2002)] as listed in Table VII. The logft-values are displayed in four groups, following Kanada-En'yo *et al.*: (i) The states at $E_{\rm x} = 0.320$ ($1/2^-$), 2.69 ($3/2^-$), and 3.89 ($5/2^-$) MeV have logft-values of 4.8–5.7. It is understood that these are the members of the rotational band with $K^\pi = 1/2^-$. (ii) The states at 3.96 ($3/2^-$) and 5.24 ($5/2^-$) MeV have larger logft-values than the first group. These are the members of the rotational band with $K^\pi = 3/2^-$, where development of α-cluster is more dominant than in the $K^\pi = 1/2^-$ band. (iii) The 8.03 and 8.82 MeV states have very small logft-values. One of these may correspond to a state for which it is predicted that the α-clustering is completely broken. (iv) The 10.8 MeV state, for which a large logft value was observed, may have dominant single particle configuration, but there is no corresponding state in AMD.

Experiment 909
Isospin symmetry breaking in superallowed Fermi β-decays
(C.E. Svensson, Guelph)

Precision measurements of the ft values for superallowed $0^+ \rightarrow 0^+$ Fermi β-decays between isobaric analogue states provide demanding tests of the standard model description of electroweak interactions. To date, superallowed ft values have been determined at the $\pm 0.1\%$ level for nine nuclei between ^{10}C and ^{54}Co and, once corrected for small radiative and isospin symmetry-breaking effects, their consistency has confirmed the conserved vector current (CVC) hypothesis at the level of 3×10^{-4}. However, the value of V_{ud} derived by comparing these β-decay data with the purely leptonic muon decay, combined with present knowledge of V_{us} and V_{ub}, indicates a violation of the unitarity of the Cabibbo-Kobayashi-Maskawa (CKM) quark-mixing matrix at the 98% confidence level [Towner and Hardy, Phys. Rev. **C66**, 035501 (2002)]. Should this discrepancy be firmly established, it would indicate the need for new physics, either in terms of explicit quark effects in nuclear structure or an extension of the minimal electroweak standard model. Before a definitive conclusion can be reached, all uncertainties contributing to the unitarity test must be carefully scrutinized and, if possible, reduced. For V_{ud}, the dominant uncer-

tainties are those associated with theoretical corrections to the ft values, and the search for systematic effects has focused on the nuclear-structure dependent δ_C corrections that account for the breaking of isospin symmetry by charge-dependent forces in the nucleus.

Experiment 909 involves a series of measurements with the 8π spectrometer and SCEPTAR β array aimed at constraining the above-mentioned isospin symmetry-breaking corrections in superallowed Fermi β-decays. This program will take advantage of the unique beams of radioactive ions available at ISAC to study particular decays in which the predicted δ_C corrections show the greatest model sensitivity. An initial focus of Expt. 909 will be on precise lifetime and branching ratio measurements for ^{34}Ar, with the aim of establishing the superallowed ft value at the $\pm 0.1\%$ level. The uncertainty in the ^{34}Ar superallowed ft value is currently dominated by the uncertainty in the half-life, 844.5 ± 3.4 ms. With high-intensity beams of ^{34}Ar expected from the new ISAC ECR ion source in the spring of 2003, the first objective will be to improve this half-life precision by approximately an order of magnitude. These measurements will be carried out by collecting samples of ^{34}Ar at the centre of the 8π and following their decay for $\sim$30 half-lives by time-stamping γ-rays emitted from excited states in the daughter ^{34}Cl populated in Gamow-Teller decay branches of ^{34}Ar.

In anticipation of ^{34}Ar beams from the ISAC ECR ion source in early 2003, two commissioning runs with radioactive ^{26}Na beams were carried out as part of Expt. 909 during 2002. This isotope was chosen because i) high yields were available from ISAC surface ion sources, ii) the half-life ($\sim$1.07 s) is similar to ^{34}Ar, iii) the daughter ^{26}Mg is stable, and iv) $\sim$99% of ^{26}Na β-decays are followed by the 1809 keV γ-ray transition in ^{26}Mg, facilitating tests of the γ-ray lifetime technique to be employed for ^{34}Ar. The first requirement was to determine a precise value for the ^{26}Na lifetime. To this end, a ^{26}Na beam was delivered in May to the fast tape system at the ISAC GPS station and its lifetime determined to high precision by the well-established and well-understood 4π gas proportional β counter technique. A sample of the data from a single run from this experiment is shown in Fig. 60. A total of 32 runs were conducted under various experimental conditions to check for systematic effects. The analysis of these data is nearing completion, and will establish the ^{26}Na lifetime at the desired $\pm 0.05\%$ level (20 times better than previously known). During the May run, the ^{26}Na beam was also delivered to the 8π spectrometer at ISAC as the first radioactive beam commissioning of the newly completed low energy beam transport to the 8π.

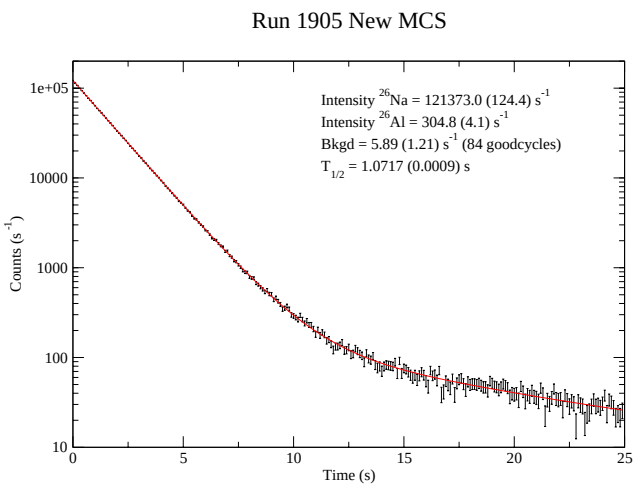

Fig. 60. Decay curve from a single run of β counting ^{26}Na samples with the 4π gas proportional counter at the ISAC GPS station.

With upgrades to the 8π electronics completed in the summer of 2002, a second ^{26}Na experiment was carried out in August, 2002. The spectrum of γ-rays from approximately the first 2.5 hours of collecting continuous ^{26}Na beam at the centre of the 8π is shown in Fig. 61. γ-rays with yields down to $\sim 10^{-5}/\beta$-decay, including many transitions above 5 MeV not previously known in ^{26}Na β-decay, were observed. These data, together with simultaneously recorded high-efficiency γ-γ coincidence data that will establish coincidence relationships between transition in the daughter nucleus, illustrate the power of a large multi-detector such as the 8π spectrometer for performing high-precision branching ratio measurements. The primary objective of the August experiment, however, was to test the γ-ray lifetime technique. For the majority of the experiment, samples of ^{26}Na ions were thus collected during a brief ($\sim$1 s) beam-on period and their

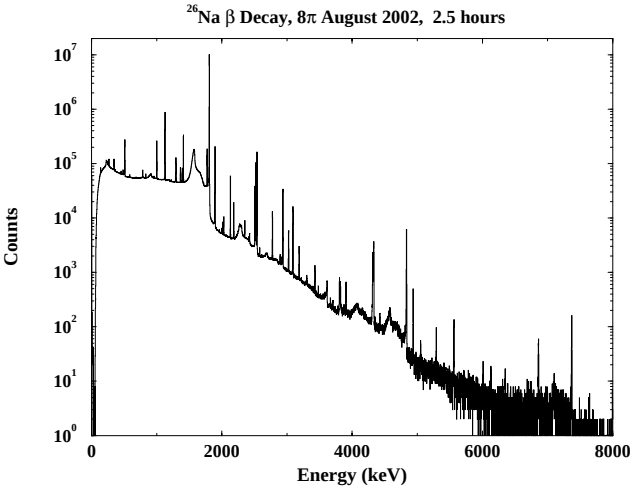

Fig. 61. γ-ray spectrum from $\sim$2.5 hours of continuous ^{26}Na beam to the 8π spectrometer at ISAC.

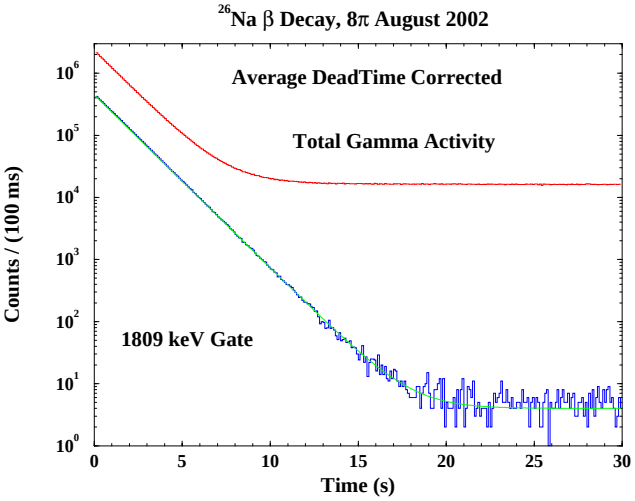

Fig. 62. Summed γ-ray decay curves from a single run of the August ^{26}Na experiment with the 8π spectrometer at ISAC. The upper curve is the total γ activity, while the lower curve has been gated on the photopeak of the 1809 keV transition in the daughter ^{26}Mg.

decay then followed over a 30 s (28 half-lives) beam-off period. Figure 62 shows the data from a single run of this experiment. While the total γ activity in the HPGe detectors of the 8π becomes dominated by room background after about 8 half-lives, the decay curve measured in coincidence with the 1809 keV photopeak from ^{26}Mg provides more than 16 half-lives before the background is reached. This single run provides a statistical precision of $\pm$0.05% for the ^{26}Na half-life. A total of 36 runs under intentionally varied experimental conditions were performed during the August experiment. These data are currently being analyzed to constrain systematic effects associated with the γ-ray lifetime technique that will be used to perform the high-precision lifetime measurement for the superallowed emitter ^{34}Ar when beams from the ISAC ECR ion source become available in early 2003.

Following measurement of the ^{34}Ar lifetime, subsequent measurements with the 8π and SCEPTAR will focus on an improved determination of the ^{34}Ar superallowed branching ratio. Large, and model-dependent, isospin symmetry-breaking corrections are also predicted for the $A \geq 62$ odd-odd $N = Z$ nuclei. A program of precision lifetime measurements (Expt. 823) for these nuclei with the 4π gas proportional counter at the ISAC general purpose station is being led by G.C. Ball of TRIUMF. Future experiments with the 8π spectrometer and SCEPTAR will provide branching ratio measurements for these short-lived isotopes. Weak non-analogue Fermi decay branches that provide direct, and absolute, information on one component of the isospin symmetry breaking will also be measured. Initial measurements of ^{74}Rb decay by our collaboration with a single HPGe detector have identified a number of high-energy γ-rays from excited states in the daughter ^{74}Kr [Piechaczek *et al.*, submitted to Phys. Rev. C]. The high γ-γ efficiency of the 8π spectrometer will be used to clarify the coincidence relationships between these γ-rays and identify further γ-ray transitions following weak Gamow-Teller decay branches, with the aim of establishing the superallowed branching ratio at the $\pm$0.05% level. With the continued development of ion source technology at ISAC, these superallowed and non-analogue Fermi β-decay branching ratio studies will be extended to include ^{62}Ga and ^{70}Br.

Experiment 925
Isospin mixing in ^{36}Ar via spin-polarized observables in ^{36}K β^+ decay

(J.A. Behr, M.R. Pearson, TRIUMF; K.P. Jackson, TRIUMF/SFU)

This experiment would measure the isospin mixing between the first two $I^\pi = 2^+$ excited states of ^{36}Ar and the lowest 2^+ T=1 isobaric analogue state, using spin-polarized ^{36}K beta decay observables with TRIUMF's neutral atom trap. The main purpose is to help test isospin mixing models in the *sd* shell needed for determination of the superallowed Fermi strength in $0^+ \rightarrow 0^+$ decays (and hence CKM matrix unitarity), as the calculation's methodology is the same. The β asymmetry A_β and neutrino asymmetry B_ν would show deviations linear in the ratio M_F/M_{GT} produced by isospin mixing from the values of 1/3 and –1/3 predicted if they were pure Gamow-Teller transitions.

^{36}K was successfully trapped, the shortest-lived isotope ($t_{1/2}$=0.34 s) for which neutral atoms have been trapped. ^{36}K was produced from the TiC target at $\sim 1 \times 10^6$/s, which allowed trapping and initial tests but was insufficient for the isospin mixing experiment. The additional Ti:sapph when frequency-locked is expected to produce 3$\times$ more capture efficiency, and we had better ^{36}K/^{37}K production ratio for Ca. There are conceptual designs for $CaZrO_3$/Zr foil hybrid targets to handle more beam than the 2.5 μA limit of our $CaZrO_3$ ceramic target.

To do a viable experiment for A_β in ^{36}K, β^+ tracking is needed to ensure the atoms decay from the trap volume. We intend to build Be-windowed wire chambers for this purpose. We did not polarize ^{36}K, but tests done with polarized ^{37}K demonstrated the difficulties of measuring A_β with a trap. The trap has a lifetime for stable species of 45 s, limited by the 3×10^{-10} torr vacuum, so some atoms decay from the walls and not from the trap, producing β singles backgrounds. Shown in Fig. 63 is the effective asymmetry measured as a function of vacuum, with vacuum deliberately spoiled to enhance this effect. A correction of $\approx$1% can be deduced by extrapolating to the known ^{37}K decay rate

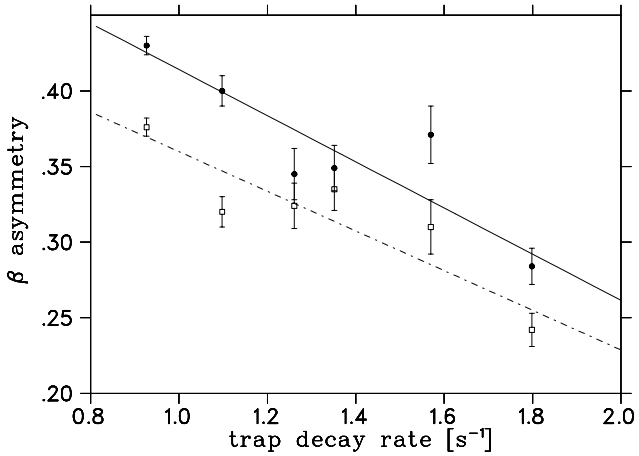

Fig. 63. The measured ^{37}K β singles asymmetry as a function of trap lifetime for the two CaF_2(Eu) detectors. This demonstrates the difficulty of measuring β singles to the accuracy required for ^{36}K isospin mixing experiments without β^+ tracking.

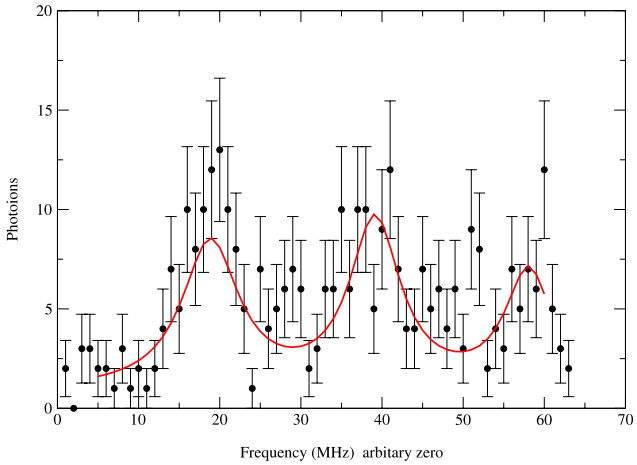

Fig. 64. Hyperfine structure of $S_{1/2}$ F=5/2 to $P_{3/2}$ F=7/2, 5/2, 3/2 states in ^{36}K, as measured by resonant excitation with the trap off followed by non-resonant photoionization.

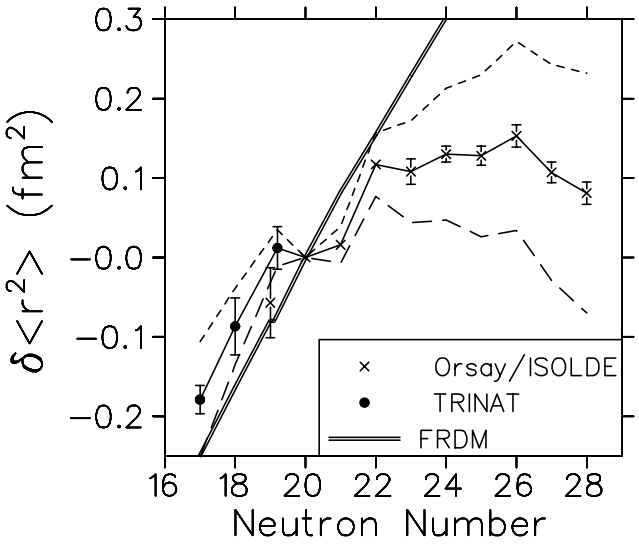

Fig. 65. Deduced ^{36}K charge radius plotted with potassium isotopes previously measured at TRIUMF and at ISOLDE [Mårtensson-Pendrill *et al.*, J. Phys. **B23**, 1749 (1990)]. The K isotopes for $N<20$ follow the finite-range droplet model (FRDM). The dashed lines show systematic effect of the specific mass shift.

of 0.81 s^{-1} (i.e., no trap losses). The lack of agreement between the two back-to-back detectors is not understood, and implies additional backgrounds.

The same isospin mixing information is contained in B_ν, which can be measured using β-recoil coincidences free of such backgrounds, but this would be severely statistics limited at present rates.

Polarization of ^{36}K was not attempted. The M.Sc. thesis of O. Aviv from Tel Aviv is to extract the $\beta-\nu$ correlation parameter a from the Gamow-Teller and the analogue transitions to the accuracy allowed from the present 600 coincidences measured. Momentum reconstruction techniques developed for the ^{38m}K experiment are being used to separate the different final states.

The optical hyperfine structure needed for future optical pumping was measured, from which the charge radius and the quadrupole moment can be derived. USD calculations [Brown, private communication] predict the quadrupole moment to be an order of magnitude smaller than for other potassium isotopes, and our preliminary result is not in agreement. We show the preliminary result for the ^{36}K measurement in Fig. 64 and the deduced ^{36}K charge radius in Fig. 65. The charge radii for $N<20$ are in agreement with the finite range droplet model, in contrast with those for $N>20$. These data were taken in 8 hours, with ~20 atoms trapped, and demonstrate the sensitivity of our two-step photoionization methods to perform accurate atomic spectroscopy on small numbers of atoms.

Experiment 928
Level structure of ^{21}Mg: nuclear and astrophysical implications
(A. Murphy, Edinburgh)

The TUDA collaboration is pleased to announce that Expt. 928 successfully took data in November. Good statistics were accrued with all necessary stable and radioactive beams, and analysis of the data taken is currently progressing.

The objective of the experiment was to measure the parameters of states in the resonant ^{21}Mg nucleus, which determine the ^{20}Na$(p,\gamma)^{21}$Mg reaction rate. This reaction is thought to be an integral link in

the path of breakout from the hot-CNO cycle to the rp-process that may occur in novae and X-ray bursts. Furthermore, accurate knowledge of these excited states may be compared to those of isobaric analogue states and thus a study of the Thomas-Ehrman shifts made.

In order to determine the parameters of resonant states in ^{21}Mg, resonant elastic scattering of protons was employed. Experimentally, this consisted of impinging a radioactive ^{20}Na beam on to a hydrocarbon foil, and then detecting the recoil protons. The beam was generated by ISAC, using a primary silicon-carbide target with a driver beam of typically 20 μA of 500 MeV protons. Typical beam currents on target in the TUDA chamber were a few pA, and during the experiment beam energies of 1.25 MeV/u and 1.60 MeV/u were requested. Accurate confirmation of the beam energies was assured by making measurements in both the Prague magnet, and then cross checking with the DRAGON spectrometer. This consisted of sending the beam in to each device and focusing the beam on to a set of exit slits (after the first magnetic dipole in the case of DRAGON), and then measuring each independently calibrated field. For the higher beam energy, where the maximum rigidity of the DRAGON MD1 magnet was unable to sufficiently bend the beam, this required first introducing gas in to the DRAGON target volume to slow the beam. Measurements of the required magnetic field were performed with various pressures of gas, and an extrapolation to zero gas pressure made. In all cases, an agreement between the beam energy measured with the Prague magnet and with DRAGON of ~1 keV/u was observed.

The target consisted of ~795 μg/cm^2 of CH_2. Such a thickness results in a significant spread of energies at which elastic scattering reactions can take place, corresponding to the depth in the target at which the reactions occur. For the lower beam energy, reactions can occur at ~0.51–1.20 MeV in the centre-of-mass, and for the higher beam energy between ~0.91–1.54 MeV.

Detection of the recoiling protons was achieved in two LEDA-design silicon detector arrays. These were placed downstream of the target at 19 and 62 cm. Preliminary spectra of protons observed in detecting elements placed at a laboratory scattering angle of 15.6° are shown in Fig. 66. This shows protons being detected with a range of energies in agreement with that predicted due to the width of the target. Rutherford scattering determines that the yield in general falls off with higher energy, but superimposed on this are three distinct resonances, with approximate energies of 4.01, 4.26 and 4.44 MeV (excitation energy in ^{21}Mg). Observation of the lowest energy state was the primary goal of this experiment. The states at 4.01 and 4.26 had already been observed, but the highest energy state is entirely new. Accurate determination of the energies, widths and spins of these states will require R-matrix analysis (multi-channel and allowing the possibility of non-zero angular momentum transfer), and this is currently getting under way.

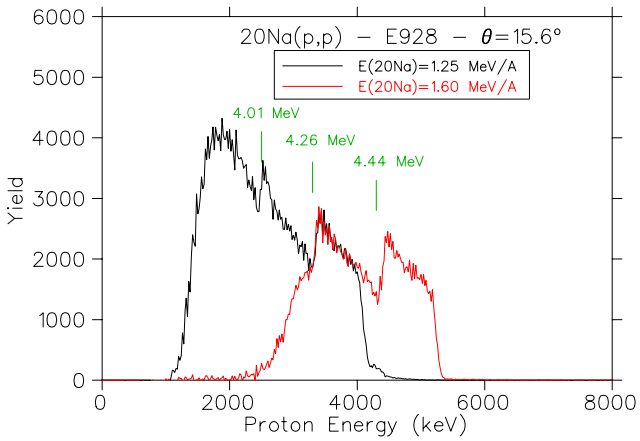

Fig. 66. Preliminary spectrum of proton energy observed in the ^{1}H(^{20}Na,^{1}H)^{20}Na reaction.

Experiment 930
π^- capture in water and light materials
(Y. Efremenko, Tennessee; T. Numao, TRIUMF)

Asymmetric production of neutrino species is an essential factor in appearance experiments of neutrino oscillation. The production of $\overline{\nu}_e$ at low energy is thought to be significantly suppressed over that of ν_e; the conventional belief is that π^+'s freely decay but π^-'s, after stopping in the beam moderator, are immediately absorbed by a nucleus without a chance of decay. This results in a large asymmetry in the $\overline{\nu}_e$ and ν_e productions, which is further enhanced by the larger π^+ production cross section by a factor of ~5. However, if a π^- stays long enough either freely or bound in an atomic orbit, it has a chance to decay to a μ^- that would subsequently produce a $\overline{\nu}_e$.

The goal of Expt. 930 is to measure the free-decay fraction of the π^- stopped in water and light materials at a sensitivity of <0.1 %. Direct modes of search are to detect delayed electrons from the decay $\pi^- \to e\overline{\nu}$ and from the main pion decay mode, the decay $\pi^- \to \mu^-\overline{\nu}$ followed by $\mu^- \to e^-\nu\overline{\nu}$, ($\pi \to \mu \to e$ chain). The backgrounds come from Compton scattering of radiative pion capture γ-rays for the decay $\pi^- \to e\overline{\nu}$ and from decay-in-flight of π^-'s in the beam (or muon contamination in the beam) for $\pi \to \mu \to e$ chain. Other modes to be sought are $\pi^- + (Z) \to (Z-1)^* + \gamma$, $\pi^- + p \to n + \pi^0$, and $\pi^- + O \to X + p$. These capture modes are almost background-free in the delayed part, but a good time resolution (about 200 ps or better) is required to reach a sensitivity of 10^{-3} in the free-decay fraction.

A 75 MeV/c π^- beam at M9A was stopped at rates of 10–30 KHz in an 8 mm thick water target after passing through two sets of wire chambers and beam counters. The decay (and reaction) products were observed by two arm telescope systems located at ±90°. Each telescope consisted of three plastic counters spanning about 2–5% in solid angle followed by a large NaI crystal (46 cmϕ × 51 cm and 36 cmϕ × 36 cm) placed about 30 cm from the beam axis. Data were taken with a π^- beam as well as a π^+ beam to calibrate the system and provide normalizations. Other possible moderator materials, such as beryllium and aluminum, were tested as well.

In the data analysis, events originating from a pion were selected based on the energy losses in the two beam counters and the time of flight (TOF) with respect to the cyclotron rf phase. Each type of decay product was selected based on the energy loss measurements in the telescope counters and the remaining energy in the NaI detectors.

Figure 67 shows energy spectra of positrons (closed triangles) and electrons (open triangles). The electron spectrum is based on a higher statistic π^- sample by more than an order of magnitude. The peak around 70 MeV in the positron spectrum is from the decays $\pi^+ \rightarrow e^+\nu$, and the bumps around 50 MeV in both spectra are from the $\pi \rightarrow \mu \rightarrow e$ chain (including the contribution from muons in the beam). For the measurements of proton time spectra, the time zero position was corrected for the time walk, momentum dependences (beam and proton) and TOF. Figure 68 shows a time spectrum of protons after π^- capture, which is consistent with a gaussian distribution with $\sigma \sim 200$ ps. No events in the region $t > 5$ ns were present in the spectrum. This preliminary result indicates that the free-decay fraction of the π^- in water is <1%. A preliminary study of the decay $\pi^- \rightarrow \mu^- \rightarrow e^-$ also provided a similar limit. The analysis that aims for a sensitivity of <0.1% is in progress.

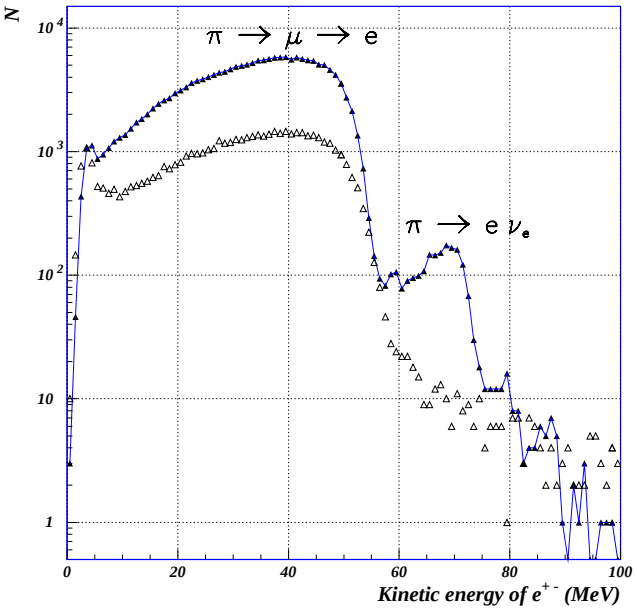

Fig. 67. Energy spectra of positrons (closed triangles, connected) and electrons (open triangles).

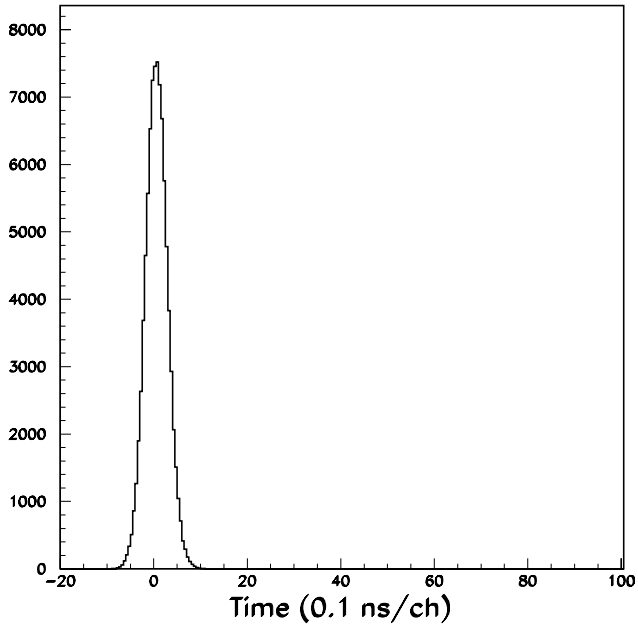

Fig. 68. Time spectrum of protons after corrections.

Other studies with the 8π spectrometer

Several nuclear physics experiments have been performed with the 8π γ-ray spectrometer in either off-line or parasitic mode. These are reported below.

The half-life of ^{176}Lu

(G.F. Grinyer, Guelph)

Measurements of the half-lives of certain long-lived isotopes are typically dominated by experimental uncertainties in detector efficiencies, solid-angle coverage, internal conversion, self-absorption, angular correlations and true-coincidence summing. In particular, published half-life values for ^{176}Lu, of interest for geochronological studies, range from 21 to 73 billion years and show scatter far greater than the experimental uncertainties. As a result, the precision of Lu-Hf deduced ages is currently limited by uncertainties in the ^{176}Lu decay constant. We have employed a unique γ-γ coincidence method that takes advantage of the inherent symmetry within the 8π γ-ray spectrometer at ISAC, and eliminates many of the above uncertainties. The experiment was performed in February, 2002, and was the first on the 8π since its relocation to TRIUMF in 2001. A small sample of enriched Lu_2O_3 powder was placed at the centre of the 8π array and data were

taken for 48 hours live time. Our method reduces the calculated corrections to only 3% and led to the result $T_{1/2} = 40.8 \pm 0.3$ billion years [Grinyer *et al.*, Phys. Rev. C (in press)] which is now sufficiently precise for geochronological work.

The spontaneous decay of ^{178m2}Hf ($T_{1/2} = 31$ y)
(P.M. Walker, TRIUMF/Surrey, UK)

Nuclear isomers provide probes into a variety of nuclear-structure facets [Walker and Dracoulis, Nature **399**, 35 (1999)], especially the interplay between individual-particle and collective modes of excitation. An outstanding isomer is the 31 year, 2.4 MeV state in ^{178}Hf. This, the second metastable state of ^{178}Hf, is designated ^{178m2}Hf. It carries 16 units of angular momentum. On account of its long half-life and high excitation energy, ^{178m2}Hf has attracted much interest. In particular, it has been reported [Collins *et al.*, Phys. Rev. Lett. **82**, 695 (1999)] that the decay of ^{178m2}Hf can be induced by X-rays, opening up the possibility of novel energy-storage devices. However, the issue remains controversial [Ahmad *et al.*, Phys. Rev. Lett. **87**, 072503 (2001)].

The X-ray-induced decay may proceed through new pathways, from the 31 year isomer at 2.4 MeV to the ground state. Also, the known [van Klinken *et al.*, Nucl. Phys. **A339**, 189 (1980)] spontaneous decay path may involve additional weak γ-ray branches, which are important for understanding the breakdown of the K quantum number. (K is the projection onto the nuclear symmetry axis of the total angular momentum.)

In order to clarify the nature of the decay of this exceptional isomer, we have used the 20-Ge detector, 8π Compton suppressed spectrometer at TRIUMF, to obtain a high statistics γ-γ coincidence data set. The 0.4 μCi source of ^{178m2}Hf (provided by SRS Technologies, Alabama) was extracted from a Los Alamos beam dump, and placed at the centre of the 8π spectrometer. No TRIUMF or ISAC beams were involved. The ^{178m2}Hf source also contained ^{172}Hf ($T_{1/2} = 1.9$ years) with an approximately equal decay rate. More than 10^9 two-fold γ-γ coincidence events have been recorded during four weeks of data-taking, including, for each event, the relative γ-ray times over a 2 μs range.

Preliminary analysis of the data has revealed two new γ-ray transitions emitted directly from the 31 year isomer, each accounting for about one part in 10^4 of the total decay rate. One is a 310 keV transition with M4 multipolarity, and the other is a 587 keV, E5 transition. The observation of these two high-multipolarity, K-forbidden transitions establishes the quality and sensitivity of the new data set. Other possible transitions are under investigation.

The β decay of ^{150g}Eu ($T_{1/2} = 36$ y)
(P. Schmelzenbach, Oregon State)

Numerous studies have been made of nuclei that are sufficiently far enough away from a closed shell that they exhibit collective behaviour. In the past, and now recently, there has been particular interest in such a region of nuclei with 90 neutrons. In these nuclei, the addition or removal of a pair of neutrons results in a sudden change in nuclear properties. The onset of this transition is observed in nuclei with 88 neutrons. By studying N = 88 nuclei, a more stringent test can be applied to transition models. In particular, it is important that nuclear levels and γ-ray intensities be well known, especially those below the pairing energy of about 2 MeV. In an effort to establish a more correct level scheme for ^{150}Sm, nuclear levels of ^{150}Sm were studied through the β decay of ^{150}Pm ($T_{1/2} = 2.9$ h, Q = 3454 keV, $J^\pi = 1^-$), ^{150m}Eu ($T_{1/2} = 12.8$ h, Q = 2303 keV, $J^\pi = 0^-$), and ^{150g}Eu ($T_{1/2} = 35.8$ y, Q = 2261 keV, $J^\pi = 5^-$). In combination with other experiments, these β decay experiments are particularly useful in determining levels because of the parent's various spins, and Q values. The three parent nuclei were all produced at the 88″ cyclotron located at Lawrence Berkeley National Laboratory. The short-lived parent nuclei were counted in 1999 at the 8π, then located at LBNL. This particular study investigated the levels of ^{150}Sm, populated through the beta decay of ^{150g}Eu ($T_{1/2} = 35.8$ y). This source was allowed to cool for 3 years. A portion of this source, with an activity of 6.8 μCi, was counted for a total of 175 h in December, 2002 at TRIUMF using the 8π spectrometer. Preliminary results have revealed approximately 165 γ-rays placed in a consistent level scheme (including about 35 new γ-rays previously unreported from this decay.) No new levels have been proposed below 2 MeV based on this decay, although some known levels have been seen for the first time from the long-lived europium. Further analysis, including angular correlations, may help determine uncertain spin assignments for some of these levels.

β-decay of ^{11}Li
(F. Sarazin, TRIUMF)

The structure of ^{11}Li, a ^{9}Li core surrounded by two distant neutrons (the so-called halo), has been investigated in many different ways in the past two decades to improve our understanding of the halo wave function. Among them, the study of the ^{11}Li β-decay has provided very useful information on how the halo wave function influences the weak interaction process. It has also been found that the daughter nucleus, ^{11}Be, has an abnormal level sequence, suggesting an inversion of the $1p_{1/2}$ and $2s_{1/2}$ single particle neutron orbits. However, discrepancies in γ-ray intensities exist among

these previous experiments, mostly due to low statistics and large background. A more precise study of the ^{11}Li β-decay is likely to resolve these discrepancies and bring new insights on these two important topics.

In August, a beam of ^{11}Li was implanted into a thin Al foil at the centre of the array of 20 HPGe detectors comprising the 8π γ-ray spectrometer. In this experiment, the ^{11}Li β-decay was investigated for the first time with a high-efficiency γ-array of Compton-suppressed germanium detectors. A total of 8.1M γ-singles and γ-γ coincidence events were collected over a 2.5 day period.

Because of the very neutron-rich nature of ^{11}Li and ^{11}Be, their mass difference is quite large (Q_β = 20.61 MeV) and their neutron separation energies are low (S_n = 0.503 MeV for ^{11}Be). Therefore, the ^{11}Li β-decay leads almost exclusively to unbound states in ^{11}Be, which subsequently decay mainly by neutron emission. To study these states, one is required to detect the neutron(s) emitted and/or the γ-ray cascades in the corresponding daughter nucleus. In the present case, the dominant β-decay path of ^{11}Li, besides the direct decay to the first and only bound excited state of ^{11}Be, is via β-delayed one-neutron emission into ^{10}Be. The level structure of ^{10}Be is well known up to the one-neutron separation energy at 6.812 MeV (see Fig. 69). It is therefore not necessary to detect the neutron to identify the states that are populated by one-neutron emission in ^{10}Be.

The γ-decay cascades of the ^{10}Be excited states observed in this experiment are shown in Fig. 69. Three new transitions have been observed for the first time in a ^{11}Li β-decay experiment, as a result of the unique capability of the 8π for decay studies.

The relatively high efficiency of the array makes it possible to observe weak branches of the decay, even at high energy. Although observed in other types of experiment, a transition at 5.96 MeV has been observed for the first time following the β-decay of ^{11}Li. It could have been assumed that only very weak branches would remain to be seen at lower γ-energy. However, thanks to the Compton suppressed configuration of the array, a new transition, shadowed in previous experiments by the strong contribution of the single escape peak of 3368 keV, has been observed at 2895 keV (see Fig. 70). This 2895 keV transition is a signature that the 6263 keV 2^- state is fed by a neutron branch never observed before.

The relative intensities of the γ-rays observed in this experiment for the β-decay of ^{11}Li are about a factor of 10 more precise than previous data [Morrissey *et al.*, Nucl. Phys. **A627**, 222 (1997)], sufficient to resolve previous discrepancies.

To push the analysis further, the neutron energies are required to determine which states in ^{11}Be are linked with which states in ^{10}Be. In this experiment, we are investigating the possibility of deducing the neutron energy information from the lineshape analysis of the γ-peaks recorded with the 8π spectrometer. Indeed, as can be seen in Figs. 70 and 71, these peaks display Doppler-broadened lineshapes, due to the ^{10}Be momentum kick induced by the β-delayed neutron emission. The lineshapes observed for the γ-decay of a given excited state in ^{10}Be depends on the relative intensities

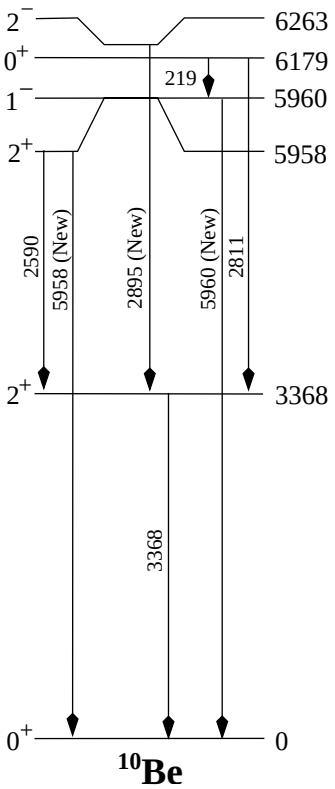

Fig. 69. Level scheme of ^{10}Be below S_n = 6.812 MeV and γ-transitions observed in this experiment.

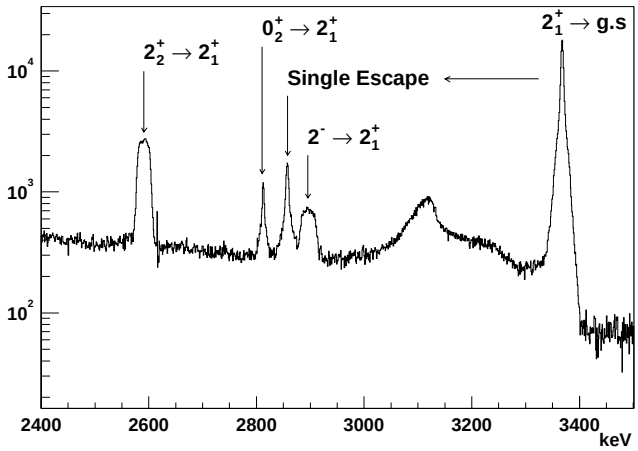

Fig. 70. γ-transitions in ^{10}Be observed in the 2.4–3.5 MeV range.

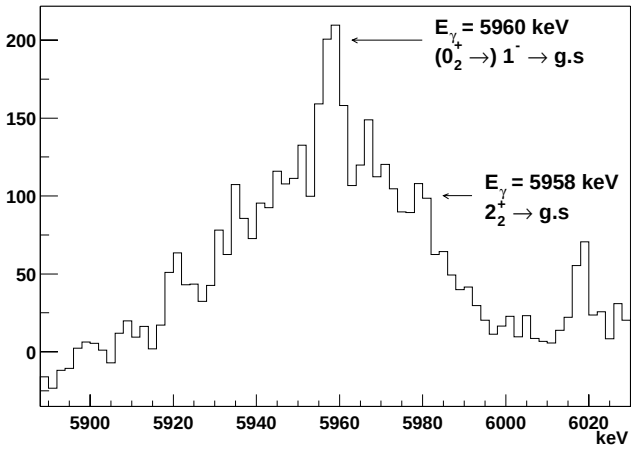

Fig. 71. Structure of the 5.96 MeV peak after room background subtraction.

of all the neutron branches feeding the state either directly or indirectly, and on the lifetimes of the excited states in ^{10}Be involved in a particular decay path. It is possible, in principle, to deduce the neutron energies of these branches from a careful lineshape analysis. A Monte Carlo simulation is under development to reproduce the lineshapes of the peaks of interest and possibly extract new information such as lifetime measurements of excited states in ^{10}Be and/or previously unobserved neutron branches.

In the meantime, one can already immediately extract information from the lineshape of the 5.96 MeV peak. As shown in Fig. 71, the lineshape of the 5.96 MeV peak clearly displays 2 separate components: a broad one corresponding to the decay of the short-lived ($\tau < 55$ fs) 5958 keV state and a sharper one corresponding to the longer-lived ($\tau \sim 800$ fs) 6179 keV state, which is observed to decay to the 5960 keV level (see Fig. 69).

The present study is complementary to Expt. 903 (Shimoda *et al.*), also being performed at ISAC, which makes use of a polarized ^{11}Li beam to measure β-n and β-n-γ coincidences and deduce the spin and parity of the excited states populated in ^{11}Be. The comparison between our lineshape analysis and the Osaka data should provide a more detailed understanding of the ^{11}Li β-decay through β-delayed one-neutron emission.

LANSCE Experiment NPDGamma
Measurement of the parity-violating gamma asymmetry A_γ in the capture of polarized cold neutrons by para-hydrogen, $\vec{n} + p \rightarrow d + \gamma$.

(S.A. Page, W.D. Ramsay, Manitoba)

Introduction

Despite several decades of intense experimental and theoretical effort, the strength of the pion exchange contribution to the weak nuclear force [Desplanques *et al.*, Ann. Phys. **124**, 449 (1980)] remains a mystery. The most precise measurements to date from parity mixing in ^{18}F [Page *et al.*, Phys. Rev. **C35**, 1119 (1987); Bini *et al.*, Phys. Rev. Lett. **55**, 795 (1985)] indicate a coupling constant consistent with zero, in contrast to a relatively large value implied by measurements of the anapole moment of ^{133}Cs via atomic parity violation. The *np* system is the only two nucleon system that is sensitive to the weak meson-nucleon coupling f_π^1 and can provide a clean measurement free of nuclear structure uncertainties. The up-down γ-ray asymmetry relative to the neutron spin direction in the reaction $\vec{n} + p \rightarrow d + \gamma$ at very low energy is sensitive almost exclusively to f_π^1. Previous measurements [Cavaignac *et al.*, Phys. Lett. **B67**, 148 (1977); Alberi *et al.*, Can. J. Phys. **66**, 542 (1988)] of A_γ failed to reach sufficient precision to test model predictions, and set only upper bounds that were less definitive than the ^{18}F experiments noted earlier. Advances in techniques for producing high intensity beams of polarized, cold neutrons now make possible for the first time a measurement of A_γ and hence f_π^1 to within 10% of model predictions [Desplanques *et al.*, Ann. Phys. **124**, 449 (1980); Bowman *et al.*, experiment proposal: "Measurement of the Parity-Violating Gamma Ray Asymmetry A_γ in the Capture of Polarized Cold Neutrons by Para-Hydrogen, $\vec{n}+p \rightarrow d+\gamma$", submitted to the US DOE (1998); Wilburn and Bowman, Phys. Rev. **C57**, 3425 (1998), and references therein].

The $np \rightarrow d\gamma$ experiment [Bowman *et al., op. cit.*; Wilburn and Bowman, *op. cit.*] will be the first of a new program of fundamental electroweak symmetry experiments to be run at the Lujan Center spallation neutron source at LANSCE, Los Alamos National Laboratory. An international team from 12 scientific institutions has been assembled to prepare the experiment.

Two University of Manitoba researchers (S.A. Page and W.D. Ramsay) joined the collaboration in the fall of 1999. We have taken responsibility for precision monitoring of the neutron beam flux, and have designed a new current mode beam monitor that was tested successfully in the fall of 2001 at LANSCE. Three additional beam monitors based on this new design are currently under construction for the experiment. During the past year we expanded our role, with vital infrastructure support from TRIUMF, to include design and construction of an integrated stand for the gamma detector array and liquid hydrogen targets. TRIUMF also engineered a computer controlled motion system to move the CsI array horizontally and vertically by precisely determined distances up to ± 5 mm. The Manitoba/TRIUMF group will work on commissioning of the apparatus and on diagnosis and minimization of systematic errors. The experiment is sched-

uled for installation and testing during 2003, followed by a full calendar year of data-taking.

Apparatus

The basic requirements of the experiment are an intense source of polarized cold neutrons, a liquid parahydrogen target, a high-efficiency, large solid angle γ-ray detector, and a means of reversing the spin of the neutron beam with minimal effect on other beam properties. At LANSCE, the neutron beam will be produced by a 200 μA 800 MeV proton beam pulsed at 20 Hz impinging on a tungsten spallation target; MeV neutrons emerging from the target will be cooled in a liquid hydrogen moderator and transported via a supermirror guide to the experimental apparatus (Fig. 72), where they will emerge with a time-of-flight distribution indicated in Fig. 73. The supermirror guide will enhance the total neutron flux in the desired energy range (0–15 meV) by about a factor of 3 with respect to the Maxwellian distribution of neutrons emerging from the moderator. The pulsed beam enables the neutron energies to be determined from their times of flight.

Neutrons will be polarized in the vertical direction by selective transmission through a nuclear-polarized ^{3}He gas cell which acts as a spin filter, producing the energy dependent polarization spectrum indicated in Fig. 73. The neutron beam intensity will be measured with a ^{3}He/N_2 ionization chamber before the ^{3}He cell, and again at the end of the beam line with a similar device. A third beam monitor will be inserted downstream of the ^{3}He cell for diagnostic purposes; the transmission of the ^{3}He cell serves as an on-line measurement of its polarization and hence that of the neutron beam.

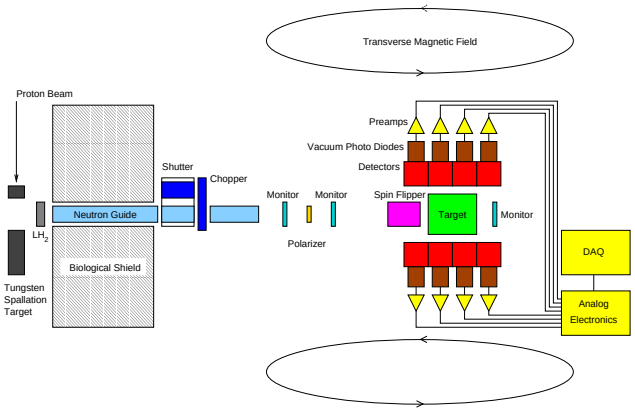

Fig. 72. $np \to d\gamma$ experimental apparatus at LANSCE. Cold neutrons from the LH_2 moderator travel through a supermirror neutron guide, are polarized by a polarized ^{3}He spin filter and are captured in the liquid para-hydrogen target. The 2.2 MeV capture γ-rays are detected by an array of CsI(Tl) crystals.

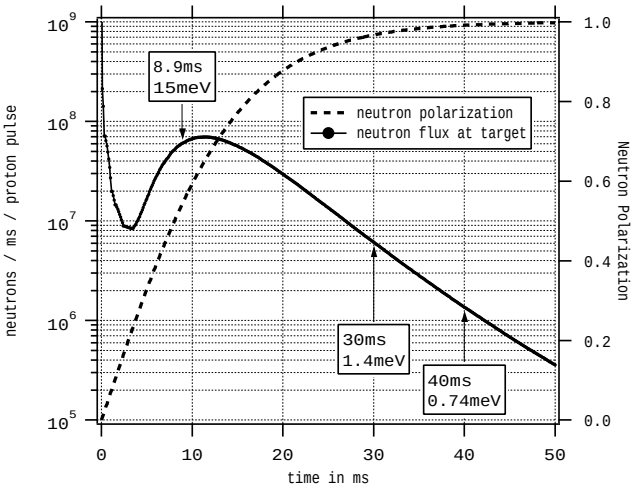

Fig. 73. Cold neutron beam flux and polarization for $\vec{n}+p \to d+\gamma$, assuming a 15 m flight path. Neutrons arriving early in the frame with energy >15 meV are energetic enough to excite para-to-ortho transitions in the target, so there is no physics asymmetry during this time. After 40 ms, a frame overlap chopper will block slow neutrons. (For the 22 m flight path of FP12, 40 ms will correspond to 1.5 meV.)

A uniform vertical guide field, $B_\circ = 10$ G, preserves the neutron beam polarization as it is transported to the liquid hydrogen target. Low energy neutrons depolarize rapidly in ortho-hydrogen, while those below 15 meV retain their polarization in a parahydrogen target; hence, it is important to ensure that the target is prepared and maintained with the very low equilibrium ortho-hydrogen concentration of <0.05%. On-line monitoring of the target transmission provides a measure of the ortho:para hydrogen ratio, since the cross sections for the two species are markedly different. Only 60% of the beam neutrons will be captured in the target; those that scatter through the target walls will be absorbed in a ^{6}Li liner surrounding the target vessel, and the remaining 15% will be transmitted to the ionization chamber at the end of the beam line for monitoring purposes.

The 2.2 MeV γ-rays from neutron capture in the target will be detected with an array of 48 (15 cm)^3 CsI(Tl) crystals read out in current mode by vacuum photodiodes coupled via low noise I-V preamplifiers to transient digitizers. The time-of-flight information from the CsI detectors will allow the γ-ray asymmetry A_γ with respect to the neutron spin direction to be deduced as a function of incident neutron energy; A_γ should be constant, but the experimental asymmetry $\varepsilon = P_n A_\gamma$ will reflect the energy dependence of the beam polarization from Fig. 73. A beam chopper will eliminate frame overlap by blocking the low energy tail of the flux distribution, which would otherwise be superposed on the spectrum of fast neutrons from the next beam pulse. A resonant rf spin flipper upstream of

the target will reverse the direction of the neutron spin every beam pulse according to a $+--+-++-$ reversal pattern, cancelling systematic drifts to second order. The expected asymmetry is $A_\gamma = -5 \times 10^{-8}$ based on the best available theoretical predictions [Bowman *et al., op. cit.*; Wilburn and Bowman, *et al., op. cit.*], and we plan to measure A_γ to $\pm 5 \times 10^{-9}$ with systematic errors less than 5×10^{-10}.

Prototype beam monitor

During 2001, a prototype beam flux monitor was constructed according to our specifications by LND, Inc., of Oceanside, NY. The beam monitor is a parallel plate ionization chamber with 12 × 12 cm^2 active area. It was filled by LND with a gas mix consisting of 50% N_2 and 50% ^{3}He at 1 standard atmosphere. The chamber consists of an outer aluminum box with entrance and exit windows each 1 mm thick, and it contains 3 internal aluminum electrodes, each 0.5 mm thick for a total of 3.5 mm Al. The outer box and central internal electrode are grounded; the other electrodes are intended to be biased at –5 kV. A current signal is derived from the sum of the ionization collected when neutrons are captured on the ^{3}He in either of the two central 1 cm gaps, as indicated in Fig. 74.

Neutron capture on ^{3}He produces a triton, a proton, and 0.77 MeV of kinetic energy. Not all of the kinetic energy released contributes to the ionization signal, because of the finite detector geometry. To design the beam monitor, a simple Monte Carlo program was written to simulate the capture of neutrons and collection of charge in the ionization medium. The program calculates the distribution of energies deposited in the detector for a uniform flux of incident neutrons distributed over a given area. For fixed detector dimensions, the mean of this distribution decreases, and the variance increases slightly, with increasing beam size. The additional noise due to the variance of the energy deposited per neutron is given by $\sqrt{1+(\sigma/E)^2}$. This noise factor depends only weakly on the choice of filling gas and the transverse detector size, for reasonable options that were considered in the design.

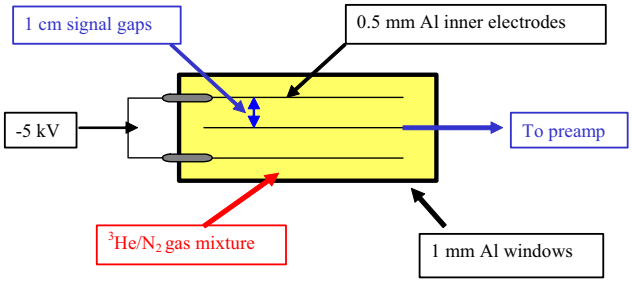

Fig. 74. Sketch of the LND 27527 prototype beam monitor. The beam enters vertically in this orientation. For the upstream monitors, enough ^{3}He is added to capture about 1% of the neutrons.

For the upstream monitors in the NPDGamma experiment, we plan to absorb about 1% of the beam to produce the signal. This corresponds to about 22 torr of ^{3}He in N_2 at 1 Atm. The reason for choosing a relatively heavy filler gas is to maximize the energy that is deposited in the sensitive region, and hence also to minimize a slow contribution to the current signal that would result from ionization occurring in the low field regions between the edges of the inner electrodes and the outer can. The lower ion mobility is compensated for by operating the chamber at a higher voltage than would be necessary with a lighter gas. At –5 kV, the response time for the 1% detectors is estimated to be 80 μs.

Test run data

A first look at M1 at the beginning of the test run produced the scope plot shown in Fig. 75. Note the significant frame overlap indicated by the tail at the start of the beam pulse. The plot is averaged over 8 beam pulses at 54 μA proton current. The Al Bragg edges at 14.1 and 16.3 ms locate the detector at 14.05 m from the source. The maximum signal is 2.7 volts at 16.9 ms, corresponding to an energy of 3.6 meV. The capture probability at 3.6 meV is 0.223. The preamp feedback resistor was 5.0 MΩ. From these data, we deduce the test run neutron flux at 3.6 meV to have been 1.4×10^6 neutrons/ms/pulse.

A detailed comparison of the fluctuations in the beam monitor signals for the prototype monitor M1 and the reference monitor M2 was carried out. The integrated charge between 2 and 40 ms within a beam pulse was recorded, and the variance in the ratio of integrated charges, R=(M1/M2), was used to assess the intrinsic noise in the two monitors, in

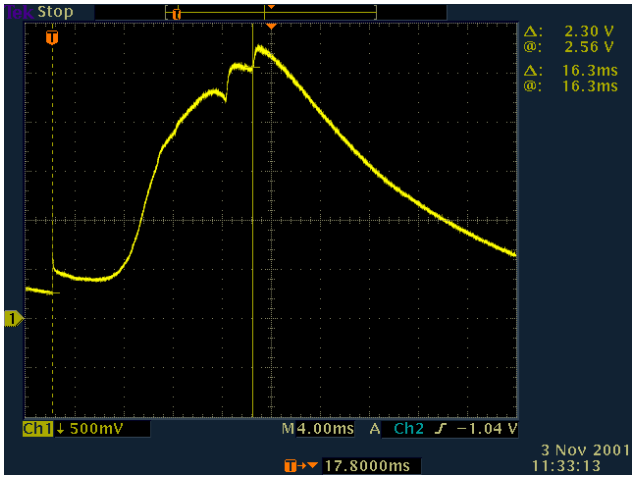

Fig. 75. Digital scope plot from prototype monitor during the test run. No frame overlap chopper was in operation, so some overlap is seen at the start of the frame. The two notches near the top are Bragg edges from aluminum.

comparison with model predictions. It was found that $\sigma_R/R = 1.0 \times 10^{-3}$, which compared well with a prediction of 0.9×10^{-3} based on the expected number of neutrons detected by the two monitors in this time window (N1, N2) and the predicted noise factors $1.1/\sqrt{N1}$ and $1.2/\sqrt{N2}$ respectively.

Finally, an absolute comparison of the neutron flux at 3.12 meV was carried out, using the prototype monitor M1, the reference monitor M2, and a ^{6}Li-doped scintillation counter for normalization purposes. The beam was tightly collimated for these measurements. The resulting flux values at 3.12 meV were deduced to be 36, 33, and 32 kn/ms/pulse for M1, M2 and the ^{6}Li counter respectively, in agreement to within the uncertainties associated with the experimental conditions.

We conclude that the performance of the prototype monitor M1 was entirely satisfactory, with gain and noise characteristics in agreement with expectations. We also found that the design was very insensitive to mechanical vibrations – one could barely detect a change in the output signal when the monitor was struck firmly on the side with a wrench. Very little 60 Hz pickup was experienced with this configuration. Based on the test run results, 3 similar beam monitors, filled to appropriate gas mixtures for the final NPDGamma experiment, have been obtained and are now at LANSCE.

TRIUMF detector stand project

A crucial issue for the experiment is the ability to determine the effective detector alignment, *in situ*, to within ±20 mr with respect to the magnetic holding field direction, in order to suppress the contribution of a small parity-allowed left-right asymmetry to the parity-violating up-down asymmetry that we are seeking to measure. One possible approach for this determination is to calibrate the detector alignment via a capture reaction with a known and relatively large left-right gamma asymmetry. Part of our test run time was spent searching for such asymmetries in several nuclei which had exhibited significant parity-violating up-down asymmetries, but no suitable candidates were found. An alternative scheme based on scanning a small target within the beam envelope in x and y was explored, but this was found to be unsuitable due to nonuniformities in the beam intensity distribution. As a result, we have concluded that the preferred method to calibrate the detector alignment is to scan the entire detector array in x and y with the liquid hydrogen target in place. This method places stringent requirements on the detector stand design and construction that were not envisioned when the experiment was originally proposed.

As part of our contribution to the project, the Manitoba/TRIUMF team has taken on the responsibility for design and construction of an integrated stand for both the CsI detector array and the liquid hydrogen target. This task relies heavily on crucial engineering and infrastructure support provided by TRIUMF. The design and construction of the stand and motion controller is now complete and the apparatus has been shipped to Los Alamos for final assembly and testing by TRIUMF and Manitoba personnel. A drawing of the integrated stand concept is shown in Fig. 76. Early in the project, one of the 4-detector support panels was shipped to LANL, where it was loaded with detectors and preamps. Deflections under load were within tolerances, as predicted by the FEA analysis of the design undertaken by TRIUMF engineer Tom Ries. Figure 77 shows Tom with the completed CsI array

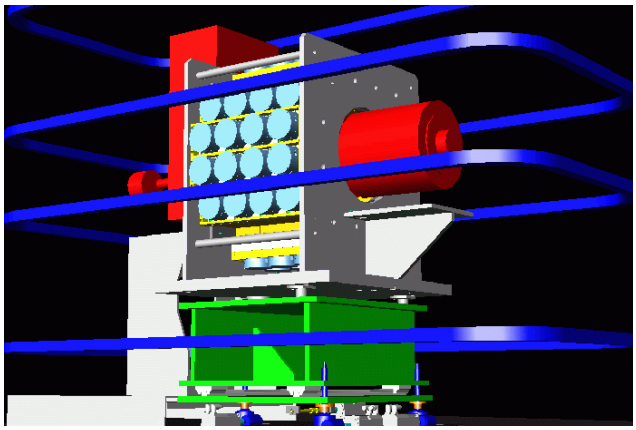

Fig. 76. Drawing of NPDGamma equipment. The CsI array is seen in the centre, supported by the TRIUMF $x-y$ motion stand. The cylinder at the right is the rf spin flipper, which moves with the CsI array. Part of the LH_2 target services box is visible at the left. The large horizontal coils provide the 10 G guide field.

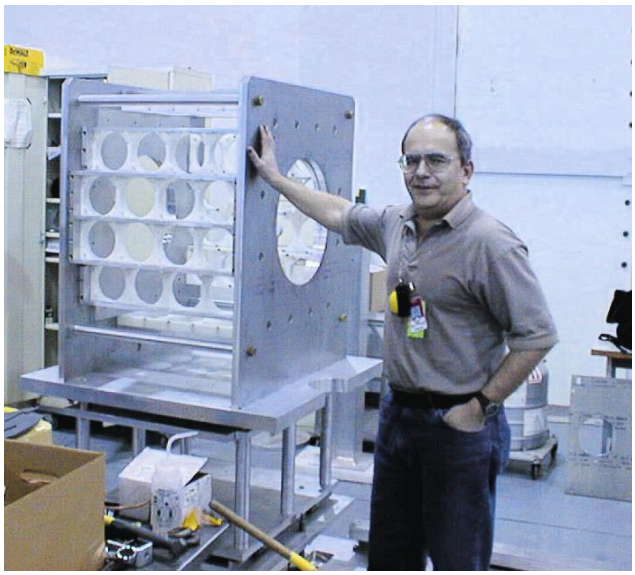

Fig. 77. CsI mounting frame during installation in the ER-2 area of Lujan Center.

mouning frame. Tom and engineering coop student, Justin Ho, will go to Los Alamos early in 2003 to set up the TRIUMF apparatus.

Future plans

The construction of the beam line is currently under way, and the cave to house the experimental equipment is planned to be ready in late May, 2003. The liquid hydrogen target should be delivered to LANL in early May, 2003, for assembly and mounting on the stand structure (Fig. 76). We will provide manpower for installation and commissioning of the apparatus. The stand assembly was completed at TRIUMF in December, 2002. The experiment is scheduled to be commissioned starting in June, 2003, followed by one year of data acquisition, starting November–December, 2003 and likely spread over 2 calendar years. A new Manitoba graduate student has been recruited and will be starting work in summer, 2003.

Collaborators: C.S. Blessinger, M. Gericke, G.L. Greene, G. Hansen, G.L. Morgan, H. Nann, W.M. Snow (Indiana University); J.D. Bowman G.E. Hogan, J.N. Knudson, S.K. Lamoreaux, G.S. Mitchell, C.L. Morris, S.I. Penttila, D.A Smith, W.S. Wilburn, V.W. Yuan (Los Alamos National Laboratory); R.D. Carlini (Thomas Jefferson National Accelerator Facility); T.E. Chupp, K.P. Coulter, R.C. Welsh, J. Zerger (University of Michigan); M.S. Dewey, T.R. Gentile, D.R. Rich, F.E. Wietfeldt (National Institute of Standards and Technology); T. Case, S.J. Freedman, B.K. Fujikawa (University of California, Berkeley); S. Ishimoto, Y. Masuda, K. Morimoto (KEK National Laboratory, Japan); G.L. Jones (Hamilton College); W.M. Hersman, M.B. Leuschner, V.R. Pomeroy (University of New Hampshire); S.A. Page, W.D. Ramsay (University of Manitoba); E.I. Sharapov (Joint Institute for Nuclear Research, Dubna); T.B. Smith (University of Dayton).